



# SPSD II

## A CONTINUOUS HOLOCENE RECORD OF ENSO VARIABILITY IN SOUTHERN CHILE (ENSO-CHILE)

M. DE BATIST, N. FAGEL, A. BERGER



### PART 2

GLOBAL CHANGE, ECOSYSTEMS AND BIODIVERSITY



ATMOSPHERE AND CLIMATE



MARINE ECOSYSTEMS AND BIODIVERSITY



TERRESTRIAL ECOSYSTEMS AND BIODIVERSITY



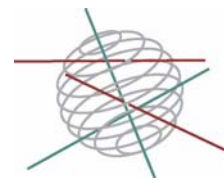
NORTH SEA



ANTARCTICA



BIODIVERSITY



**Part 2 :**  
**Global change, Ecosystems and Biodiversity**

FINAL REPORT



**A CONTINUOUS HOLOCENE RECORD  
OF ENSO VARIABILITY  
IN SOUTHERN CHILE  
(ENSO-CHILE)**

**EV/10**



M. De Batist<sup>1</sup>, N. Fagel<sup>2</sup>, M.F Loutre<sup>3</sup>, E. Chapron<sup>4</sup>  
A. Berger<sup>3</sup>, X. Boës<sup>2</sup>, S. Bertrand<sup>2</sup>, F.Charlet<sup>1</sup>, F.  
De Vleeschouwer<sup>2</sup>, E. Juvigné<sup>2</sup>, M. Pino<sup>5</sup>, V. Renson<sup>2</sup>  
E. Roche<sup>2</sup>, M. Sterken<sup>6</sup>, J. Thorez<sup>2</sup>, R. Urrutia<sup>7</sup>, L. Vargas<sup>2</sup>  
E. Verleyen<sup>6</sup>, W. Vyverman<sup>6</sup>

<sup>1</sup> *Department of Geology and Soil Science  
Universiteit Gent, Belgium*

<sup>2</sup> *Département de Géologie,  
Université de Liège, Belgium*

<sup>3</sup> *Institute of Astronomy and Geophysics Georges Lemaître,  
Université catholique de Louvain la Neuve, Belgium*

<sup>4</sup> *Geological Institute, ETH Zürich, Switzerland*

<sup>5</sup> *Instituto de Geociencias, Universidad Austral de Chile, Valdivia,  
Chile*

<sup>6</sup> *Department of Biology, Universiteit Gent, Belgium*

<sup>7</sup> *EULA, Universidad de Concepcion, Chile*



BELGIAN SCIENCE POLICY



D/2007/1191/50

Published in 2007 by the Belgian Science Policy

Rue de la Science 8

Wetenschapsstraat 8

B-1000 Brussels

Belgium

Tel: + 32 (0)2 238 34 11 – Fax: + 32 (0)2 230 59 12

<http://www.belspo.be>

Contact person: M<sup>me</sup> Martine Vanderstraeten

Secretariat: + 32 (0)2 238 36 10

Neither the Belgian Science Policy nor any person acting on behalf of the Belgian Science Policy is responsible for the use which might be made of the following information. The authors are responsible for the content.

No part of this publication may be reproduced, stored in a retrieval system, or transmitted in any form or by any means, electronic, mechanical, photocopying, recording, or otherwise, without indicating the reference.

---

**TABLE OF CONTENTS**


---

<b>ABSTRACT</b> .....	5
<b>I. INTRODUCTION</b> .....	7
I.1. Why studying paleoclimate in southwestern South America ? .....	7
I.2. Regional setting of the Chilean Lake District, southwestern South America .....	9
I.3. Exploration of the Chilean Lake District and selection of the study sites .....	11
I.4. Study site: Lago Puyehue .....	11
I.5. Data collected in Lago Puyehue .....	14
<i>Seismic data</i> .....	14
<i>Sediment cores</i> .....	14
<b>II. LONG-TERM RECORD OF CLIMATE CHANGE</b> .....	17
II.1. Materials and methods .....	17
II.1.1. <i>The PU-II long core: lithology</i> .....	17
II.1.2. <i>Sedimentological, mineralogical and geochemical analysis</i> .....	19
II.1.3. <i>Tephrostratigraphical analysis</i> .....	20
II.1.4. <i>Diatom analysis</i> .....	21
II.1.5. <i>Pollen analysis</i> .....	21
II.1.6. <i>Age-depth model</i> .....	22
II.2. Results .....	23
II.2.1. <i>Seismic stratigraphy</i> .....	23
II.2.2. <i>Sedimentological, mineralogical and geochemical variations</i> .....	25
II.2.3. <i>Diatom stratigraphy</i> .....	29
II.2.4. <i>Pollen stratigraphy</i> .....	31
II.3. Discussion .....	34
II.3.1. <i>Timing of glacier retreat from Lago Puyehue ?</i> .....	34
II.3.2. <i>Long term climate evolution</i> .....	36
II.3.3. <i>Millennium-scale abrupt climate changes</i> .....	38
<i>A new record of a southern medium- to high-latitude Late-Glacial Cold Reversal ?</i> ...	38
<i>Other millennium-scale abrupt climate changes: 3400-2900 cal. yr BP</i>	
<i>cold/humid event</i> .....	40
<i>Other millennium-scale abrupt climate changes: Little Ice Age</i> .....	40
<b>III. HIGH-RESOLUTION RECORD OF PRECIPITATION</b> .....	43
III.1. Materials and methods .....	43
III.1.1. <i>Varve analysis</i> .....	43
<i>Varve counting</i> .....	43
<i>Manual varve thickness measurements</i> .....	44
<i>Semi-automatic varve counting</i> .....	44
<i>Calendar years estimation from varve counting</i> .....	44
<i>Grey-scale-based varve-thickness measurements</i> .....	45
<i>The varve-thickness index</i> .....	46
III.1.2. <i>Spectral analysis</i> .....	46
III.2. Results .....	47
III.2.1. <i>Sedimentation rates obtained from varve counting</i> .....	47
III.2.2. <i>Varve micro-facies and the origin of the varves</i> .....	49
III.2.3. <i>Quantitative climate-varve relationships</i> .....	50
<i>Local climate control on varve thickness</i> .....	50
<i>Correlation between varve thickness and global climate factors</i> .....	53
<i>Varve thickness and ENSO</i> .....	54

III.3. Discussion .....	56
III.3.1. A 600 yr record of changes in precipitation in Lago Puyehue .....	56
Varve-thickness record .....	56
Regional precipitation changes since 1400 .....	57
III.3.2. Spectral analysis of ENSO variability over the last 600 yrs .....	59
Dominant climate periodicities in the Lago Puyehue record .....	59
A 600 yr record of ENSO-related periodicities and links with other climate modes.....	62
III.3.3. Precipitation and ENSO variability during millennium-scale abrupt climate changes .....	63
ENSO variability during millennium-scale abrupt climate changes:	
the Little Ice Age .....	63
A varve-thickness record of a Late-Glacial millennium-scale abrupt climate change: the Huelmo/Mascardi Cold Reversal .....	63
<b>IV. CONCLUSIONS .....</b>	<b>69</b>
<b>ACKNOWLEDGEMENTS .....</b>	<b>73</b>
<b>REFERENCES .....</b>	<b>75</b>
<b>PROJECT OUTPUT .....</b>	<b>85</b>

## ABSTRACT

An 11-m-long sediment core was collected in Lago Puyehue (40°S, Lake District, Chile). The coring site was selected on basis of a thorough seismic-stratigraphic analysis that highlighted it as an area of relatively condensed, continuous and undisturbed sedimentation in this otherwise highly dynamic post-glacial lake. The 11-m core extends back to 17,915 cal. yr BP and a substantial part of it is annually laminated. An age-depth model was established by 9 AMS  $^{14}\text{C}$  dates, constrained by  $^{210}\text{Pb}$ ,  $^{237}\text{Cs}$ ,  $^{241}\text{Am}$  measurements, by the identification of event deposits related to earthquakes and/or volcanic eruptions, and by varve counting for the past 600 yrs. The core was submitted to a multi-proxy analysis, including sedimentology, mineralogy, grain-size, major geochemistry and organic geochemistry (C/N ratio,  $\delta^{13}\text{C}$ ), loss-on-ignition, magnetic susceptibility, diatom analysis, palynology and varve thickness analysis.

Interpretation of the seismic data and extrapolation of the age-depth model puts the age for the onset of open-water conditions in Lago Puyehue at ca. 28,000 cal. yr BP. This contrasts with previous glacial-history reconstructions from the area based on terrestrial records, which date the complete deglaciation of the basin as ca. 14,600 cal. yr. BP.

Along-core variations in sediment composition reveal that the area of Lago Puyehue was characterised since the Last Glacial Maximum (LGM) by a series of rapid climate fluctuations superimposed on a long-term warming trend. Among these climate fluctuations are: i) a first warming pulse sometime between 19,500 and 17,150 cal. yr BP, ii) a well-marked cold and humid interval at 13,100-12,300 cal. yr BP, roughly coeval with the Huelmo/Mascardi Cold Reversal (and out-of-phase with the Northern-Hemisphere Younger Dryas and the Antarctic Cold Reversal), iii) a second pulse towards warmer and dryer conditions between 12,300 and 11,800 cal. yr BP, marking the onset of the Holocene, iv) warm and dry climate conditions between 11,800 and 7,800 cal. yr BP, reflecting an early Holocene climatic optimum, v) relatively stable climate conditions since 7,800 cal. yr BP, except for vi) an interval of cold and/or humid conditions at 3,400-2,900 cal. yr BP, and vii) a wet period during the interval 1490-1700.

Regional present-day climate around Lago Puyehue is dominated by the southern Westerlies and associated strong precipitation. Precipitation peaks during the transition from austral autumn to winter and during winter. Detailed re-analysis of available instrumental data shows El-Niño years to be characterized by lower-than-normal precipitation, particularly during the autumn/winter transition. Since precipitation during autumn/winter is the dominant factor controlling the thickness of the varves, varve-thickness and color-intensity records can be used as proxy for precipitation and as a tracer of El Niño activity over time. Spectral analysis of varve-thickness records over the last 600 yrs reveals periodicities of 3, 3.2 and 4-4.4 yrs. The dominant period over the last 100 yrs is that of 3 yrs, which is consistent with the most common frequency of the present-day El Niño phenomenon. The record also contains multi-decadal periodicities of 15 and 41 yrs, which are consistent with other South Pacific and even North Pacific indexes (QBO, PDO, PNI or NOI). The dominant period over the last 600 yrs is 4-4.4 yrs and appears in the record during

the period 1490-1700 (i.e., the Little Ice Age). The climate during the Little Ice Age thus appears to have been characterized by successive pronounced El Niño events. Varve-thickness analysis of the laminated interval at the bottom of the long core allows sub-dividing the Huelmo/Mascardi Cold Reversal into two separate cold/humid intervals, interrupted by a dryer and warmer phase.

The sedimentary record obtained from Lago Puyehue provides the very first long-term, continuous, high-resolution record from the Pacific side of southern South America, and will undoubtedly emerge as a reference paleoclimate record.

Key words: paleoclimate; climate change; El Niño Southern Oscillation; lake; Chile

## I. INTRODUCTION

The overall objectives of the ENSO-CHILE project were:

1. To study the regional impacts of "El Niño Southern Oscillation" (ENSO) climatic events in southwestern South America, and more specifically in an area that is very sensitive to them, but in which their effects and history are still poorly known;
2. To analyse the long-term evolution and variability –both in terms of intensity and dominant periodicity– of these events during the Late-Glacial and Holocene, in order:
  - to identify possible multi-decadal cyclicity overprints on ENSO intensities and to evaluate possible teleconnections with Northern Hemisphere or Equatorial multi-decadal climate modes,
  - to identify possible millenium-scale variations in climate, and how they impact on ENSO behaviour, and to evaluate possible links with Northern Hemisphere millenium-scale abrupt climate shifts and/or with intertropical millenium-scale complex climate phases.

### I.1. Why studying paleoclimate in southwestern South America ?

The "El Niño Southern Oscillation" (ENSO) is one of the most important processes affecting the present-day climate of the Earth, with impacts on an almost global scale. It is caused by variations in trade-wind intensity and unstable ocean-atmosphere interactions in the tropical Pacific Ocean. It is expressed by an alternation of positive/negative ("El Niño" and "La Nina") climatic anomalies that especially affect the Western and Eastern Pacific areas. ENSO occurs quasi-cyclical with a multi-annual to decadal period. It has a profound impact on precipitation (droughts, floods) and average seasonal temperature (warm, cold), with subsequent effects on fisheries, agriculture, economy, public health,... A better understanding of the ENSO phenomenon requires detailed studies in several contrasted areas and settings, because its effects can be highly variable: i.e., droughts in Brazil, floods of the Nile, etc. The Pacific coasts of the Americas have received particular scientific attention in the recent past (e.g. PEP1) because it is one of the areas most affected by the ENSO system: i.e., El Niño years are expressed by extremely wet conditions in Northern Peru, by storms in Central Chile, etc. However, the effects of the ENSO phenomenon further south in South America, where climate is essentially controlled by the interaction of the humid-air-advecting Westerlies and the topography of the Andes, are less well-known.

- Question 1: What are the effects of ENSO along the Pacific coast of southern South America ?

In recent years it has become clear that ENSO intensity has increased throughout the 20<sup>th</sup> century and that its impact is now felt almost on a global scale. ENSO effects have even been identified in southern Europe, while the climate of other parts of Europe appears to be dominated by a similar ocean-atmosphere interaction: i.e., the "North Atlantic Oscillation" (NAO). Both ENSO and NAO systems are receiving increased scientific attention. Recent studies have shown the presence of a multi-

decadal (i.e. 50-70 yrs) cyclicity overprinted on ENSO intensity (Markgraf et al., 2000), not only in intertropical areas but also in the North Pacific. Similar multi-decadal cycles of NAO have been identified in the North Atlantic area, and are attributed to changes in the North Atlantic thermohaline circulation pattern. However, it remains unclear whether a similar ocean-driven cyclicity also occurs in the South Pacific. A long continuous high-resolution climate record from the South Pacific area could reveal such a cyclicity, and whether or not it is connected with any of the Northern Hemisphere cycles.

- Question 2: Are multi-decadal cycles also present in the South Pacific and do they correlate with Northern Hemisphere ones ?

Some of the most spectacular natural climate fluctuations since the end of the Last Glacial Maximum (LGM; i.e. 18,000 yr BP) occurred during the transition from the last glacial into the current interglacial period, and were characterized by rapid, drastic, millennium-scale temperature excursions: e.g., the "Younger Dryas cold reversal" (YD). Although they are recorded in various natural archives around the World, recent data seem to indicate that they were asynchronous in both hemispheres and, probably, triggered by processes in the Southern Hemisphere. Recent data have also shown that also the Holocene itself has been affected by several abrupt cooling periods, which are especially well-documented in the North Atlantic region. The most recent and probably strongest of these cooling periods is the "Little Ice Age" (LIA). These LIA-like cold periods appear to have occurred more or less regularly with an interval of about 2,500 yr, and they are attributed to interactions between North Atlantic oceanic circulation, the Greenland ice sheet and polar atmospheric circulation. Possibly, they are also controlled by solar activity and consequently could be of global importance, although they have not yet been clearly documented in the Southern Hemisphere (except for the LIA itself). These uncertainties clearly indicate that additional, high-resolution, well-dated post-LGM climate reconstructions from the mid- to high-latitude regions in the South (i.e. between 40 and 70°S) are urgently needed to reveal the extent, timing and duration of Southern Hemisphere climate fluctuations and the connection between the Northern and Southern Hemispheric climate systems.

- Question 3: Is the post-LGM period in southern South America also characterized by millennium-scale abrupt climate changes and do they relate to the tropical and/or the North Atlantic ones ? What is the long-term evolution of the ENSO system through the Holocene ?

South-Central Chile is well suited to produce valuable paleoclimate records for the study of inter-hemispheric linkages throughout the Late Quaternary, given its location in the Southern Westerly zone (40-55°S), which is influenced by both equatorial (i.e., ENSO) and Antarctic climate expressions. The continuous distribution of large lakes across a wide latitudinal belt (Fig. 1) at the northern boundary of the Southern Westerly zone makes the region of the Chilean Lake District particularly interesting to investigate spatio-temporal patterns in past climate variability using a paleolimnological approach.

## **I.2. Regional setting of the Chilean Lake District, southwestern South America**

The Chilean Lake District extends from ca. 37° to 42° S (Fig. 1). At this latitude, Chile is about 200 km wide and it can be sub-divided from West to East into three main physiographic provinces (Fig. 1): the Coastal Ranges, the Central Valley and the Andes. The Coastal Ranges, on average 500-800 m high, are composed of a Late Paleozoic accretionary prism and magmatic arc (Willner et al. 2004) and are dominated by primarily low-grade metamorphic rocks. The Central Valley has a mean altitude of 150-200 m and consists of Eocene-Miocene volcano-sedimentary deposits that are overlain by Pliocene-Quaternary volcanics and volcanoclastics and by fluvial and fluvio-glacial deposits. The Andes, at an average elevation of 2,500-1,500 m, consist of plutonic basement and volcanic rocks, resulting from Pliocene to Recent volcanic activity (SERNAGEOMIN 2003).

This outspoken physiographic segmentation is a direct result of the subduction of the Nazca oceanic plate below the adjacent continental margin (Fig. 1). Ongoing subduction is also reflected in the distribution of the seismicity, with very frequent and strong earthquakes. The largest ever instrumentally recorded earthquake ( $M_w = 9.5$ ), the Valdivia earthquake of 22 May 1960, devastated large parts of the area and reportedly even triggered an eruption of the Puyehue Volcano, at 70 km distance (Lara et al. 2004).

The subduction-related geodynamic setting also makes this area one of the most active volcanic regions in the World. It is part of the South American South Volcanic Zone (SVZ) and comprises a whole series of very large and highly active volcanoes (Fig. 1): e.g. the Llaima (3,060 m), Villarrica (2,847 m), Osorno (2,652 m) and Puyehue Volcanoes (2,111 m). Many of these are quite recent in age (i.e. Late-Glacial to Holocene). Most are stratovolcanoes composed of basaltic to andesitic lavas and pyroclastics. The volcanic activity in this part of Chile is so pervasive that the whole region is covered by a thick layer of volcanic ashes, on top of which the typical andosols (so-called "trumaos") have formed (Langohr 1971, 1974, Bertrand & Fagel in press).

Apart from the volcanic activity, also the Quaternary glaciations have been very important in shaping the region. Large glacial valleys drain the interior of the Andes, which was covered by the Northern Patagonian Ice Cap during Quaternary glaciations, and terminate at the piedmont of the mountains, at the boundary with the Central Valley (Fig. 1). The maximum extension of the glaciers is marked by well-developed moraine complexes. There are two main generations of moraines that mark the maximum extension of the Patagonian Ice Cap during the ultimate and penultimate glaciations, locally called the Llanquihue and Casma or Colegual glaciations, respectively. Three successive Llanquihue moraine belts are clearly visible in the morphology throughout the Lake District (Laugenie 1982). They document different glacial stages, and have been radiocarbon-dated at ca. 73-65 kyr BP, ca. 28-18 kyr BP and ca. 15-14 kyr BP (Clapperton 1993). The youngest and

most internal system of moraine ridges often functions as dams for the several large glacial piedmont-type lakes that characterize the area.

In total, the Lake District comprises up to 17 medium- to large-sized lakes (Fig. 1). They range from about 5 to 45 km across and are on average between 100 and 350 m deep. In general, they show a distinct tendency of increasing in size and depth and decreasing in altitude from North to South. The pioneering work of H. Campos and his co-workers in the '80s has uncovered the general characteristics of their morphology and bathymetry and has illustrated that most of the lakes are composed of a complex combination of several sub-basins separated by shallower ridges or sills.

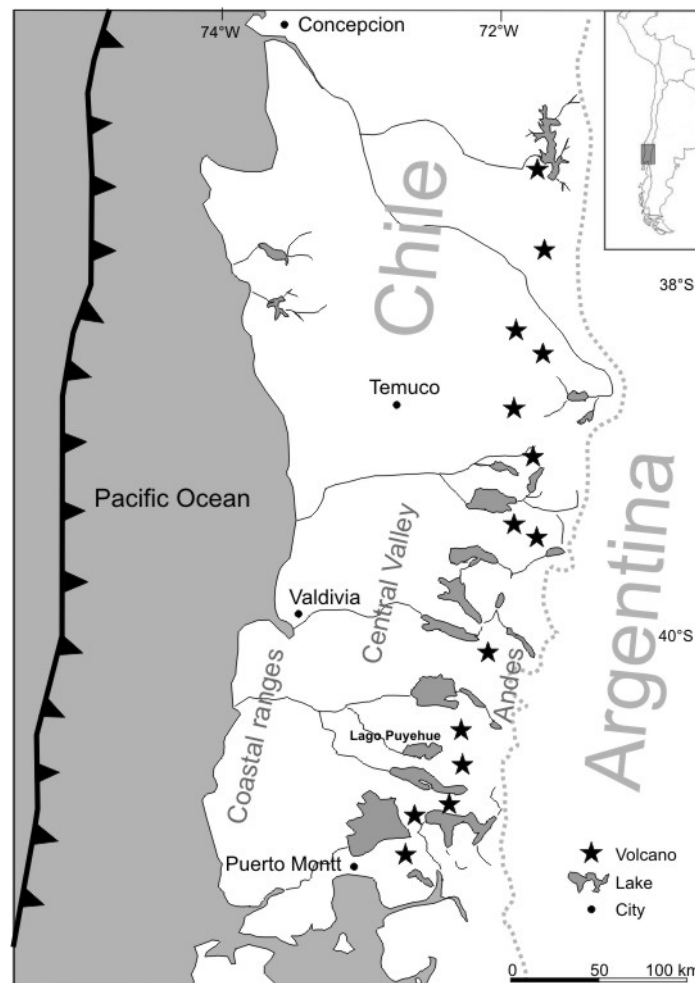


Figure 1: Regional location map of the Chilean Lake District, with indication of the main lakes and volcanoes.

The limnology of these lakes has been studied by a.o. Campos et al. (1987, 1988, 1989, 1990, 1992a, 1992b) and Urrutia et al. (2000). They are all oligotrophic and temperate monomictic, with a summer stratification from December to March (slightly variable depending on altitude).

### **I.3. Exploration of the Chilean Lake District and selection of the study sites**

A first expedition in the framework of the ENSO-CHILE project was carried out from 10 December 2001 to 15 March 2002. This expedition consisted of four main parts:

#### Part 1: Reflection seismic reconnaissance of all suitable lakes in the region

Regional reflection-seismic reconnaissance profiles were acquired in six suitable (i.e. maximum water depth < 150 m) and accessible lakes: i.e., Lagos Laja, Icalma, Lleulleu, Villarrica, Puyehue, Todos los Santos (total length: 500 km). Based on these seismic data, the potential of the lakes to contain a useful sedimentary record was evaluated, and two lakes were selected as most suitable: i.e., Lagos Icalma and Puyehue.

#### Part 2: Detailed reflection seismic study of the selected lakes

More detailed grids of high-resolution and very-high-resolution reflection-seismic profiles were then collected in Lagos Icalma and Puyehue. Seismic-stratigraphic interpretation of these data allowed the selection of two coring sites in each of the lakes: i) one site influenced by detrital, riverine sediment input, and as such most likely having recorded a precipitation-driven history of floods from the drainage basin, and ii) one site dominated by open lacustrine sedimentation, and as such most likely having recorded climate-driven changes in limnological parameters of the lake water body.

#### Part 3: Reconnaissance of the drainage basins

Extensive fieldwork was carried out in the region, and in the drainage basins of Lagos Icalma and Puyehue in more detail. Data and samples were collected with regards to geomorphology, mineralogy, source rocks, pollen and vegetation.

#### Part 4: Coring survey

Two long cores were collected from each of the two selected lakes (Lagos Icalma and Puyehue), from the two pre-selected coring sites. In addition, several short cores were also collected from different parts of the lake.

In this report, we will focus on the sedimentary record of Lago Puyehue, which proved to contain the best paleoclimate record and to be most suited to accomplish the goals of the ENSO-CHILE project.

### **I.4. Study site: Lago Puyehue**

Lago Puyehue (40°40'S, 72°28'W) is one of the medium-sized moraine-dammed piedmont lakes of the Lake District. It is located at the foothill of the Andes (Figs. 1, 2) at an elevation of 185 m a.s.l. The lake is bordered at its western margin by a series of moraine belts formed during the different stages of the Llanquihue glaciation (Fig. 2; Laugenie 1982, Bentley 1997). The innermost moraine ridges have been dated as being ca. 16,100-12,200 <sup>14</sup>C yr BP in age (Bentley 1997). Lago Puyehue is surrounded by several active volcanoes (Fig. 2): i.e., the Casablanca Volcano at ca.

20 km to the south-east of the lake (1,990 m a.s.l.) and the Puyehue Volcano (2,240 m a.s.l.) and its fissural prolongation Cordon de Caulle at ca. 30 km to the east of the lake. The history of the Puyehue volcano dates back to > 200 ka (Gerlach et al. 1988).

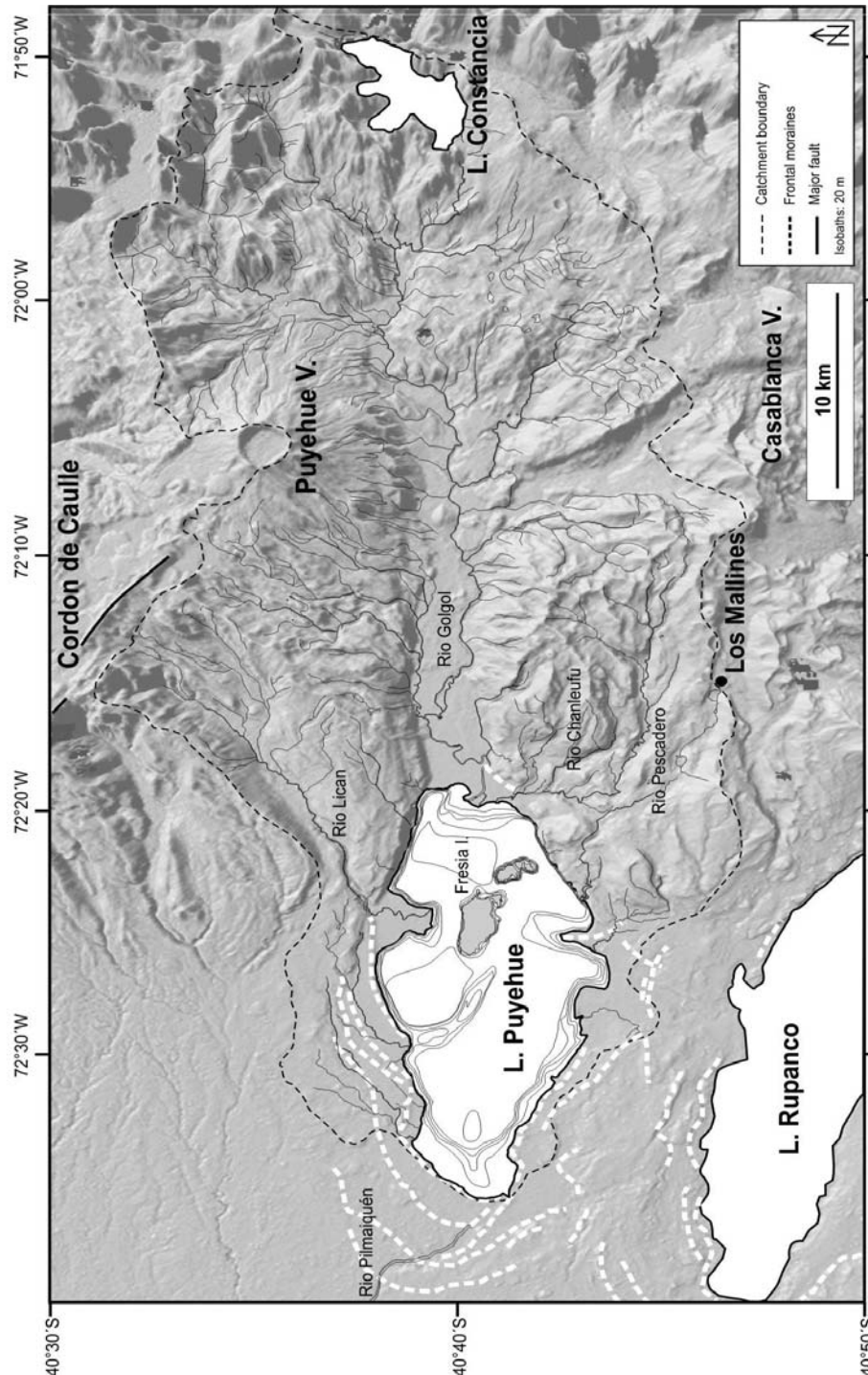


Figure 2: Grey-shaded, SRTM-derived Digital Elevation Model (DEM) of Lago Puyehue and its catchment, with indication of drainage network, main rivers, volcanoes and moraine ridges (after Bentley 1997). Location of peatbog Los Mallines is also indicated. Bathymetry of Lago Puyehue is based on Campos et al. (1989); bathymetry of Lagos Rupanco and Constanica is not included.

Lago Puyehue has a surface area ( $A_0$ ) of 165.4 km<sup>2</sup>, a water volume of 12.6 km<sup>3</sup> and a maximum depth of 123 m (Campos et al. 1989). Its bathymetry is highly complex (Figs. 2, 3b) and reveals three interconnected sub-basins, separated by bathymetric sills or ridges: 1) a large western sub-basin, 5 x 12 km across and about 100 m deep, 2) a small northern sub-basin, 4 x 4 km across and 120 m deep, and 3) a large, irregularly-shaped eastern sub-basin, 5 x 8 km across and 123 m deep. Several islands (a.o., Fresia Island, Cuicui Island) cluster in the central and eastern part of the lake (Fig. 2). They consist of bedrock and their surface is characterized by glacial striae and grooves (Laugenie 1982). A shallow platform occurs in the southern part.

The catchment area ( $A_D$ ) covers 1,510 km<sup>2</sup>, and extends far to the East from the lake (Fig. 2) into the Andes. It consists of Quaternary volcanic rocks, Pleistocene glacial and fluvio-glacial deposits and isolated outcrops of Mesozoic and Cenozoic intrusions, and it is quasi totally covered by several metres of post-glacial andosols. The lake's main tributary is the Rio Golgol, which enters the lake at its eastern border (Fig. 2). Here, the river has developed a large alluvial plain (ca. 3 by 7 km) and a distinct, steep-sloped delta. Several smaller rivers also flow into the lake from the North, South and Southeast (Fig. 2). Rio Pilmaiquén forms the outlet of the lake, which cross-cuts several of the frontal moraine ridges (Laugenie 1982, Bentley 1997) before merging with the Rio Bueno and eventually flowing into the Pacific. There is presently no glacier in the catchment of Lago Puyehue. The  $A_D/A_0$  index (catchment to lake surface ratio) is large, indicating that the sedimentary input into the lake is determined by the drainage from the catchment and that the infill is dominated by river-borne sedimentation.

Lago Puyehue is an oligotrophic and temperate monomictic lake. The lake is stratified with a thermocline at ~20 m depth in summer and mixed during the austral winter months (Campos et al. 1989). The lake temperature (epilimnion) is maximum in summer (~ 18 °C) and water mixing in winter leads to a 9-10 °C homothermy. Maximum nutrient concentrations (phosphorus and nitrogen) occur in autumn and winter (Campos et al. 1989). Its high silica concentration (15 mg/l; Campos et al. 1989) is characteristic for lakes located in volcanic setting. Phytoplankton (e.g., *Melosira*, *Asterionella*) is more abundant in austral autumn and winter (Campos et al. 1989); phytoplankton other than diatoms (e.g., *Cyanophyceae*) is dominant in austral summer months.

Climate around Lago Puyehue is characterized by temperate, humid conditions and is largely controlled by the strength and position of the westerly winds. Mean annual air temperature in the catchment varies between 6 and 9 °C, with maxima of 20 °C in January, and minima of 2 °C in July (Schick 1980). Freezing sometimes occurs at night in winter, but complete ice covering of the lakes has never been observed (Thomasson 1963). Snow cover occurs from May to November, and the current Equilibrium Line Altitude lies at 1,700-1,600 m a.s.l. (Laugenie 1982, Hubbard 1997). Winds are strongest during the transition from austral autumn to winter (~4 m/s in May) and during winter. In spring, wind speeds are lower and reach only ca. 1 m/s (Kalnay et al. 1996). Precipitation trends follow those of the wind velocity and

precipitation peaks during the transition from austral autumn to winter (450-520 mm in May and June) and during winter (Miller 1976, Heusser 2003). Annual precipitation increases with elevation, from ca. 2000 mm/yr around the lake up to ca. 5,000 mm/yr on the slopes and summits of the volcanoes in the region (Parada 1973). During El Niño years precipitation and wind speeds during summer months are significantly lower than during normal climate conditions.

The humid temperate climate is responsible for the development of dense, temperate rainforests, which are essentially of the Valdivian and North-Patagonian type (e.g., Moreno and León 2003, Moreno 2004). Natural vegetation is still well preserved in the catchment; only the shores of Lago Puyehue have been affected by human activities.

## **I.5. Data collected in Lago Puyehue**

### Seismic data

A regional grid of 47 high-resolution and very-high-resolution reflection seismic profiles was acquired across the entire lake (Fig. 3a). The high-resolution data were collected using a multi-electrode sparker (300 J, main frequency: 400-1,500 Hz) as seismic source, and a single-channel, high-resolution streamer as receiver, while the very-high-resolution data were acquired using a 3.5 kHz GeoAcoustics sub-bottom profiling system. A Simrad Shipmate GPS was used for positioning and navigation of the R/V Huala-II of the Universidad Austral de Chile (Valdivia, Chile). The seismic and positioning data were recorded digitally on an Elics Delph-2 system. Processing, which included signal deconvolution, frequency filtering and true-amplitude recovery, was carried out with Landmark ProMAX seismic processing software, and seismic-stratigraphic and structural interpretation and mapping was conducted on an SMT Kingdom Suite seismic interpretation system. Since the single-channel data do not provide information on seismic velocities, an average velocity of 1,600 m/s was used for time-depth conversions.

In total, 65 km of sparker profiles and 73 km of sub-bottom profiles were acquired (Fig. 3a). The sparker data penetrate the entire sedimentary infill in the western part of the lake (> 200 m thick) with a vertical resolution of < 1 m. Elsewhere in the lake, penetration is restricted to ~20 m due to gas blanking. The sub-bottom profiles are predominantly located in the eastern part of the lake (Fig. 3a). They penetrate the upper sedimentary infill to a depth of about 20 m with a vertical resolution of 25-30 cm.

### Sediment cores

Several long and short cores were collected in Lago Puyehue. The long cores were taken with a Uwitec piston-coring system and the short cores with a Uwitec gravity corer, both operated from a Uwitec platform. The coring equipment was provided and operated by the Université de Savoie (Chambéry, France).

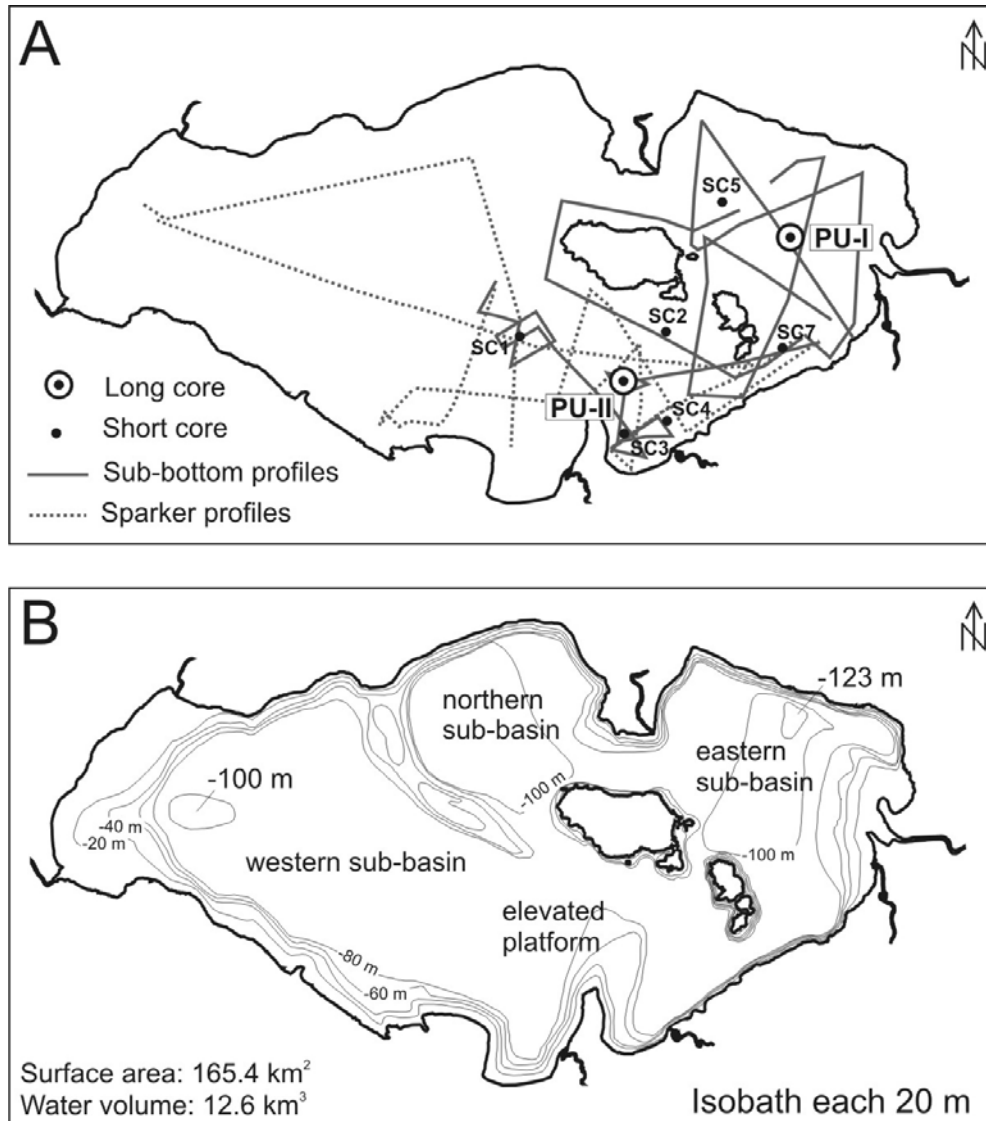


Figure 3: A. Location map of the seismic profiles (sparker and sub-bottom profiles), of the PU-I and PU-II long cores, and of the short cores. B. Bathymetry map, compiled by combining the seismic data with the data of Campos et al. (1989).

Long cores were retrieved from two sites in the lake: site PU-I and site PU-II (Fig. 3a, Tab. 1). Site PU-I is located in the eastern sub-basin, at 122.4 m water depth, close to the inflow of the Rio Golgol. Site PU-II is situated on the shallow platform in the southern part of the lake at 48.4 m depth, where sedimentation is dominated by open lacustrine sedimentation. The composite length of the two long cores is 236 cm (PU-I) and 1,122 cm (PU-II); they have a diameter of 6 cm.

At each of these two sites, also five short cores were taken, and six additional short cores were retrieved from secondary sites across the lake (SC1 to SC7, Fig. 3a, Tab. 1). The length of these short cores varies between 25 and 95 cm

In this report, we will focus on the PU-II long core for the long-term (LGM to Holocene) paleoclimate record, and on a selection of short cores and specific

sections of the PU-I and PU-II long cores for the high-resolution paleoclimate and ENSO reconstructions.

<b>Coring site</b>	<b>Latitude (°S)</b>	<b>Longitude (°W)</b>	<b>Water depth (m)</b>
<b>PU-I</b>	40°39.766'	72°22.155'	122.4
<b>PU-II</b>	40°41.843'	72°25.341'	48.4
<b>SC1</b>	40°41.261'	72°27.377'	90.0
<b>SC2</b>	40°42.645'	72°25.311'	53.6
<b>SC3</b>	40°42.418'	72°24.527'	110.2
<b>SC4</b>	40°41.194'	72°24.521'	108.7
<b>SC5</b>	40°39.302'	72°23.447'	
<b>SC7</b>	40°41.407'	72°22.261'	113.5

Table 1: Location and depth of the long and short cores obtained in Lago Puyehue.

## II. LONG-TERM RECORD OF CLIMATE CHANGE

### II.1. Materials and methods

The PU-II long core was scanned for magnetic susceptibility and gamma-density with a Geotek multi-sensor core logger on non-opened sections (at GFZ-Potsdam, Germany). After opening of the core in Belgium, sediment texture was described (colour, grain-size, structure, contacts) and whole-core magnetic susceptibility (MS) was re-measured at higher resolution on open sections with a Bartington MS2E point sensor (provided by EAWAG, Dübendorf, Switzerland) every 5 mm. The two halves of the composite core were sub-sampled according to the sampling sketch shown in Fig. 4. U-channels (5 mm thick) were taken in the upper part of the archive-half for grain-size analyses. In the same half core, small samples were taken every 5 mm in order to determine the different diatom species. The remaining sediment was impregnated by polymers for the preparation of thin sections. The working half of the composite core was sub-sampled with plastic discs in 1 cm thick slices. Each slice was then divided into 3 equal aliquots for i) mineralogical and geochemical analyses, ii) palynological analysis and iii) tephrostratigraphic analysis (Fig. 4).

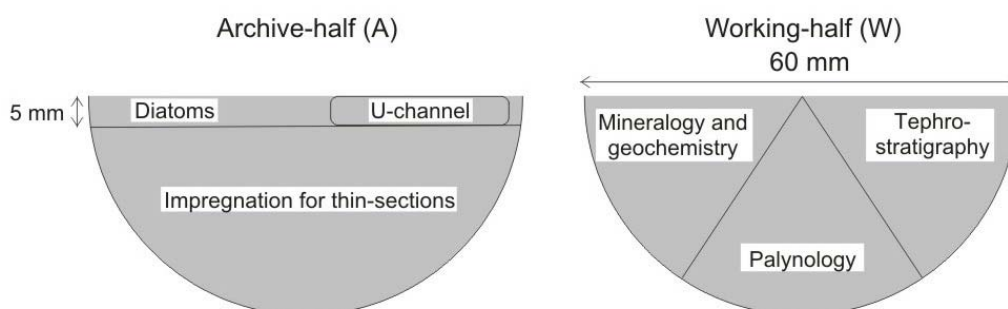


Figure 4: Sampling sketch of the PU-II long core.

#### II.1.1. The PU-II long core: lithology

The sediment is composed of finely laminated to homogeneous brown silt-sized particles (Fig. 5). Four main sedimentary facies can be discerned: homogeneous, slightly laminated, laminated and finely laminated (Fig. 5). In addition, the PU-II long core also contains 81 volcanic sand layers with a thickness ranging from 1 to 75 mm. Seventy-eight of these layers are *in situ* tephras (i.e., coarse grained, net contacts, embedded in a fine matrix and generally less than 1 cm thick). Their cumulative thickness is 52.3 cm. The thickest tephra occurs at 102.3-109.8 cm depth. These *in situ* tephras were studied in terms of tephrostratigraphy and the recent ones were dated by varve-counting and could be attributed to historical eruptions. The 3 remaining sand layers represent the base of turbidites (at 379.5-381 cm, 396.5-397.25 cm and 956-971 cm). Several layers (~1 cm thick) of green clays, frequently containing millimetre-sized pebbles of altered pumice, are interpreted as *in situ* weathering products of pumice deposits.

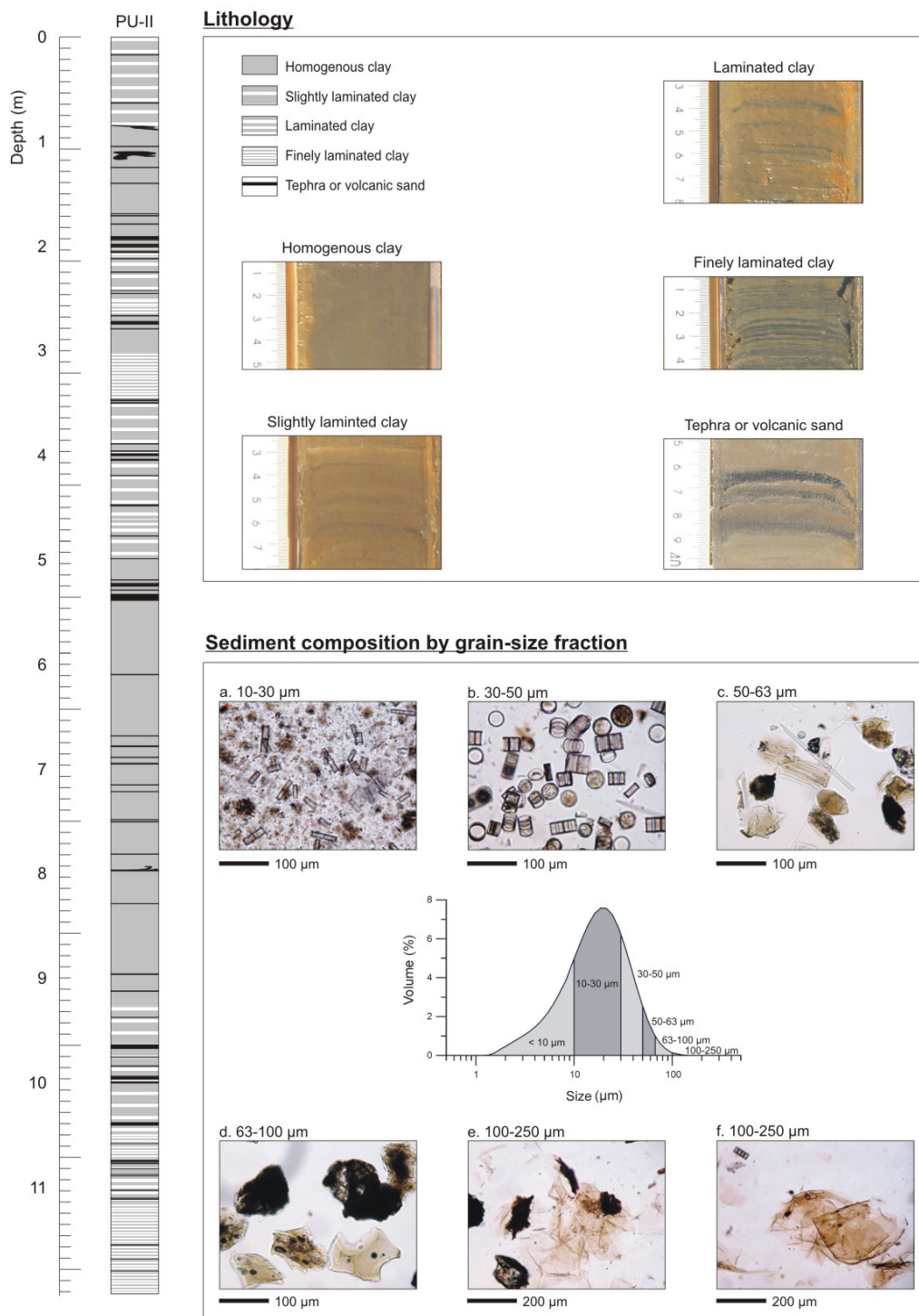


Figure 5: Sedimentary facies types encountered in the PU-II long core. In addition, microscopic illustrations of the different grain-size fractions composing the sediment are shown.

Smear slides show that the 10-30 µm fraction contains detrital clays and diatoms. The 30-50 µm fraction is entirely composed of diatoms. The main species are *Aulacoseira sp.* and *Cyclotella sp.* Between 50 and 100 µm, the sediment contains various minerals and volcanic glasses, as well as sponge spicules. Finally, the 100-250 µm fraction only represents a very small part of the sediment (< 2 %), and

consists of organic matter remains and volcanic minerals. Some organic matter remains are attributed to Cladocera (lacustrine zooplankton).

### ***II.1.2. Sedimentological, mineralogical and geochemical analysis***

The methods that were used for the further sedimentological analysis of the PU-II long core, were chosen after a preliminary high-resolution and multi-methodological investigation of one of the short cores from the PU-II site (Bertrand et al. 2005).

- Grain-size measurements were performed on bulk sediment using a Malvern Mastersizer 2000 laser-diffraction particle analyser detecting particle sizes in the range between 0.02 and 2000  $\mu\text{m}$ . Samples were introduced into a tank with 100 ml deionized water free of additive dispersant, split with a 2000 rpm stirrer and crumbled with ultrasonic waves. Sample quantity was adjusted in order to obtain a laser beam obscuration between 10 and 20 %. Grain-size parameters were averaged over 10,000 scans. Distribution parameters were calculated following Folk and Ward (1957). Grain-size analyses were performed with a 5 mm sampling step between 0 and 430 cm, and then every 2 cm between 430 and 1122 cm.
- Loss-on-ignition (LOI) was measured after 24 h at 105 °C (LOI<sub>105</sub>), after 4 h at 550 °C (LOI<sub>550</sub>) and after 2 h at 950 °C to estimate water content, organic matter content and inorganic carbonate content, respectively (Heiri et al. 2001).
- Bulk mineralogy was analysed by X-ray diffraction (XRD) on a Bruker D8-Advance diffractometer with CuK $\alpha$  radiations. Bulk samples were powdered to 100  $\mu\text{m}$  using an agate mortar. An aliquot was separated and mounted as non-oriented powder by the back-side method (Brindley and Brown 1980). The powder was scanned by XRD between 2° and 45° 2 $\theta$ . The data were analysed in a semi-quantitative way following Cook et al. (1975).
- Clay mineralogy was analysed on the < 2  $\mu\text{m}$  fraction obtained after 50 min of sedimentation (Stokes's settling law). Oriented mounts were constructed by the "glass-slide method" (Moore and Reynolds 1989) and subsequently scanned on the diffractometer. Slides containing crystallized clays after air drying (N) were also scanned after ethylene-glycol solvation during 24 h (EG) and after heating at 500 °C during 4 h (500). Since amorphous clays are abundant in the samples, the crystallized clay content was estimated using the intensity of the most intense clay diffraction peak on the natural (N) diffractogram.
- Major elements were determined by X-ray fluorescence (XRF) on Li-borate glass after loss-on-ignition at 950 °C. Analyses were performed on an ARL 9400. Accuracy is 0.50 %, 3.07 % and 1.69 % for SiO<sub>2</sub>, TiO<sub>2</sub> and Al<sub>2</sub>O<sub>3</sub>, respectively (Bologne and Duchesne 1991). Biogenic silica was deduced by normative calculation (Leinen 1977):

$$\text{SiO}_2 \text{ bio} = \text{SiO}_2 \text{ tot} - x \cdot \text{Al}_2\text{O}_3$$

in which x is the SiO<sub>2</sub>/Al<sub>2</sub>O<sub>3</sub> ratio of terrigenous sediments. When normalizing with Al, it was assumed that all Al derives from detrital material, and that the detrital material has a constant Si/Al ratio. Soils and rocks in the lake catchment represent the main sources of lacustrine detrital particles. Their SiO<sub>2</sub>/Al<sub>2</sub>O<sub>3</sub> ratio was calculated by XRF analyses (mean: 3.5, Bertrand et al. 2005).

Except for grain-size and magnetic susceptibility, all analyses were done on a sample of 1 cm thickness, taken every 10 cm, avoiding samples containing macroscopically visible tephra layers and turbidites. Samples below tephra layers were preferred in order to discard a possible tephra influence on the sediment composition.

### II.1.3. Tephrostratigraphical analysis

The samples containing the 18 thickest tephras were used for tephrostratigraphic analysis. Samples were sieved at 75  $\mu\text{m}$  to remove most of the host sediment. To avoid the presence of coarse grains in smear slides, samples were sieved at 420  $\mu\text{m}$  and only the 75-420  $\mu\text{m}$  fraction was investigated. Bulk samples of the 75-420  $\mu\text{m}$

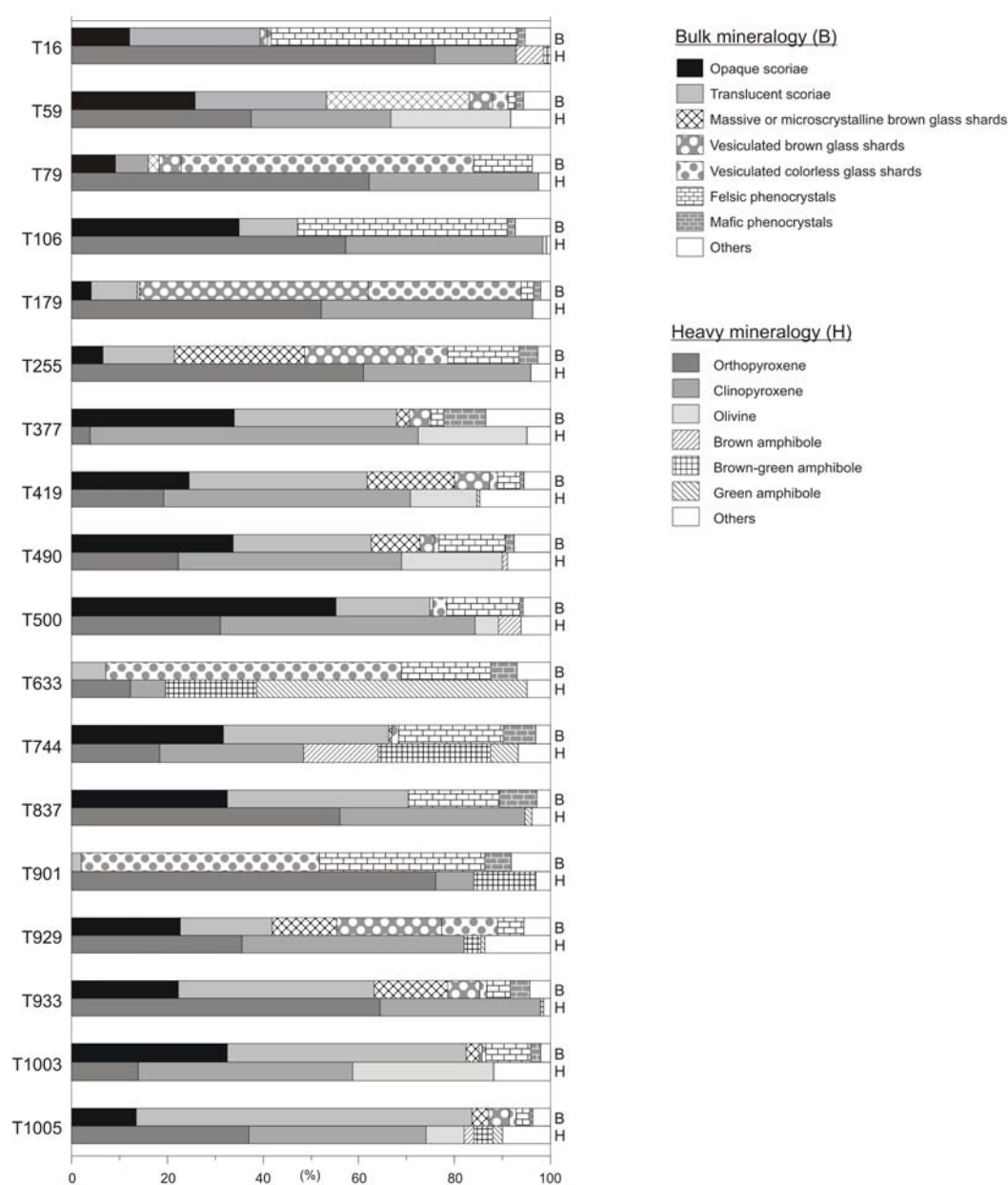


Figure 6: Bulk and heavy mineralogy of the 18 thickest tephra layers in the PU-II long core.

fraction were investigated under a binocular lens in reflected light. In addition, each sample was treated with H<sub>2</sub>O<sub>2</sub>, HCl and 3 HNO<sub>3</sub> + H<sub>2</sub>SO<sub>4</sub> and two smear slides of this cleaned material were mounted for investigation under polarizing microscope: i.e., the bulk sample and a sample of the heavy minerals separated in bromoform (density 2.8) using centrifugation. Between 105 and 176 grains were counted from each smear slide (Fig. 6). Several minerals were identified in the bulk fraction according to their typical characteristics under binocular lens and microscope. High amounts of glass shards were found in eight samples. Their chemical composition (major elements) was determined using an electron microprobe Cameca SX50 at the CAMST (UCL, Louvain-la-Neuve, Belgium). The accelerating voltage was 15 kV and the beam current was 20 nA. Counting times were 20 s for all elements.

#### **II.1.4. Diatom analysis**

Sub-samples of approximately 0.5 cm<sup>3</sup> were taken at intervals of 20 cm. The samples were weighed, dried at 60 °C for 24 h, and weighed again to calculate the water content. Samples for diatom analyses were diluted in distilled water, without oxidation treatment, and were spiked with polystyrene microspheres (concentration:  $4.92 \cdot 10^6$  per liter) to allow for quantitative analysis (Battarbee and Kneen 1982). Frustules were mounted in Naphrax<sup>®</sup> medium. Transects were scanned at a magnification of 10x 100x with a Leitz Diaplan and a Zeiss Axioplan II light microscope. A minimum of 200 valves was counted per sample. Diatoms were identified to generic or specific level, according to Round et al. (1990), Rumrich et al. (2000), Round and Bukhtiyarova (1996) and Frenguelli (1942). The genus *Naviculadicta* was used according to Rumrich et al. (2000). Total diatom biovolume calculations were based on size measurements of all taxa having a mean abundance greater than 1 % in the core. A minimum of 25 valves was measured for each taxon. All measured taxa comprised on average 96 % of the total diatom abundances in the core.

Cluster analysis, constrained by sample depth, was performed on the relative diatom abundances using the programs CONISS (Grimm 1987) and Tilia 2.0b4 (Grimm 1991). Graphs were plotted using Tilia Graph and TG View 1.1.1.1. (Grimm 2001). For grouping samples according to their species composition without any restriction to sample depth, an ordination was done on the relative abundance data of all samples. An initial Detrended Correspondence Analysis (DCA) was applied, in which detrending was by segments, species data were log (x+1) transformed, and downweighting of rare species was applied. The results show that the length of gradient of the first axis was short (1.56 standard deviation units), implying that Principal Components Analysis (PCA) was applied (cf. ter Braak and Prentice 1988). Ordinations were carried out using the program CANOCO 4.5 (ter Braak and Smilauer 1997-2002).

#### **II.1.5. Pollen analysis**

For pollen analysis, ~ 2-6 g of samples were collected at 10 cm intervals from 0 to 300 cm core depth, and at 20 cm intervals from 320 to 1120 cm core depth. All

samples were processed using HF and acetolysis (Erdtman 1960). Tablets with *Lycopodium* spores were added to all samples in order to calculate pollen concentration values (Stockmarr 1971). Samples were filtrated with 12  $\mu\text{m}$  sieve. In each sample, a minimum of 200 pollen grains were counted whenever possible. Pollen of trees, shrubs and herbs (terrestrial pollen) form the pollen sum. Pollen grains from local vegetation (mainly *Cyperaceae*) were excluded from the pollen sum. For pollen identification, we used the pollen morphological studies by Heusser (1971) and Villagrán (1980). Pollen diagrams were drawn using WellPlot 1.0 (Zippi 1996). Zones in the pollen diagrams were selected on the basis of related presence-absence of ecological groups of the main vegetation communities, in order to recognize the main changes in forest development.

### II.1.6. Age-depth model

The age-depth model of PU-II long core is based on 9 AMS radiocarbon dates, obtained on samples of bulk sediment (Poznan Radiocarbon Laboratory, Poland; Czernik and Goslar 2001). Radiocarbon ages were calibrated with BCal using atmospheric data of Stuiver et al. (1998) and the weighted average of each calibrated age was used to construct the age-depth model (Tab. 2). The age obtained at 1,119 cm was rejected because it was stratigraphically inconsistent. This decision was supported by the very low carbon content of this sample (0.4 mg), making the result unreliable.

Depth (cm blf)	Lab #	$^{14}\text{C}$ age $\pm 1\sigma$ (yr BP)	$2\sigma$ error range calibrated ages (OxCal) (cal. yr BP)	Weighted Average (BCal) (cal. yr BP)
120.5	Poz-5922	2570 $\pm$ 35	2490 - 2770 (95.4 %)	2655
156.5	Poz-1406	2590 $\pm$ 40	2490 - 2790 (95.4 %)	2681
306.5	Poz-7660	4110 $\pm$ 40	4510 - 4830 (92.7 %)	4648
400.5	Poz-2201	5300 $\pm$ 40	5940 - 6200 (95.4 %)	6074
463.7	Poz-5923	5760 $\pm$ 40	6440 - 6670 (95.4 %)	6560
627.7	Poz-5925	7450 $\pm$ 50	8160 - 8390 (93.9 %)	8262
762.0	Poz-1405	10010 $\pm$ 60	11,200 – 11,750 (91.0 %)	11,494
908.0	Poz-7661	11440 $\pm$ 80	13,100 – 13,850 (95.4 %)	13,407
1,012.0	Poz-2215	13410 $\pm$ 100	15,250 – 16,750 (95.4 %)	16,063
1,119.0	Poz-7662	12880 $\pm$ 90	14,350 – 15,950 (95.4 %)	15,355

Table 2: AMS radiocarbon dates on samples of bulk sediment of the PU-II long core. The range of calendar ages is calculated with OxCal v3.9 (Bronk Ramsey 2001). The weighted average is calculated with BCal and used for age-depth modelling.

In addition, two tephra layers dated by varve-counting were used as chronostratigraphic markers. These tephras originate from historical eruptions of the Puyehue – Cordon de Caulle Volcano (1921-1922) and the Osorno Volcano (1575).

The upper part of the age-depth model was further calibrated with the aid of sedimentation rates derived from  $^{210}\text{Pb}$ ,  $^{137}\text{Cs}$  and  $^{241}\text{Am}$  analyses conducted on short cores from the PU-II site (Arnaud et al. 2006).

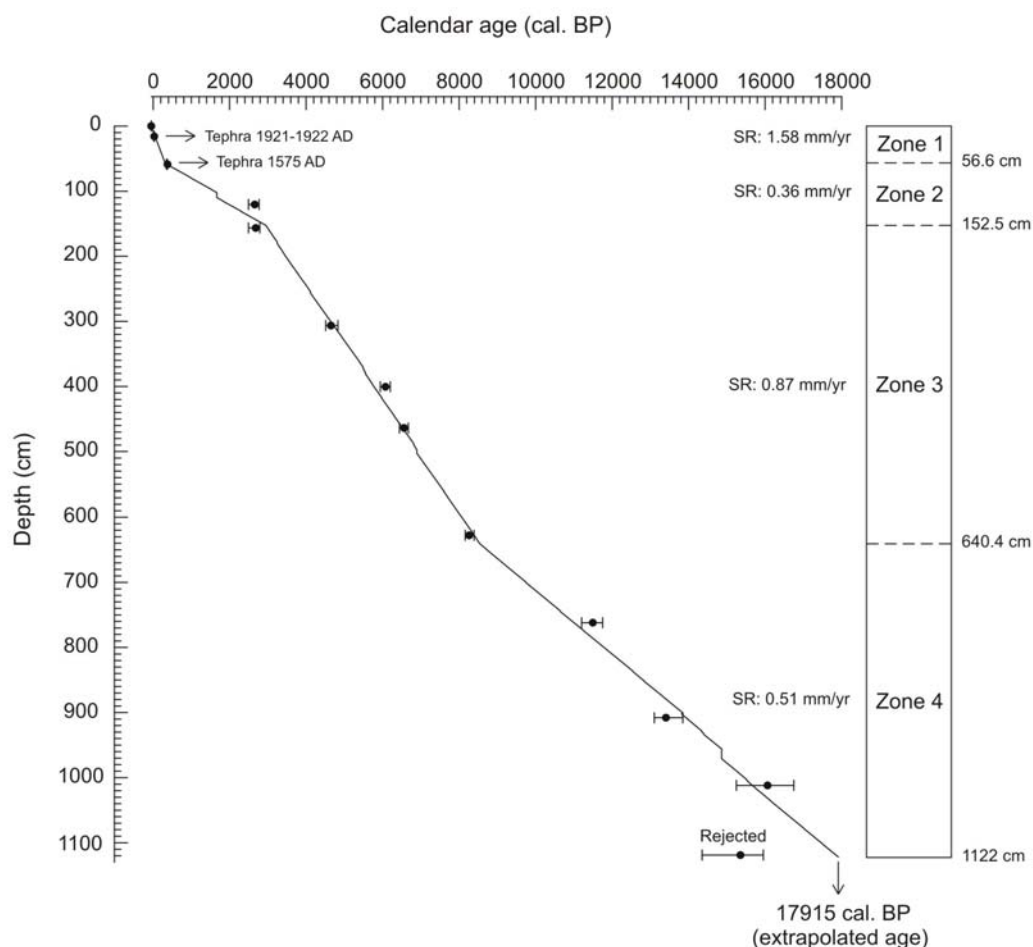


Figure 7: Age-depth model of the PU-II long core based on 4 linear regressions. Mean weighted average calibrated ages were used. Error bars represent the range of calibrated radiocarbon ages (see Tab. 1).

The 78 tephra layers and the 3 turbidites were considered as instantaneous deposits and this was taken into account when constructing the age-depth model (Fig. 7). No continuous age-depth model was able to fully reproduce the  $^{14}\text{C}$  distribution (cubic splines and polynomial with up to 8 terms were tested). We thus use a discontinuous age-depth model assuming constant sedimentation rates in 4 domains for which linear regressions on the  $^{14}\text{C}$  ages were calculated. The resulting temporal sampling resolution (10 cm) varies between 63 and 278 yr with a mean of 162 yrs.

## II.2. Results

### II.2.1. Seismic stratigraphy

The sparker seismic data from the western sub-basin of Lago Puyehue reveal a sedimentary infill composed of 5 seismic-stratigraphic units, each with its own

characteristic seismic facies (Fig. 8). The succession of these seismic facies throughout the infill reflects the evolution of the sedimentary processes in the lake basin through time. A more or less similar 5-fold seismic stratigraphy has been observed in many other glacial lake basins, and this has led to the definition of a "type stratigraphy" for glacial lakes (Van Rensbergen et al. 1998).

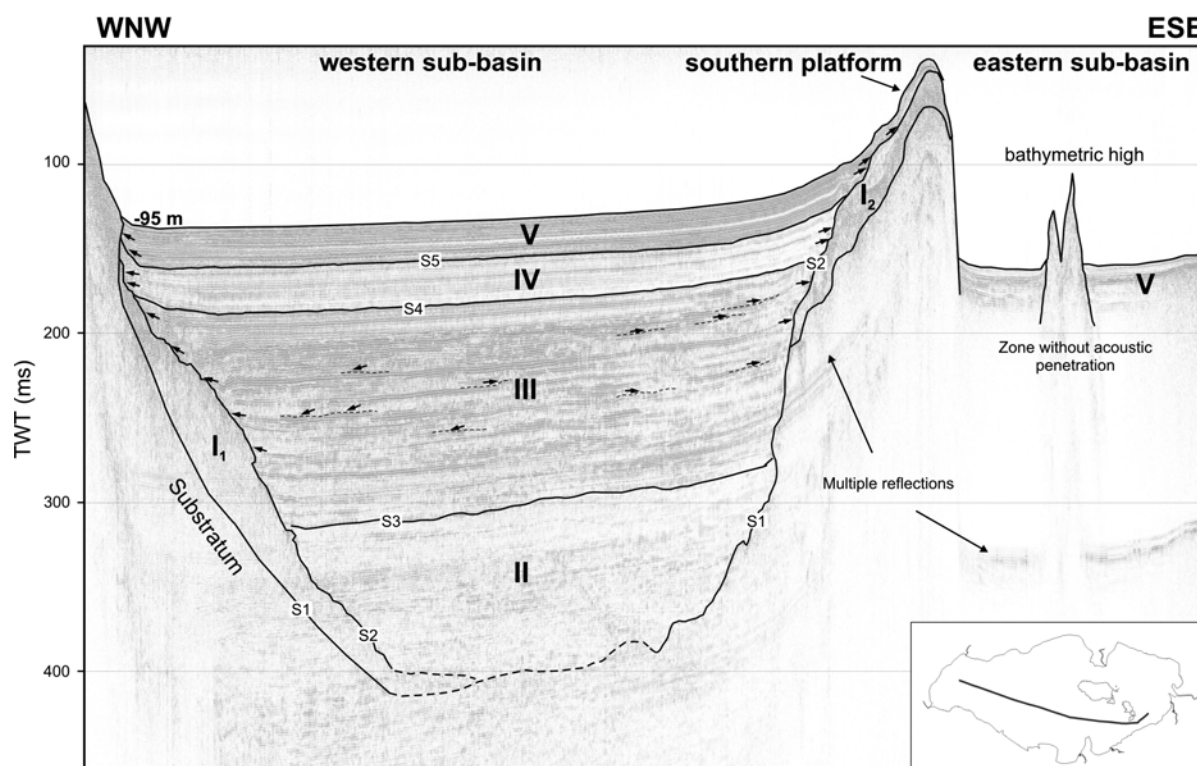


Figure 8: Sparker seismic profile across the western sub-basin, the southern platform and part of the eastern sub-basin (see inset for location), with indication of substratum and seismic-stratigraphic units (Unit I to Unit V). Arrows in Units III, IV and V indicate onlapping and downlapping reflection terminations

Lago Puyehue's seismic stratigraphy consists of the following units:

- **Unit I:** an assemblage of chaotic to irregularly stratified seismic facies units with irregular external form that overly the substratum (e.g., I<sub>1</sub> and I<sub>2</sub>), and that occur in the lake basin immediately adjacent to where moraine belts and outwash sediments have been identified and mapped onshore. This unit is interpreted to represent morainic, ice-contact or outwash deposits, associated to sub-aqueous meltwater discharge in a sub- or proglacial lake or even to sub-aerial accumulation.
- **Unit II:** a thick, mostly reflection-free, basin-fill unit that ponds the central deep of the basin. This unit is interpreted as comprising glacio-lacustrine sediments that have been deposited very rapidly in a proglacial or subglacial lake at the onset of the deglaciation of the basin.
- **Unit III:** a stratified, ponded basin fill, with parallel, continuous, high- to medium-amplitude reflections onlapping towards the basin margins. This unit is interpreted to represent lacustrine fan deposits that were fed by sediment-laden meltwater

streams (i.e. underflows) in a proglacial (i.e., ice-contact) lake. The highly dynamic character of this depositional environment is reflected in the strong lateral variability in reflection characteristics (i.e. amplitude, continuity) and in the presence of abundant internal erosional truncations and of small-scale onlap and downlap terminations. The upward decrease in abundance of these erosive surfaces suggests that depositional energy has gradually subsided during accumulation of Unit III. The sometimes very high reflection amplitudes in this unit indicate that these meltwater-generated underflow pulses may have delivered coarse-grained, sandy sediments to the central parts of the basin. This facies could be genetically related to the massive glacio-fluvial outwash terraces that have been described onshore in between the moraine belts (Bentley 1996, 1997). As field data suggest that the glaciers retreated rapidly from the Andes in the Chilean Lake District at the end of the LGM (Lowell et al. 1995, McCulloch et al. 2000), the associated meltwater streams probably did not persist for a long time. Therefore, Unit III was probably deposited in a relatively short period of time, despite its considerable thickness.

- Unit IV: a mostly parallel-stratified basin fill with continuous, low- to medium-amplitude reflections. This unit is interpreted as composed of fluvially derived sediment deposited in an open, post-glacial (i.e., non-ice-contact) lake. The inflowing rivers carried much less sediment than the meltwater streams of Unit III and underflow activity was consequently much reduced, except during seasonal or exceptional floods, which could explain the presence of sporadic higher-amplitude reflections in Unit IV and the slight basinward-thickening of the unit in the western sub-basin. Most of the main inflowing rivers enter the lake either at its northern, eastern and southeastern margins. Consequently, the more proximal, prograding fan delta deposits of Unit IV are probably restricted to those areas, while the western sub-basin and the southern platform receive only the finer, more distal fraction.
- Unit V: a basin fill with concordant, low-amplitude, continuous reflections. Unit V has a draping geometry on the southern platform, but a slightly marginward-thinning and onlapping geometry in the deeper western sub-basin. The lithology of core PU-II confirms that the sediments of Unit V on the southern platform have indeed accumulated mainly by suspension settling of fine-grained, silt-sized particles of predominantly biogenic origin. They do, however, still contain a terrigenous component and it is likely that this component is more important in the deep western sub-basin towards where it can be transported by sporadic flood-generated underflows. This could also explain the anomalously high reflection amplitudes of this open-lake deposit. Nevertheless, the sub-bottom profiler data illustrate that the Unit V strata in the western sub-basin are only slightly thicker than those on the southern platform, confirming that the main component in both environments is indeed suspension settling of fine-grained sediment.

### ***II.2.2. Sedimentological, mineralogical and geochemical variations***

Figs. 9 and 10 demonstrate that clear relationships exist between independent proxies.  $\text{Al}_2\text{O}_3$ ,  $\text{TiO}_2$  and MS show a striking behaviour. On the other hand,  $\text{LOI}_{105}$ ,

LOI<sub>550</sub>, grain-size and SiO<sub>2 bio</sub> seem to co-vary. Principal component analysis (PCA) performed on these data has demonstrated the occurrence of 2 data groups. The first association is made of Al<sub>2</sub>O<sub>3</sub>, TiO<sub>2</sub> and MS. The second group is made of LOI<sub>105</sub>, LOI<sub>550</sub>, mean grain-size and biogenic silica. These two data groups are strongly anti-correlated arguing for a two end-members system, made of i) terrigenous and ii) biogenic particles.

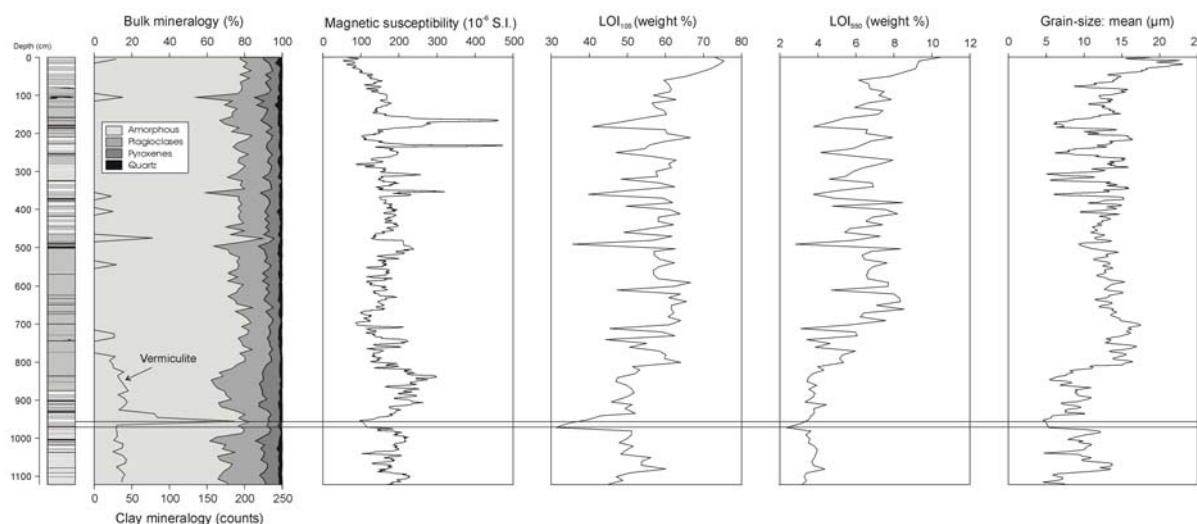


Figure 9: Bulk mineralogy, magnetic susceptibility (MS), water content (LOI<sub>105</sub>), organic matter content (LOI<sub>550</sub>) and grain size of the PU-II long core.

- **Terrigenous particles:** Al<sub>2</sub>O<sub>3</sub> and TiO<sub>2</sub> are positively correlated ( $r = 0.68$ ) and used as markers of the terrigenous fraction of the sediment. These elements mainly originate from regional andosols by river discharge. The relatively high mean MS values reflect the volcanic setting, responsible of a high percentage of magnetic minerals in the sediment. Because magnetic minerals are contained in the terrigenous fraction of the sediment, the MS signal clearly reflects the detrital supply, as proved by its positive correlation with Al<sub>2</sub>O<sub>3</sub> ( $r = 0.53$ ) and TiO<sub>2</sub> ( $r = 0.37$ ). *Down-core variations of the MS signal can thus be used to infer variations in the terrigenous supply.* These are mainly linked to precipitation, but, in the highly active volcanic context of the area, the rejuvenation of the erodable sedimentary stock by volcanic eruptions may also influence the terrigenous supply.
- **Biogenic particles:** Biogenic silica and LOI<sub>550</sub> represent the siliceous organisms and organic matter preserved in the sediment, respectively. Biogenic silica is mainly determined by the amount of diatoms, and in particular of *Aulacoseira*, while e.g. sponge spicules and phytoliths are rare. Organic matter mainly originates from in-lake productivity, as demonstrated by Bertrand et al. (2005). These two parameters are positively correlated ( $r = 0.62$ ) and are assumed to represent the overall lake paleoproductivity. PCA analysis and correlation coefficients demonstrate that LOI<sub>105</sub> and grain-size data are positively correlated with these parameters. LOI<sub>105</sub> variations are closely linked to lithological changes, i.e. diatoms and organic matter content, because their ability to retain water

compared to the terrigenous sediment. Variations of  $LOI_{105}$  are thus related to changes in the biogenic content of the sediment. Similarly, a close relation between grain-size and biogenic silica ( $r = 0.71$ ) and  $LOI_{550}$  ( $r = 0.67$ ) is observed. The coarser the sediment, the higher the biogenic content is. This relation is due to the coarse size of diatoms and organic matter. Indeed, the bulk grain-size distribution can be decomposed in two fractions: the fine terrigenous sediments and the coarse biogenic fraction, mainly made of diatoms, but also vegetal tissue remains. This result is comforted by the size of diatoms (20-60  $\mu\text{m}$ ) observed in smear slides. *A coarse grain-size thus reflects a high biogenic content and can be interpreted as a high lake paleoproductivity.*

Because MS and grain-size data were measured at high resolution, these signals can be used for tracing relative changes in terrigenous and biogenic components.

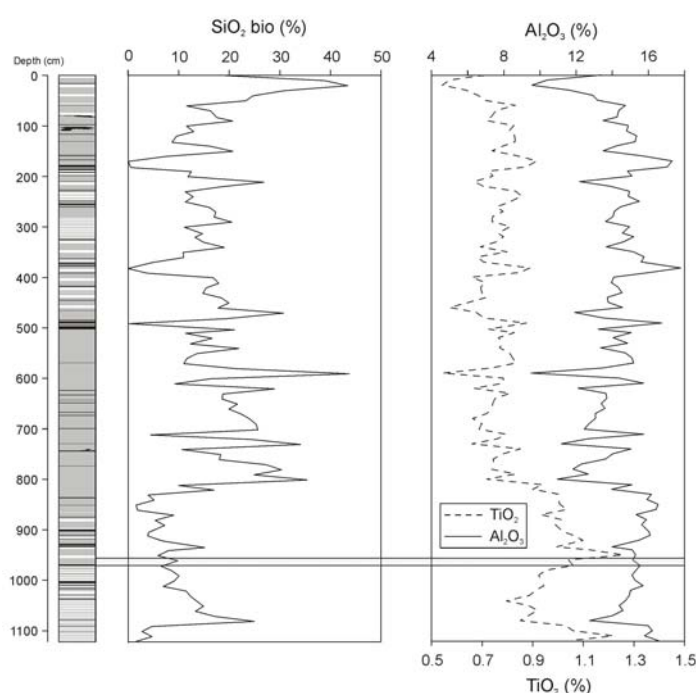


Figure 10: Biogenic silica, and geochemistry of the PU-II long core.

In order to discuss the variations of each sediment component independently, mass accumulation rates (MARs) were calculated. The sediment was assumed to be composed of 3 main types of particles: i) terrigenous particles, ii) biogenic silica and iii) organic matter and MARs were calculated for each group. Because MAR calculation is biased by the age-depth model shape, MARs were only calculated between 18,000 and 9,000 cal. yr BP., where the age-depth model is linear. High detrital terrigenous supply is interpreted as reflecting a stronger erosion in the catchment, linked to increased precipitation. Paleoproductivity variations are interpreted as due to changes in temperature and/or nutrient supply. The choice between both can be deduced from the parallelism with the detrital supply results (assuming that nutrients are primarily introduced from the catchment). The temporal distribution of sediment composition and supply (MARs), mean grain-size and

magnetic susceptibility reveals 7 periods (zones A to G), reflecting changes in productivity and rate of detrital supply during the last 18,000 yrs (Fig. 11):

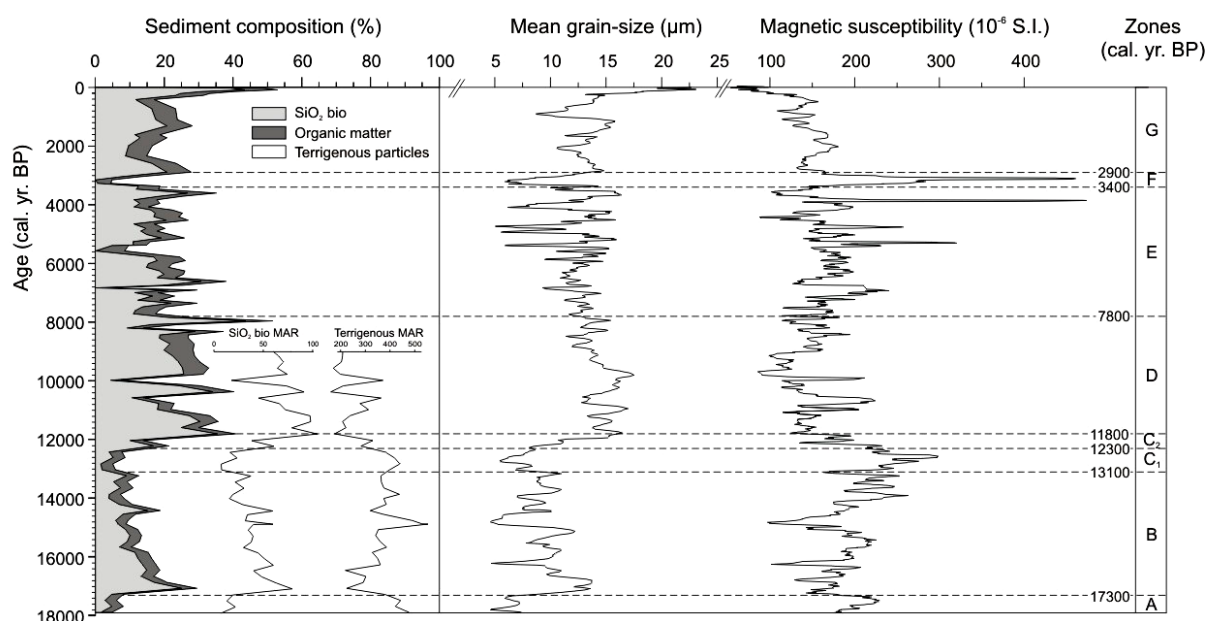


Figure 11: Sediment composition changes as a function of time, and delimitation of 7 main periods (zones A-G).

- Before 17,300 cal. yr BP (zone A): the sediment is mainly composed of terrigenous particles (90 %) and is characterized by a very low MAR of SiO<sub>2</sub> bio, indicating a very low lake paleoproductivity. This period is interpreted as cold and humid. The end of this period is marked by an abrupt increase in lake paleoproductivity at 17,300 cal. yr BP, interpreted as the result of a warming pulse, enhancing lake plankton development and probably marking the end of the last glacial. The decrease of the terrigenous supply at 17,300 cal. yr BP probably reflects also a slightly drying climate.
- 17,300 to 13,100 cal. yr BP (zone B): this abrupt climate change at 17,300 cal. yr BP is followed by a progressive cooling until 13,100 cal. yr BP, as can be deduced from the decreasing content in biogenic particles and in grain-size data. The terrigenous supply starts to increase at 15,000 cal. yr BP., reflecting a strengthening of precipitation. This increase last until ca. 12,500 cal. yr BP.
- 13,100 to 11,800 cal. yr BP (zone C): the most outstanding feature of low paleoproductivity occurs in the zone C<sub>1</sub>, between 13,100 and 12,300 cal. yr BP, delimitating one of the coolest periods between the Late Glacial Maximum (LGM) and present. All proxies agree for a cold climate. The end of this period is marked by a gradual warming between 12,300 and 11,800 cal. yr BP (zone C<sub>2</sub>). Before 13,300 cal. yr BP (zones A and B), the MAR of terrigenous particles remains generally high, reflecting significant precipitation in the watershed and/or low vegetation cover enhancing sediment availability. Terrigenous MARs decrease during the zone C<sub>2</sub>, in conjunction with an increase in the MAR of SiO<sub>2</sub> bio. This reflects a warming and drying climate at the beginning of the Holocene.

- 11,800 and 7,800 cal. yr BP (zone D): paleoproductivity reaches its maximum and terrigenous MARs are low, reflecting high temperatures and low precipitation in the Early Holocene. Higher concentrations of organic matter are recorded since ~ 10,000 cal. yr BP, probably in relation to the development of vegetation in the watershed.
- After 7,800 cal. yr BP (zones E-G): paleoproductivity slightly decreases, but remains rather high until the second part of the last millennium (zones E to G). Two exceptions to this general trend are i) the high variability of paleoproductivity between 6,000 and 3,500 cal. yr BP and ii) a cold and/or humid event between 3,400 and 2,900 cal. yr BP. Both its onset and end are abrupt.

### **II.2.3. Diatom stratigraphy**

Diatom analysis allowed distinguishing three main biostratigraphical zones (Puyehue Diatom Zones; PDZ): PDZ 1 to 3 (Fig. 12). These three groups, as defined by the cluster analysis, were clearly separated from each other on a PCA biplot, indicating that diatom composition changed over time without reversal to previous compositions.

In general, large eutrophic species (PDZ 1) were followed by high abundances of epiphytic taxa (PDZ 2), and finally by more oligotrophic indicator species (PDZ 3). The CONISS sub-divisions of each diatom zone are described below:

- 17,900 to 9,550 cal. yr BP (PDZ 1): this period is characterized by a high mean abundance of *Aulacoseira* cf. *granulata*. *Aulacoseira* is a planktonic genus (Round et al. 1990), although some species, such as *A. granulata* and *A. distans*, are often also mentioned as being tycho planktonic (e.g. Jenny et al. 2002). *A. granulata* favours well-mixed waters, with a high Si/P ratio (Cox 1996; Blinn et al. 1994; Kilham et al. 1986). Both PDZ 1 and PDZ 2 contain relatively high abundances of tycho planktonic (i.e. *Nitzschia* and *Staurosira*) (Round et al. 1990; Patrick and Reimer 1966) and planktonic taxa that thrive well in nutrient enriched, turbid waters (e.g. *Cyclostephanos*) (Håkansson 2002; Cholnoky 1968).

PDZ 1 can be further divided into three sub-zones and starts with a remarkable peak in both total and relative diatom abundances (PDZ 1a, 17,900 to 16,850 cal. yr BP). The two samples in this zone are primarily characterized by low percentages of *Nitzschia* and *Staurosira*. Both *Cyclostephanos* and *Cyclotella* sp. 1 are relatively abundant, and some epiphytic taxa, characterizing zones PDZ 1c and PDZ 2, also appear in this zone. Absolute diatom abundances rise. This is accompanied by a decline in *Cyclotella stelligera* and a rise in *Aulacoseira* cf. *granulata*. As the volume of *A. cf. granulata* is about 178 times larger than that of *C. stelligera*, the former species is more likely to drive total diatom biovolume.

PDZ 1b (16,850 to 12,810 cal. yr BP) is less variable in taxonomic composition. This zone contains slightly lower percentages of *Aulacoseira* cf. *granulata* and higher percentages of *Cyclotella stelligera*. Increased but more variable abundances of *Nitzschia* and *Staurosira* are observed in this zone. Sub-dominant taxa are *Cyclostephanos*, *Cyclotella* sp. 1 and *Fragilaria*. Diatom biovolume and total abundance are low through this zone.

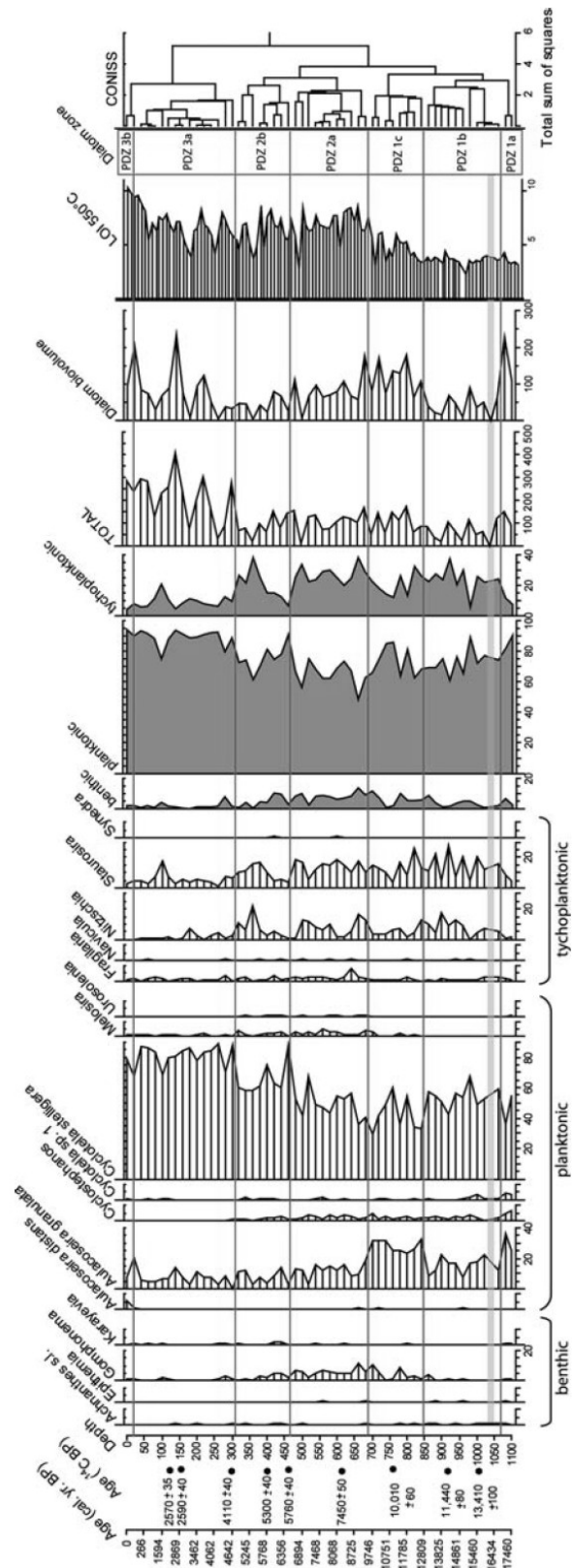


Figure 12: Diatom stratigraphy and CONISS cluster analysis. Relative abundances of taxa with an average relative abundance of more than 0.5 % are shown. The relative abundances of all benthic, planktonic and tychoplanktonic taxa together are given, as well as the total diatom concentration and calculated diatom biovolumes. LOI<sub>550</sub> is plotted as % of dry weight. The grey shading between 956 and 971 cm depth represents a turbidite layer.

PDZ 1c (12,810 to 9,550 cal. yr BP) is marked by the appearance of the epiphytic taxa *Gomphonema* and *Melosira*. Total diatom abundances rise. This is largely due to an increase in *Aulacoseira* cf. *granulata*, resulting in an even stronger increase in diatom biovolume.

- 9,550 to 4,760 cal. yr BP (PDZ 2): is generally characterized by increased numbers of epiphytic taxa (*Gomphonema*, *Melosira*, *Naviculadicta* and *Fragilaria*), and mesotrophic genera, such as *Synedra* and *Urosolenia* (Diaz et al. 1998). The benthic/epiphytic taxa account for 6.4 % of the diatoms in PDZ 2, instead of 1.7 % in PDZ 3, and 4.3 % in PDZ 1. *Cyclostephanos*, a planktonic genus favouring higher nutrient concentrations is present in the same relative amounts as in PDZ 1, as well as *Cyclotella* sp. 1. A gradual increase of the relative abundance of *C. stelligera* is observed in PDZ 2, coinciding with declines in relative abundances of *Nitzschia* and *Staurosira*.

Zone PDZ 2 can be further divided into two sub-zones, which are characterized by decreasing *Aulacoseira* cf. *granulata* abundances of 12.4 % for PDZ 2a (9,550 to 6,600 cal. yr BP) and 7.8 % for PDZ 2b (6,600 to 4,760 cal. yr BP). In PDZ 2b total diatom abundances decline towards  $94 \cdot 10^3$  valves per g dry weight.

- After 4,760 cal. yr BP (PDZ 3): the diatom communities in PDZ 3 are very distinct from those in PDZ 1 and PDZ 2, and show a lower variability in taxonomic composition (Fig. 12). Zone PDZ 3 is characterized by very high abundances of *Cyclotella stelligera* and by the absence of *Cyclostephanos* and *Cyclotella* sp. 1.

The upper diatom zone can be further divided into two sub-zones due to a last shift in diatom taxonomic composition near 30 cm core depth. The relative abundances of *Aulacoseira* cf. *granulata*, *Nitzschia* and *Staurosira* are low. Epiphytic diatoms, as well as *Synedra* and *Urosolenia* are rare. Absolute diatom abundances rise in this zone from  $166 \cdot 10^3$  towards  $2,316 \cdot 10^3$  valves per g dry weight. This increase is observed in most diatom taxa, including *A. cf. granulata* and most epiphytic taxa, and is most pronounced in *C. stelligera*. Likewise, total diatom biovolume increases to a maximum (Fig. 12), as it is mostly driven by *A. cf. granulata*.

Zone PDZ 3b (500 cal. yr BP – present) only contains two samples, of which the sample at 20 cm core depth contained an increased percentage of *Aulacoseira* cf. *granulata*. Both samples were devoid of *Nitzschia*, and contained low amounts of *Staurosira*. A remarkable maximum of *A. distans* (6.1 % or  $88 \cdot 10^3$  valves per g dry weight) occurred at 0.5 cm depth.

#### **II.2.4. Pollen stratigraphy**

The results of the pollen analysis are shown in Fig. 13. Five main pollen zones were identified (PU-II-1 to PU-II-5):

- 17,400 to 11,600 cal. yr BP (Zone PU-II-1): this zone is characterized by the marked dominance of *Nothofagus dombeyi*-type and sub-divided into three sub-zones (PU-II-1a to PU-II-1c).

Relatively low carbon content and pollen concentration values in sub-zone PU-II-1a (17,400 to 15,500 cal. yr BP) indicate low production of biomass, suggesting open vegetation was common around the lake. The high representation of

*Poaceae* and ferns spores confirms this interpretation. Regionally, the forest was mainly composed of *Nothofagus dombeyi*, and *Myrtaceae*, indicating the presence of Valdivian rainforest and thus low temperatures and humid climatic conditions.

The pollen concentration shows a slight increase in sub-zone PU-II-1b (15,500 to 14,000 cal. yr BP), suggesting a more dense vegetation cover. Considering also the sedimentological evidence, it is inferred that precipitation became less seasonal and sediments accumulated in a low energy environment. Regionally, the abundant presence of *Nothofagus dombeyi* and *Nothofagus obliqua*, and the decreasing presence of *Myrtaceae* indicates the presence of abundant Valdivian rainforest, and lowland deciduous forest. This indicates that temperate and semi-humid climatic conditions prevailed during this period.

The regional presence of *Nothofagus dombeyi*, *Nothofagus obliqua*, and characteristic shrubs of mid and high-altitudes suggests the proximity of Valdivian rainforest and lowland deciduous forest during this period (sub-zone PU-II-1c, 14,000 to 11,600 cal. yr BP). The representation of *Poaceae* and shrub reflects the presence of open vegetation at higher elevation, indicative for cooler and semi-humid climatic conditions.

- 11,600 to 8,000 cal. yr BP (Zone PU-II-2): this zone is characterized by a replacement of *Nothofagus dombeyi*-type by *Nothofagus obliqua*-type and other thermophilous taxa, such as *Caldcluvia/Eucryphia* and *Aextoxicon punctatum*. An increased carbon content and pollen concentration is indicative of a greater plant cover in the basin, and a low sediment supply. A significant contribution of *Nothofagus dombeyi* and *Nothofagus obliqua*, and a more diverse pollen spectra indicate Valdivian rainforest, lowland deciduous forest, and North-Patagonian rainforest was present. More abundant thermophilous taxa, characteristic of the lowland deciduous forest, suggest higher temperatures. The signal of *Poaceae* may reflect the understorey of dry forest, in which other xerophytic taxa, such as *Chenopodiaceae*, also grew. These observations point to warm and semi-arid climatic conditions during this period.
- 8,000 to 6,800 cal. yr BP (Zone PU-II-3): this zone is characterized by a further increase in *Nothofagus dombeyi*-type. This zone differs from the previous one by a slight increase of *Pilgerodendron/Fitzroya* and a representation of *Nothofagus obliqua*-type between 13 % and 23 %. Maximum pollen concentration values suggest a maximum in biomass production during stable environmental conditions. The abundant presence of *Nothofagus dombeyi* and *Nothofagus obliqua* and the diverse pollen spectra point to the presence of thermophilous forest: Valdivian rainforest, lowland deciduous forest, and North-Patagonian rainforest. *Poaceae* and ferns reflect open vegetation, either in the understorey of relatively dry forest and/or at higher elevation above the upper forest line. This suggests that temperate and semi-humid climatic conditions prevailed during this period.
- 6,800 to 520 cal. yr BP (Zone PU-II-4): this zone is characterized by the increasing representation of *Pilgerodendron/Fitzroya*, and is sub-divided into two sub-zones (PU-II-4a and PU-II-4b).



Abundant pollen of *Nothofagus dombeyi* and *Nothofagus obliqua* in sub-zone PU-II-4a (6,800 to 5,300 cal. yr BP) indicate the presence of diverse thermophilous forest. *Nothofagus dombeyi* is gradually replaced by *Pilgerodendron/Fitzroya*, suggesting that Valdivian rainforest was replaced by North-Patagonian rainforest: decreasing temperatures and higher climatic humidity may be inferred from this. *Poaceae* and ferns reflect open vegetation, either in the understorey of dry forest and/or at higher elevation above the upper forest line. This may indicate temperate and humid climatic conditions.

Sedimentological parameters indicate that in sub-zone PU-II-4b (5,300 to 520 cal. yr BP) stable conditions in the basin were interrupted several times by the input of coarse material and volcanic ash reflecting ash-fall events and/or short periods of abundant precipitation with subsequent ash transport. Pollen of *Pilgerodendron/Fitzroya* and *Nothofagus dombeyi* indicate the presence of North-Patagonian rainforest, and the pollen of *Nothofagus obliqua* show the presence of lowland deciduous forest. These observations point to a continuous presence of diverse thermophilous forest, but with cool North Patagonian rainforest close to the lake. *Poaceae* and ferns reflect open vegetation, either in the understorey of dry forest and/or at higher elevations above the upper forest line. Temperate and semi-humid climatic conditions characterized this period.

- After 520 cal. yr BP (Zone PU-II-4): Sedimentological parameters and increasing values of the pollen concentration and carbon content suggest the vegetation and biomass production increased, while the supply of sediments was reduced. Abundant pollen of *Pilgerodendron/Fitzroya* and *Nothofagus dombeyi* show the presence of North-Patagonian rainforest. Lower pollen representation of *Nothofagus obliqua* suggests lowland deciduous forest decreased, indicating cooler temperatures. *Poaceae* and ferns reflect open vegetation, either as patches in the forest and/or at higher elevation above the upper forest line. During the last part of this period, the high representation of grassy vegetation reflects human-induced deforestation; in addition, the sudden increase of shrub may point to human impact. Cool to cold and humid climatic conditions are inferred for the last five centuries.

## II.3. Discussion

### II.3.1. Timing of glacier retreat from Lago Puyehue ?

The PU-II long core penetrates the upper  $\frac{3}{4}$  of seismic-stratigraphic Unit V on the southern platform (Fig. 14). The base of the core is dated as 17,915 cal. yr BP.

According to the sedimentological and geochemical analyses and to the diatom content, Lago Puyehue was an open lake that was not in contact with glacier ice and that was disconnected from direct glacier meltwater input for the entire time interval covered by the core. This is also supported by the interpretation of the seismic facies of seismic-stratigraphic Unit V as resulting from open-lake suspension settling. But, as the core only penetrates the upper  $\frac{3}{4}$  of Unit V on the southern platform and as the seismic facies of Unit V does not significantly change in its basal part (Fig. 13),

the same open-lake conditions must have existed from the beginning of the deposition of Unit V. Extrapolating sedimentation rates from the base of the core yields an estimated age of ca. 24,750 cal. yr BP for the base of Unit V. Moreover, Unit IV's seismic facies indicates that it also accumulated in open-water conditions, and probably even unit III was deposited when most of the lake was ice free, i.e. when it was a proglacial or ice-contact lake. By extrapolating the sedimentation rate of Unit V, the age of the base of Unit IV on the southern platform –or of the onset of open-water conditions in Lago Puyehue– can be estimated as ca. 28,000 cal. yr BP, and the base of Unit III as several thousands of years older. These are maximum estimates as sedimentation rates were probably higher during deposition of Unit IV and significantly higher during deposition of Unit III than during deposition of Unit V.

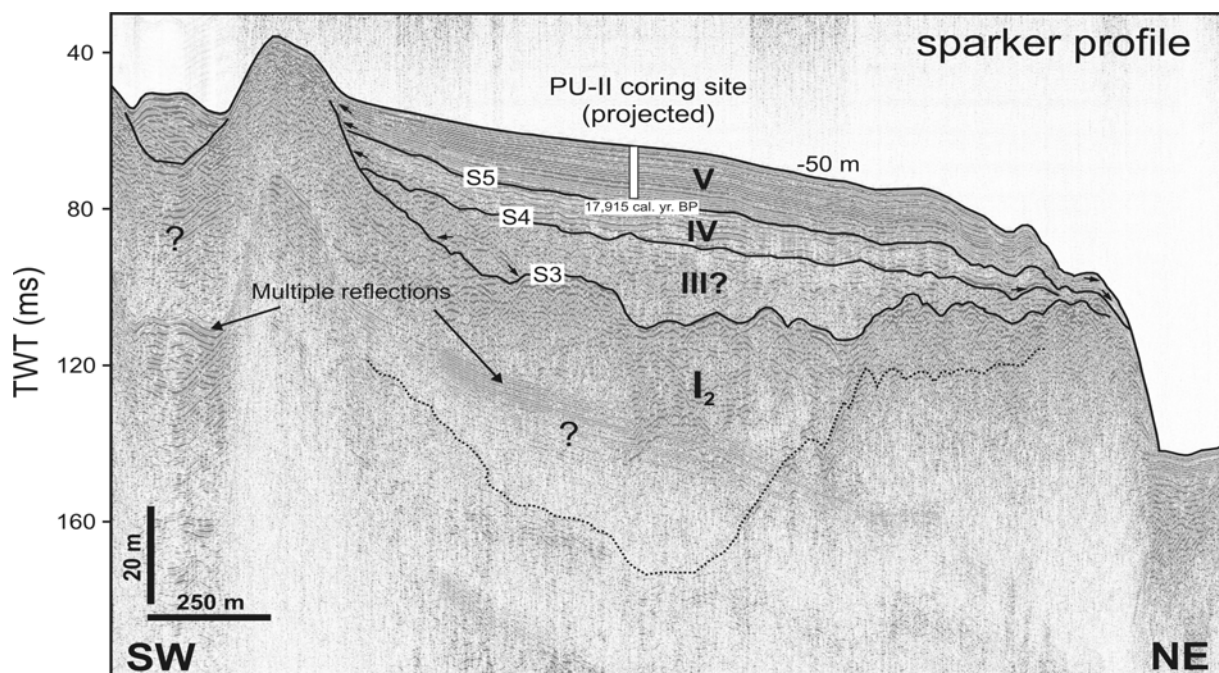


Figure 14: Seismic profile across (or very close to) the PU-II coring site on the southern platform, with indication of seismic-stratigraphic units.

The deglacial history of the Chilean Lake District has been intensively studied during the past decades, a.o. by Mercer (1972; 1976), Porter (1981), Laugenie (1982), Lowell et al. (1995) and Denton et al. (1999). Bentley (1997) focussed in particular on Lago Puyehue and neighbouring Lago Rupanco and reconstructed glacier fluctuations using geomorphological and stratigraphic analysis and detailed radiocarbon dating of moraine ridges and outwash deposits. According to this onshore evidence, deglaciation of the Lago Puyehue basin was only complete by ca. 14,600 cal. yr BP. This age is largely consistent with ages derived for other lake basins in the area (e.g. Lowell et al. 1995). Our derived age of 28,000 cal. yr BP for the onset of open-water conditions in Lago Puyehue is difficult to reconcile with the consensus view of the deglacial history of the region. We are confident about our age model because it is based on a combination of multiple dating methods (AMS  $^{14}\text{C}$ ,  $^{210}\text{Pb}$  and  $^{137}\text{Cs}$ , varve counting) yielding consistent age values and sedimentation

rates. Furthermore, paleoclimate trends that have been derived from the core (see below) and that were dated using our age-depth model, produce results that are consistent with other paleoclimate records from the area (e.g. Ariztegui et al. 1997; Moreno 1997; Moreno 2000; Moreno et al. 2001; Hajdas et al. 2003).

### ***II.3.2. Long term climate evolution***

The sedimentological and geochemical parameters, the pollen stratigraphy and the diatom stratigraphy of the PU-II long core provide a combined record of the long-term trends in the evolution of precipitation and temperature in the area of Lago Puyehue (Fig. 15).

The sedimentological and geochemical data evidence a number of climate fluctuations and shifts that are superimposed on a gradual and continuous climate improvement since the LGM (Fig. 15). A first abrupt warming and reduction in precipitation is inferred to have occurred at 17,300 cal. yr BP. This is largely in agreement with other records from the region (e.g., Moreno et al. 1999, Lamy et al. 2004) that report a distinct warming pulse sometime between 19,500 and 17,150 cal. yr BP, which ended the full glacial conditions in the area. This climate shift was followed by a gradual cooling starting at about 16,000 cal. yr BP and culminating in a well-marked cold and humid interval at 13,100-12,300 cal. yr BP. The timing of this cold and humid interval is roughly similar to that of the Huelmo/Mascardi Cold Reversal (Hajdas et al. 2003) that was identified in the Huelmo Mire (41.5°S, Chile) and in Lago Mascardi (41°S, Argentina), both located at nearly the same latitude as Lago Puyehue. This cold spell ended rapidly with a shift towards warmer and dryer conditions between 12,300 and 11,800 cal. yr BP, marking the onset of the Holocene. The period between 11,800 and 7,800 cal. yr BP was characterized by warm and dry climate conditions, corroborating earlier indications for the existence of an early Holocene climatic optimum in the Southern Hemisphere (e.g. Moreno 2004; Masson et al. 2000; Williams et al. 2003; Ciais et al. 1992). After 7,800 cal. yr BP, the climate did not vary significantly, except for a period between 6,000 and 3,500 cal. yr BP, characterized by unstable and variable conditions, and for an interval of cold and/or humid conditions at 3,400-2,900 cal. yr BP.

The pollen stratigraphy only starts at 17,400 cal. yr BP and has therefore probably not recorded the warming and drying event at 17,300 cal. yr BP that was inferred from the sedimentological data. Instead, it shows that climate was still relatively cold and humid until 15,500 cal. yr BP. This was followed by more temperate climate conditions between 15,500 and 14,000 cal. yr BP, as indicated by pollen assemblages highlighting the arrival of deciduous forest. The period between 14,000 and 11,600 cal. yr BP was marked by a return to cold conditions. This was followed by warm and dry conditions between 11,600 and 8,000 cal. yr BP, roughly in agreement with the warm and dry period between 11,800 and 7,800 cal. yr BP inferred from the sedimentological data, and reconfirming the existence of an early Holocene climate optimum in the area. This warm period was followed by temperate,

humid to semi-humid conditions until ca. 500 yrs ago, after which the present-day cool, humid climate conditions took over.

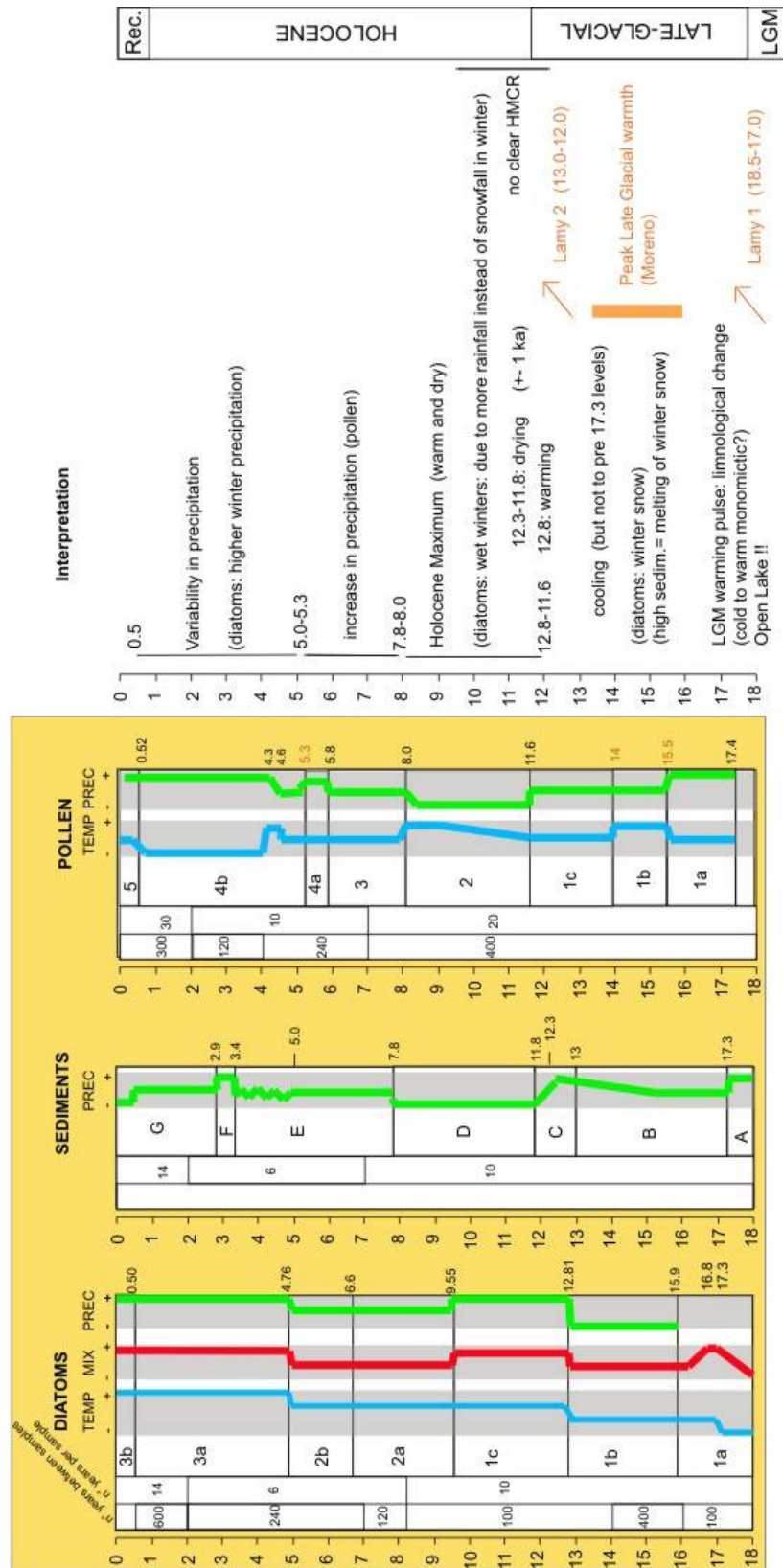


Figure 15: Composite sedimentological, pollen and diatom record of PU-II and interpretation of the long-term trends in the evolution of precipitation and temperature.

The diatom stratigraphy does not fully corroborate the presence of a Late-Glacial cold reversal in the region, although it indicates that some environmental instability may have occurred between 13,400 and 11,700 cal. yr BP. Instead, low absolute abundances and biovolumes between 16,850 and 12,810 cal. yr BP suggest an extended period of low rainfall and/or temperatures. A marked transition at 12,810 cal. yr BP points to an increase in the moisture supply to the lake, possibly associated with enhanced seasonal variability of the southern Westerlies and/or a rise in sea-surface temperatures in the South Pacific. After 9,550 cal. yr BP, stronger and longer persisting summer stratification can be inferred from the diatom data, which may have been the result of the higher temperatures associated with an early Holocene thermal optimum. The mid-Holocene is characterized by a decrease in precipitation, culminating around 5,000 cal. yr BP, and rising again after 3,000 cal. yr BP. An increase in precipitation from 3,000 cal. yr BP to present could point to an increased frequency of El Niño occurrences, leading to drier summers and slightly moister winters in the area.

### ***II.3.3. Millennium-scale abrupt climate changes***

#### A new record of a southern medium- to high-latitude Late-Glacial Cold Reversal ?

The sedimentological and geochemical data clearly highlight the presence of a Late-Glacial cold reversal, i.e., a cold and humid interval at 13,100-12,300 cal. yr BP, following a period of gradual increase in humidity since 16,000 cal. yr BP. This cold spell ended rapidly with a shift towards warmer and dryer conditions between 12,300 and 11,800 cal. yr BP, marking the onset of the Holocene. Also the pollen record provides evidence for a return to colder conditions between 14,000 and 11,600 cal. yr BP. The diatom data, on the contrary, do not really show clear evidence of a cold reversal, although they indicate that some environmental instability may have occurred between 13,400 and 11,700 cal. yr BP.

The timing of this cold and humid interval at ~13,100-12,300 cal. yr BP (Fig. 16) is roughly similar to that of the Huelmo/Mascardi Cold Reversal (i.e., 13,475 to 12,000 cal. yr BP, Hajdas et al. 2003) that was identified in the Huelmo Mire (41.5°S, Chile) and in Lago Mascardi (41°S, Argentina), both located at nearly the same latitude as Lago Puyehue. This Late-Glacial cold reversal is interpreted as the local counterpart of the Northern-Hemisphere Younger Dryas cold period (12,800 to 11,600 cal. yr BP).

The Lago Puyehue continuous lacustrine record thus provides new support to the ideas:

- i) that millennium-scale abrupt climate changes have also affected the Southern-Hemisphere climate on a regional scale during the transition from the LGM to the Holocene,
- ii) that this Southern-Hemisphere event precedes is out of phase with similar cold reversals observed in the polar North Atlantic and the Antarctic: i.e., it precedes the Northern-Hemisphere Younger Dryas by about 500 yrs, and post-dates the Antarctic Cold Reversal (i.e., 14,500 to 12,800 cal. yr BP) by about 1,400 yrs (Fig. 16).

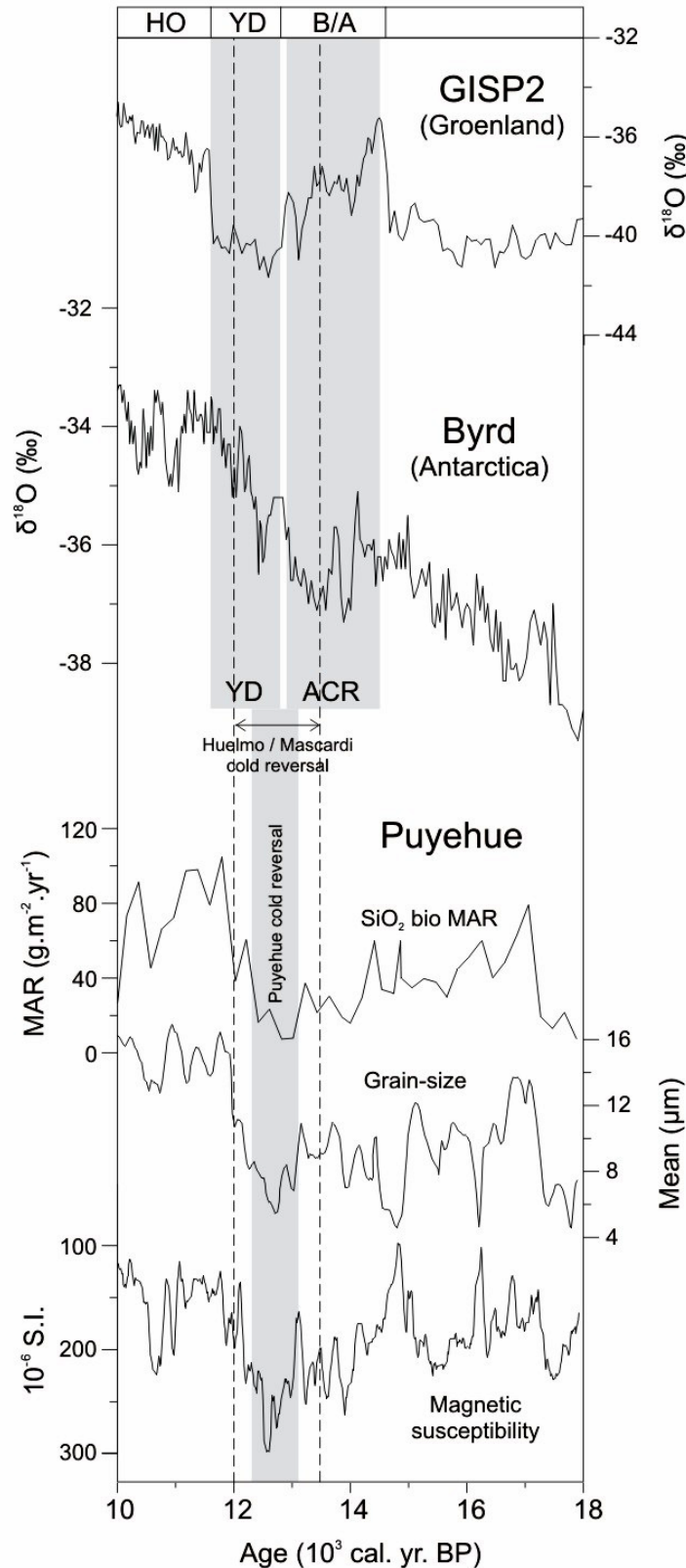


Figure 16: Climate changes between 18 and 10 ka, from Greenland, Antarctica and Lago Puyehue. Grey bands mark duration of Younger Dryas Cold Reversal (as recorded in Greenland ice core, Grootes et al. 1993), the Antarctic Cold Reversal (as recorded in Antarctic ice core, Blunier & Brook 2001) and Puyehue Cold Reversal. Dashed lines mark duration of Huelmo/Mascardi Cold Reversal (Hajdas et al. 2003).

### Other millennium-scale abrupt climate changes: 3400-2900 cal. yr BP cold/humid event

The sedimentological data also clearly evidence a period of cold and/or humid conditions at 3400-2900 cal. yr BP, starting and ending abruptly. This period is not picked up in the diatom and pollen record. In northern Chile, at 29°S, glaciers readvanced during the same period, and this was attributed to an increase in moisture supply (Grosjean et al. 1998). Additional evidences exist elsewhere in South America and in many places of the world (van Geel and Renssen 1998, van Geel et al. 2000). In Chile, however, previous studies have not revealed any abrupt climate change during this period, and also marine sediments demonstrate a continuous paleo-productivity throughout the last 8000 yrs (Lamy et al. 2002) and do not evidence any climate disturbance close to 3000 cal. yr BP. An accurate dating of this event by radiocarbon is difficult because the plateau in the calibration curve characterizing this period. According to van Geel et al. (2000), rapid climate changes at this period are due to a decreasing solar activity.

### Other millennium-scale abrupt climate changes: Little Ice Age

A detailed high-resolution sedimentological and geochemical investigation of one of the short cores from the PU-II site (Fig. 17), encompassing the last 600 yrs (Bertrand et al. 2005), also demonstrated the occurrence of a distinct wet period during the interval 1490-1700. This wet period was followed by a drying climate during 1700-1900. These results are in agreement with several other observations from the literature.

- In Northern Patagonia (41°S, Chile and Argentina), Villalba (1990) recognized two periods characterized by glacier advances: 1270-1380 and 1520-1670. By means of a tree-ring study in the same area, Lara and Villalba (1993) and Villalba (1994) evidenced a long interval with below-average temperatures from 1490 to 1700 and the most recent warm periods from 1720 to 1750 and from 1800 to 1880. The coincidence of periods with low temperatures and glacier advances is manifest. Glacier advances during the last millennium seem to be related to a combination of higher precipitation and lower temperatures (Villalba, 1994). More recently, a tree-ring study by Villalba et al. (2001) of 17 records from Northern Patagonia demonstrates a long cold interval extending from ca. 1500 to 1660.
- Jenny et al. (2002) described high flood periods at 34°S during the 1300-1700 and 1850-1998 intervals. These periods are linked to moisture increase due to strengthening of the Westerlies.
- In Peru, Quelccaya ice-core data (14°S) present high snow accumulation rates during the 1500-1720 period (Thompson et al. 1985, 1986). This interval is interpreted as the wettest period of the last millennium, at the onset of the Little Ice Age (LIA). It is followed by a dry period at 1720-1860. Moraines deposited before 1650 were described close the Quelccaya ice cap (Goodman et al., 2001).

The wet interval deduced from Lago Puyehue sediments during the 1490-1700 period is strikingly consistent with higher ice-accumulation rates in the Quelccaya ice core (Thompson et al., 1985), as well as with colder temperatures deduced from tree-ring evidence in Northern Patagonia (Luckman and Villalba, 2001). The subsequently

drying climate (i.e., from 1740 to 1900) corresponds with the recentmost dry periods of Lara and Villalba (1993).

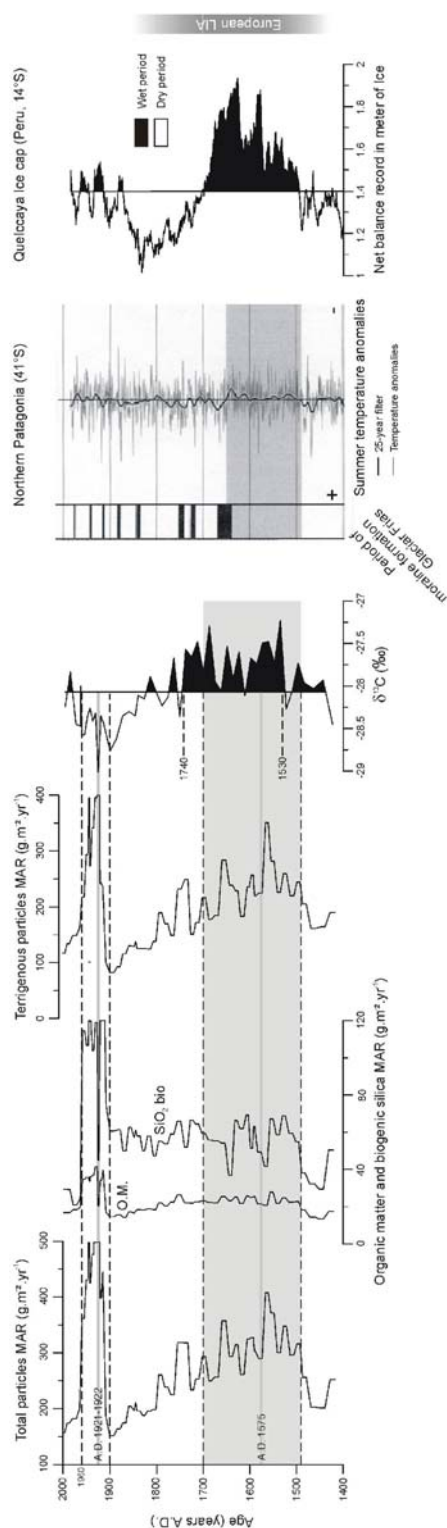


Figure 17: Mass-accumulation rates and  $\delta^{13}\text{C}$  data of PU-II-P5 short core (Bertrand et al. 2005), indicating a wetter period between 1490-1700. The record is compared with data from the Quelccaya ice cap (Thompson et al., 1985) and from northern Patagonia (Luckman and Villalba, 2001).

These observations emphasize that precipitation changes during the last 600 yr in southern America seem to be contemporaneous and seem to underscore a consistent picture. All data suggest a strengthening of the Westerlies north of 50°S during the 1490-1700 period. This would have increased the precipitation in the Andes leading to an increase in terrigenous-particle supply in the lakes.

In the Northern Hemisphere, the Little Ice Age (LIA) was characterized by colder temperatures and glacier readvances. Its onset is dated between 1430 and 1550 and its end between 1700 and 1850 (Bradley et al., 2003). The recent literature review of Soon and Baliunas (2003) attests for an interhemispheric presence of the LIA. The Puyehue data do not show significant paleoproductivity changes in favor of a cooler climate. However, the high rainfall reconstructed for the 1490-1700 period could be the local signature of the onset of the LIA. At the same latitude, Lamy et al. (2001) interpreted increased rainfall contemporaneous with the LIA period. These results evidence that the Southern Hemisphere LIA could have been initiated by a wet climate contemporaneous with the beginning of the Northern Hemisphere cold period.

Other records from South America (< 40°S) have demonstrated that this period with high precipitation was accompanied by cold temperatures until the end of the 19<sup>th</sup> century (Thompson et al. 1985, 1986; Luckman and Villalba, 2001, Valero-Garcés et al., 2003). Further South, in Gran Campo Nevado (53°S), major glacier advances are dated from the 1870s, reflecting probably the end of the Southern Hemisphere LIA (Koch and Kilian, 2005). The end of the cold period is ambiguous and seems to vary with latitude. In Tierra del Fuego (55°S), the LIA seems to be absent (Mauquoy et al., 2004).

### III. HIGH-RESOLUTION RECORD OF PRECIPITATION

#### III.1. Materials and methods

The high-resolution analysis of the sedimentary record of Lago Puyehue has concentrated on those sections of the record that are characterized by laminated sediments. In addition to selected (i.e., laminated) sections of the long core PU-II, two short cores were also studied: PU-I-P3a and PU-II-P5a. Short core PU-I-P3a (61 cm) was taken on the PU-I coring site, while short core PU-II-P5a (53 cm) was retrieved from the PU-II coring site.

All cores were scanned for magnetic susceptibility and gamma-density with a Geotek multi-sensor core logger on non-opened sections (at GFZ-Potsdam, Germany).. Moreover, magnetic susceptibility was measured on opened cores with a Bartington MS2 point sensor every 5 mm. The cores were then sub-sampled in a similar fashion as described above for the PU-II long core (see chapter II.1). Several sedimentological analyses were carried on PU-II-P5a every centimeter, following the procedures described in chapter II.1: LOI<sub>105</sub>, LOI<sub>550</sub> and LOI<sub>950</sub>, bulk and clay mineralogy by XRD and major-element geochemistry by XRF. In addition, TOC and TON were determined with a FISONs elemental analyzer and  $\delta^{13}\text{C}$  with an Optima IR-MS. Biogenic silica was extracted by  $\text{Na}_2\text{CO}_3$  and quantified by blue-spectrophotometry on 32 samples (Mortlock and Froelich 1989). Grain-size was measured every 5 mm with a Malvern Mastersizer 2000 laser-diffraction particle analyzer.

##### III.1.1. Varve analysis

###### Varve counting

Half cores were dried by lyophilization and impregnated under low vacuum, then polished with diamond discs to prepare large-format thin sections from undisturbed samples (Boës and Fagel, 2005). All laminations were checked by optical microscopy to identify the internal sediment micro-structures, composition and origin (e.g., Brauer and Negendank 2002, Brauer 2004). Varve-like laminations (e.g., Fig. 18), only visible in thin-sections, are formed by couplets or mixed couplets. Couplets are defined by a light diatom-rich layer and a terrigenous layer rich in organic matter and with few diatoms. Mixed couplets are characterized by indistinct limits between the two different layers. The annual character of the laminations was confirmed by inter-core correlations, and supported by  $^{210}\text{Pb}$  and  $^{137}\text{Cs}$  chronologies (Arnaud et al. 2006) and by independent chronostratigraphical markers (i.e., the seismite created by the 1960 mega-earthquake, and tephra layers resulting from historical eruptions). Sediment-accumulation rates were derived through varve counting after correction for intercalated instantaneous deposits. Varve counting was done on thin sections at low magnification (5x, 10x). Varve years were counted with a constant 5 mm progression and the homogeneous sediments related to the intercalated units, or the fine-grained layers, were measured. For the PU-II-P5a short core, the same sequences were counted three times per 10 cm step to estimate the counting errors

expressed as the cumulative varve number difference. The occurrence of mixed couplets requires a constant visual control of the lateral sediment variations observed in the large format thin-sections. Core chronologies were constructed by varve counting, after Hajdas-Skowronek (1993) and Lotter and Lemcke (1999).

#### Manual varve thickness measurements

The varve thickness was measured on digitized images in order to compare the annual thickness with instrumental climate data. For a constant image acquisition, large thin sections were prepared from the polymerized blocks until an equal thickness was reached. The thin sections were then digitized with a slide scanner with a constant image acquisition in black-and-white mode. The varve thickness was measured on 8-bit grey-scale (0-black; 256-white) TIF images to capture the maximum variation of the thin light clayey laminations enriched with diatoms and to increase the accuracy of the measurements performed (Nederbragt and Thurow 2001). On the digitized images, the maximum light intensities represent the light diatom-rich layers and the minimum light intensities represent the dark diatom-poor sediments. The annual thickness (distance in pixels) was manually measured from the thin-section images with ImageJ software. Only the total varve thickness was measured, as limits between the light diatom and dark brownish layers were not systematically observed. The varve thickness was extracted manually from single pixel lines applied on the different laminations. The thickness was measured along several parallel lines to assess possible lateral variations in thickness. The pixel measurements were automatically converted into microns by calibration with a micrometer, after which the results were expressed on an age-versus-depth scale.

#### Semi-automatic varve counting

The relative reflectance (or grey-scale intensity) of the light-coloured layers rich in phytoplankton (~ 100 to 500  $\mu\text{m}$ ) can also be used for (semi-)automated varve counting (Hughen et al. 1998). We used the grey-scale values obtained from the digitized thin-section images. Each grey-scale measurement was compared to a five adjacent averaging value (i.e., 100  $\mu\text{m}$  distance) in order to correct for the evolution of the mean grey-density value through the core. The measured difference between the dark and light values were expressed into a binary format (0=dark, 1=light). A varve year was counted when a light layer thicker than 100 or 125  $\mu\text{m}$  was detected by the grey-scale analysis. The two different detection thresholds correspond to the minimum thickness of the light phytoplankton-rich layers observed under the microscope. In the thickest varve sequences (i.e., light varve layers > 125  $\mu\text{m}$ ), the use of the 100  $\mu\text{m}$  filter may overestimate the real number of varve years, while in the thinnest varve sequences (i.e., light varve layers < 125  $\mu\text{m}$ ) the use of the 125  $\mu\text{m}$  filter may underestimate the real number of varve years.

#### Calendar years estimation from varve counting

The number of varve years was calculated from the 100 and 125  $\mu\text{m}$  grey-scale filters. The counts were carefully checked and counting errors caused by the presence of homogeneous horizons (i.e., instantaneous deposits, tephra) were removed from the database. The reproducibility of this semi-automatic grey-scale

varve-counting approach was also evaluated. Measurements of the same section, but along three different measurement axes, produced very similar results: i.e., 107, 109 and 105 varve years (Fig. 18). These results are consistent with the manual counting, especially for the central axis (Fig. 18). The central axis is also less affected by lateral sediment compaction during coring. Therefore, it was decided not to calculate a mean value from the three parallel axes, as this procedure would have introduced counting errors. The counting performed on the central axis constrained the results obtained by manual varve counting, as it provided an independent and automatic estimate of the number of varve years.

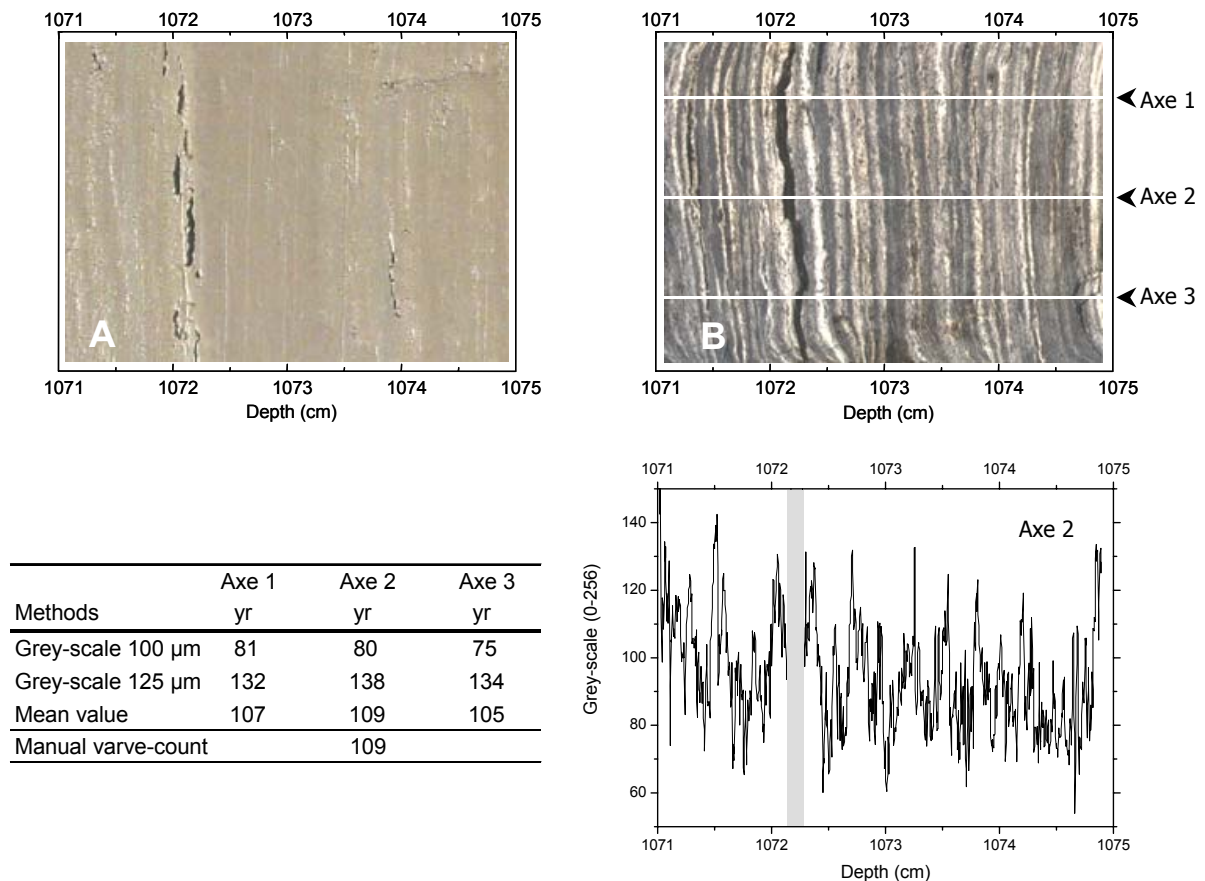


Figure 18: (A) Seemingly homogeneous fresh core surface. (B) Micromorphological picture of the same core section after varve pre-treatment. Lower right: example of grey-scale record, measured along axis 2 along a section of the sediment core. Lower left: comparison of the grey-scale results obtained along three different axes.

### Grey-scale-based varve-thickness measurements

The accurate grey-scale measurements were used to establish a continuous varve-thickness record. The seasonal varve thickness related to dark/light layers was directly extracted from the binary (0/1) grey-scale database, as each grey-scale measurement represents a distance of 25  $\mu\text{m}$ . For instance, ten successive 1-units correspond to an individual light varve layer of 250  $\mu\text{m}$  thickness composed of phytoplankton accumulated after winter turn-over. The same procedure was applied to the dark layers accumulated during lake-water stratification periods (summer and

spring). Finally, the total laminae thickness was calculated as it represents “one year” of sediment accumulation.

### The varve-thickness index

The varve-thickness record was compared to local instrumental climate data and to historical volcanic/seismic activity reports to understand sedimentary processes and climate-varve relationships. A standardized varve-thickness index was calculated according to Zolitschka (1996). The occurrence of mixed couplets did not allow a seasonal record to be extracted, limiting the approach to an annual resolution: i.e., the varve-thickness index is thus based on total varve thickness.

### **III.1.2. Spectral analysis**

Several methods of spectral analysis were applied to the varve-thickness records to identify potential periodicities in the signal. Blackman-Tuckey, Maximum Entropy, Multi-Taper Methods (MTM) and singular spectrum analysis were applied on the whole record. In addition evolutive MTM and wavelet analyses allow to identify temporal influence of some periodicities.

The Blackman–Tuckey method (Blackman and Tukey 1958) is a classical method for spectral analysis. The power spectrum is computed from the Fourier-transform of the autocovariance of the data multiplied by a lag-window (weighting function). This method helps to reduce the bias, variance and leakage, which makes it unlikely to present spurious spectral feature. In return it has a poor resolution in the spectral domain.

The maximum entropy method (MEM) is based on approximating the studied time series by a linear autoregressive process (Burg 1978; Childers, 1978). MEM is useful for its high resolution but it tends to identify spurious peaks and therefore must be used in conjunction with a more robust method.

The MTM (Thomson 1982; Percival and Walden 1993) is used to estimate the total power spectrum of the time series. It is designed to estimate sharp spectral peaks in the presence of white noise using harmonic analysis. Moreover it also gives satisfactory results in the presence of red noise (which is the case in most geophysical series) and it provides a high spectral resolution (Dettinger et al. 1995). According to this method, the data are pre-multiplied by orthogonal tapers that minimise the spectral leakage due to finite length of the series. MTM models time series as the sum of sinusoids and calculates the corresponding amplitude by a least-square procedure. A statistical test (i.e., Fischer-Snedecor test) for the significance of the amplitude spectra is also provided (Kendall and Stuart 1977). MTM allows for detection of weak peaks with high degree of statistical significance and also for signal reconstruction using the detected significant peaks (Park 1992).

Singular spectrum analysis (SSA) is designed to extract as much reliable information as possible from short, noisy time series without knowledge of the dynamics

underlying the series (Broomhead and King 1986; Fraedrich 1986; Vautard and Ghil 1989). The method is a form of principal component analysis in the time domain. It allows the decomposition of time series into trends, oscillations and noise. Selected components of the time series can be reconstructed from SSA. The Reconstructed Components (RCs) preserve not only the amplitude and the frequency but also the phase of the time series. Therefore RCs can be used to isolate specific components and to determine the periodic oscillations in the time series (using a spectral technique such as MTM for example).

The Wavelet Transform (WT, Daubechies 1992; Lau and Weng 1995; Torrence and Compo 1997; Mallat 1998) is designed to study the time-frequency variations of a time series. Thus transient or intermittent components can be detected. Here we used the Morlet wavelet (Morlet 1983) to decompose the series: WT gives a measure of the comparison between the signal and the dilated-translated wavelet.

For further detailed of the different methods see Ghil et al. (2002). Toolkits for spectral analysis are freely available at <http://www.atmos.ucla.edu/tcd/ssa> or upon request at paillar@lsce.saclay.cea.fr.

## III.2. Results

### III.2.1. Sedimentation rates obtained from varve counting

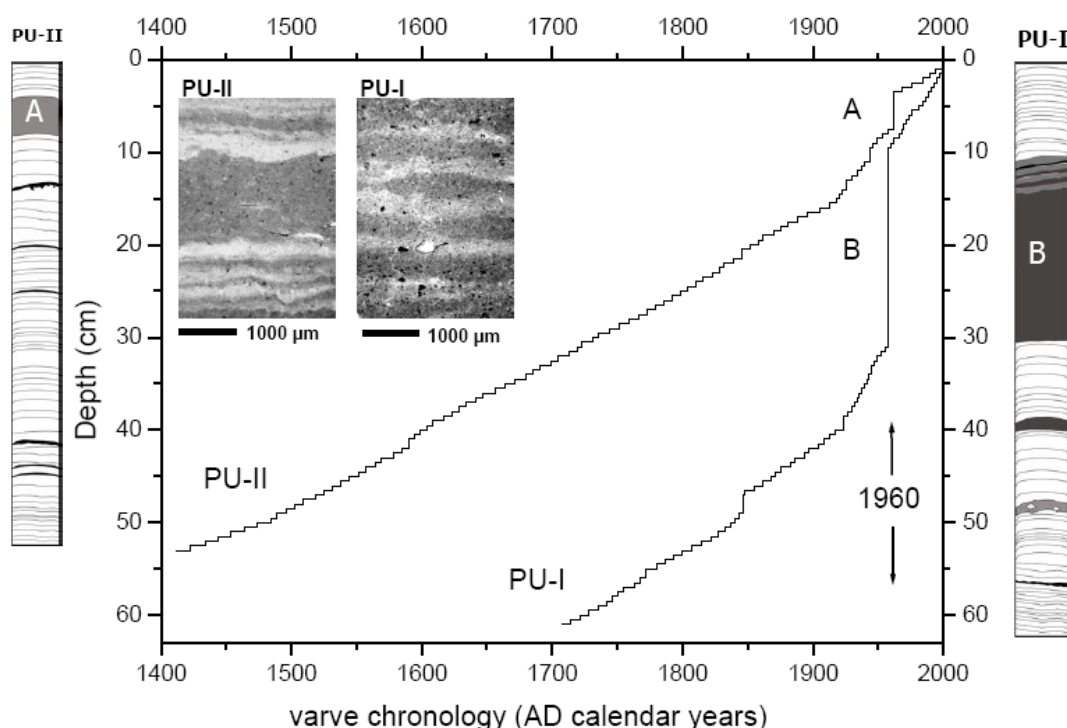


Figure 19: Sedimentological logs and varve chronologies of the PU-I-P3a and PU-II-P5a short cores. Varve chronologies are constrained by  $^{137}\text{Cs}$  and  $^{210}\text{Pb}$  (Arnaud et al. 2006) and by the occurrence of a seismite induced by the large 1960 Valdivia earthquake (A: from 4 to 7 cm depth in PU-II-P5a, B: from 14 to 30 cm depth in PU-I-P3a).

In the PU-I-P3a core, 294 varve years ( $\pm 6\%$  error) were counted, i.e. encompassing the time window between 1706 and 2000 (Fig. 19). The sedimentation rates derived from varve counting and corrected for the presence of intercalated deposits vary between  $\sim 0.9$  mm/yr and  $\sim 2.3$  mm/yr. Two main periods stand out:

- i) a period with a sedimentation rate of  $\sim 2.20$  mm/yr, between  $\sim 1920$  and 2000, and
- ii) a period with a sedimentation rate of  $\sim 0.95$  mm/yr, between  $\sim 1700$  (bottom of core) and  $\sim 1920$ .

The gaps in the counts are caused by four thick intercalated deposits occurring in  $\sim 1958$ ,  $\sim 1924$ ,  $\sim 1846$ ,  $\sim 1772$ .

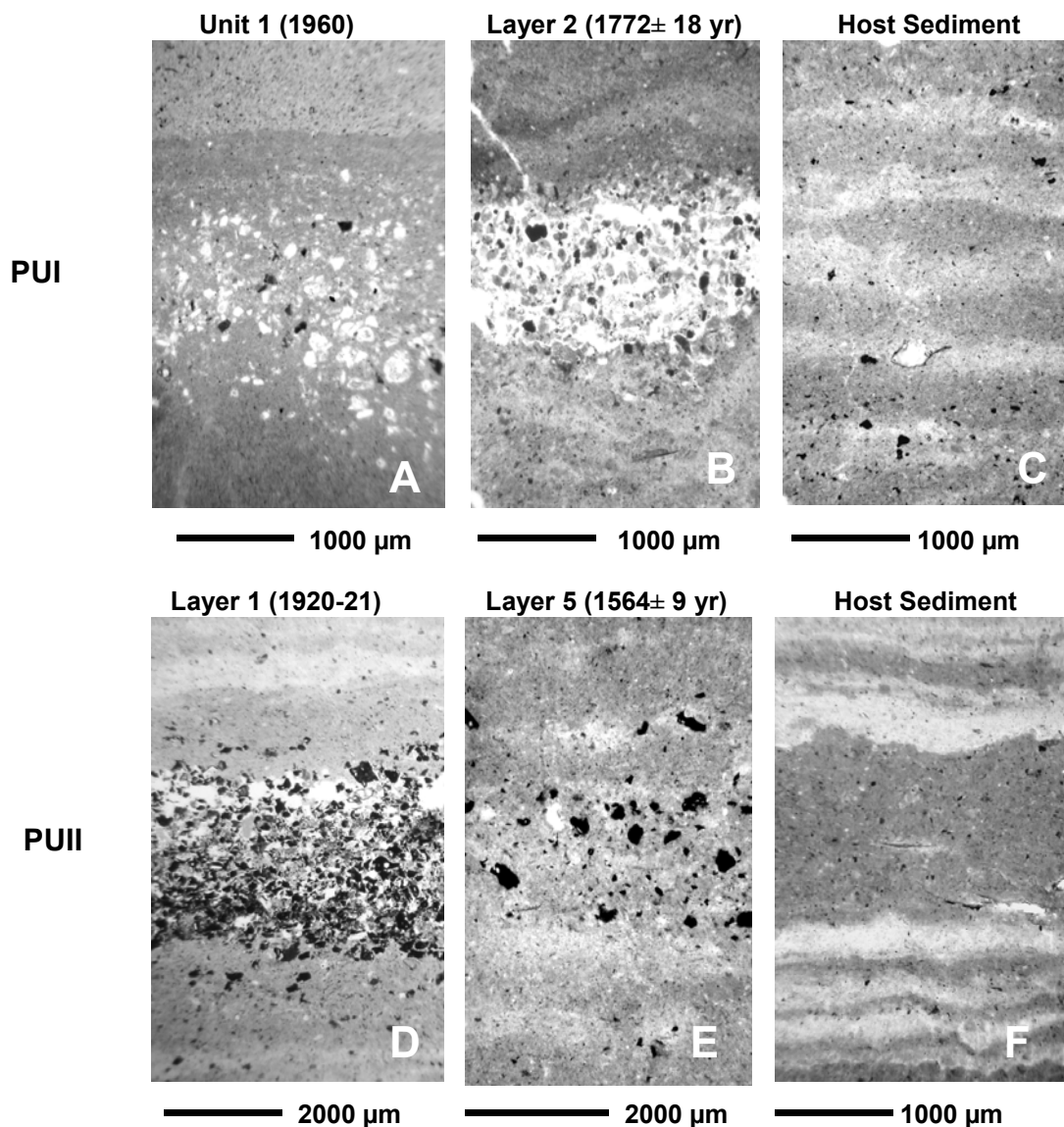


Figure 20: Micromorphological pictures of sections of the PU-I-P3a and PU-II-P5a cores. (A) fine-grained layer composed of rounded heterogeneous grains ( $< 500$   $\mu\text{m}$ ) of volcanic origin, mixed with diatomaceous clays (PU-I-P3a, Unit 1); (B) tephra layer. Note absence of diatomaceous clay matrix (PU-I-P3a, Layer 2); (C) varve couplets (PU-I-P3a, host sediment); (D) tephra layer (PU-II-P5a, Layer 1); (E) tephra layer (PU-II-P5a, Layer 5); (F) varve couplets, note varve-thickness variability (PU-II-P5a, host sediment).

In the PU-II-P5a core, 592 varve years ( $\pm 2\%$  error) were counted, i.e. encompassing the time window between 1408 and 2000 (Fig. 19). The obtained sedimentation rates vary between  $\sim 0.6$  mm/yr and  $\sim 1.5$  mm/yr, which is approximately half of the values for PU-I site. Four main periods can be identified:

- i) a period with a sedimentation rate of  $\sim 1.30$  mm/yr, between  $\sim 1920$  and 2000,
- ii) a period with a sedimentation rate of  $\sim 1$  mm/yr, between  $\sim 1840$  and  $\sim 1920$ ,
- iii) a period with a sedimentation rate of  $\sim 1.80$  mm/yr, between  $\sim 1540$  and  $\sim 1840$ ,
- iv) a period with a sedimentation rate of  $\sim 0.60$  mm/yr, between  $\sim 1408$  (bottom of core) and  $\sim 1540$ .

Seven thick intercalated deposits events occur in  $\sim 1962$ ,  $\sim 1926$ ,  $\sim 1845$ ,  $\sim 1799$ ,  $\sim 1590$ ,  $\sim 1564$ ,  $\sim 1544$ .

An estimation of the accuracy of the measurements was determined by three successive countings. The given error bar corresponds to the cumulative error, maximum at the bottom of the core. The basal age of the PU-I-P3a core is 1706 ( $\pm 18$  yr); the basal age of the PU-II-P5a core is 1408 ( $\pm 12$  yr).

### **III.2.2. Varve micro-facies and the origin of the varves**

In both cores, the sedimentary matrix contains a finely laminated micro-structure under the microscope. In PU-I-P3a, laminations are formed by the alternation of light yellowish clays and dark brownish clays (Fig. 20C). The laminations are micrometer- to millimetre-scale (1600  $\mu\text{m}$  average value). In PU-II-P5a, laminations are micrometer-scale (900  $\mu\text{m}$  average value) and characterized by rhythmic light yellowish clayey mud and dark brownish clayey mud forming series of couplets (Fig. 20F). The components making up the laminae were analyzed by optical microscope. The thin light-brownish or yellowish clayey layers are composed of diatom frustules, while the darker layers correspond to organic-rich silty-clay material mixed with terrigenous and organic particles with a few diatoms. No disturbance of the sedimentary texture due to bioturbation was observed.

Based on analysis of the varve micro-facies, variations in varve thickness appear to be mainly related to variations in the amount of diatoms making up the light layer, which itself is related to nutrient supply in winter. According to Soto (2002), deep mixing could be a regulating factor of productivity and biomass. The formation of the annually laminated sediments of Lago Puyehue is here attributed to nutrient turn-over cycles and water circulation in the lake (Fig. 21). The lake water is mixed once a year, in winter time. One dominant winter-climate forcing factor that controls lake mixing is the winter precipitation induced by the strong southern westerly winds. In winter, the strong precipitation ( $> 500$  mm) and winds ( $\sim 4$  m/s) break the lake stratification, and promote water circulation, deep mixing and homothermy (Fig. 22). Water mixing drives nutrient turn-over, resulting in significant increases in diatom productivity, which helps to explain why diatoms (i.e. *Melosira*, *Asterionella*) are more abundant in autumn and winter (Campos et al. 1989). In spring and summer, the lake

is oligotrophic and stratified, and diatoms are less abundant due to a shallow epilimnion (Fig. 22, Campos et al. 1989).

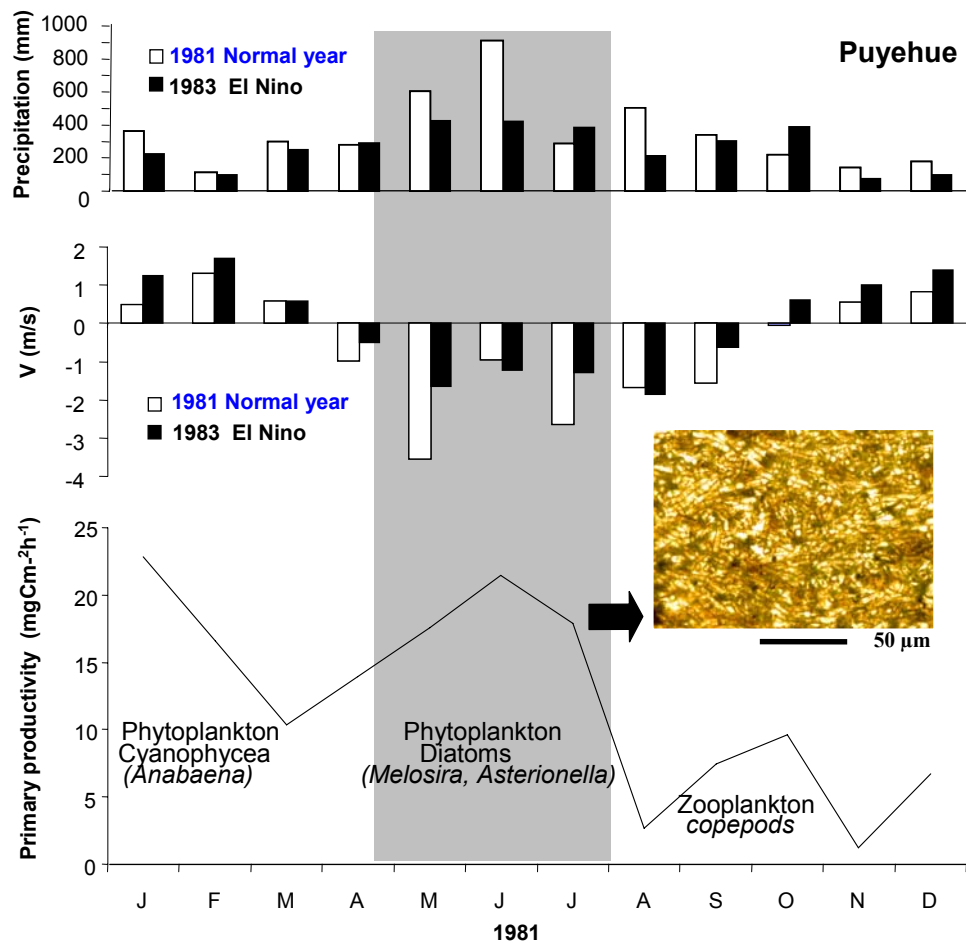


Figure 21: Precipitation in Lago Puyehue (station: Aguas Calientes) during a normal year (1981) and during an El Niño year (1983). Wind speed data at 40°S (from: NOAA, NCEP). Primary productivity of the lake in 1981 (Campos et al. 1989): diatom primary productivity increases during the strong precipitation/winds in autumn/winter. The inset represents a diatom layer deposited after the winter turn-over.

### III.2.3. Quantitative climate-varve relationships

#### Local climate control on varve thickness

The standardized varve-thickness measurements were compared with the available local (i.e., station: Aguas Calientes, Parque Nacional Puyehue) instrumental climate data to better understand the above-suggested climate-varve relationships (Zolitschka 1996). Instrumental data are available for the period 1980-2000. To estimate the strength of the linear relationships between the local climatic indices ( $x$ ) with the standardized varve thickness ( $y$ ), we use the coefficient of determination ( $r^2$ ) (Tab. 3).

In both sites, there is no linear regression between the varve thickness and the monthly air temperatures ( $r^2 < 0.05$ ). As an exception, austral summer temperatures

in February present a negative relation with the varve thickness ( $r^2 = 0.43$ ;  $r = -0.66$ ), whereas austral autumn/winter temperatures provide a poor explanation of the varve-thickness variability ( $r^2 = 0.26$ ;  $r = 0.51$  in May).

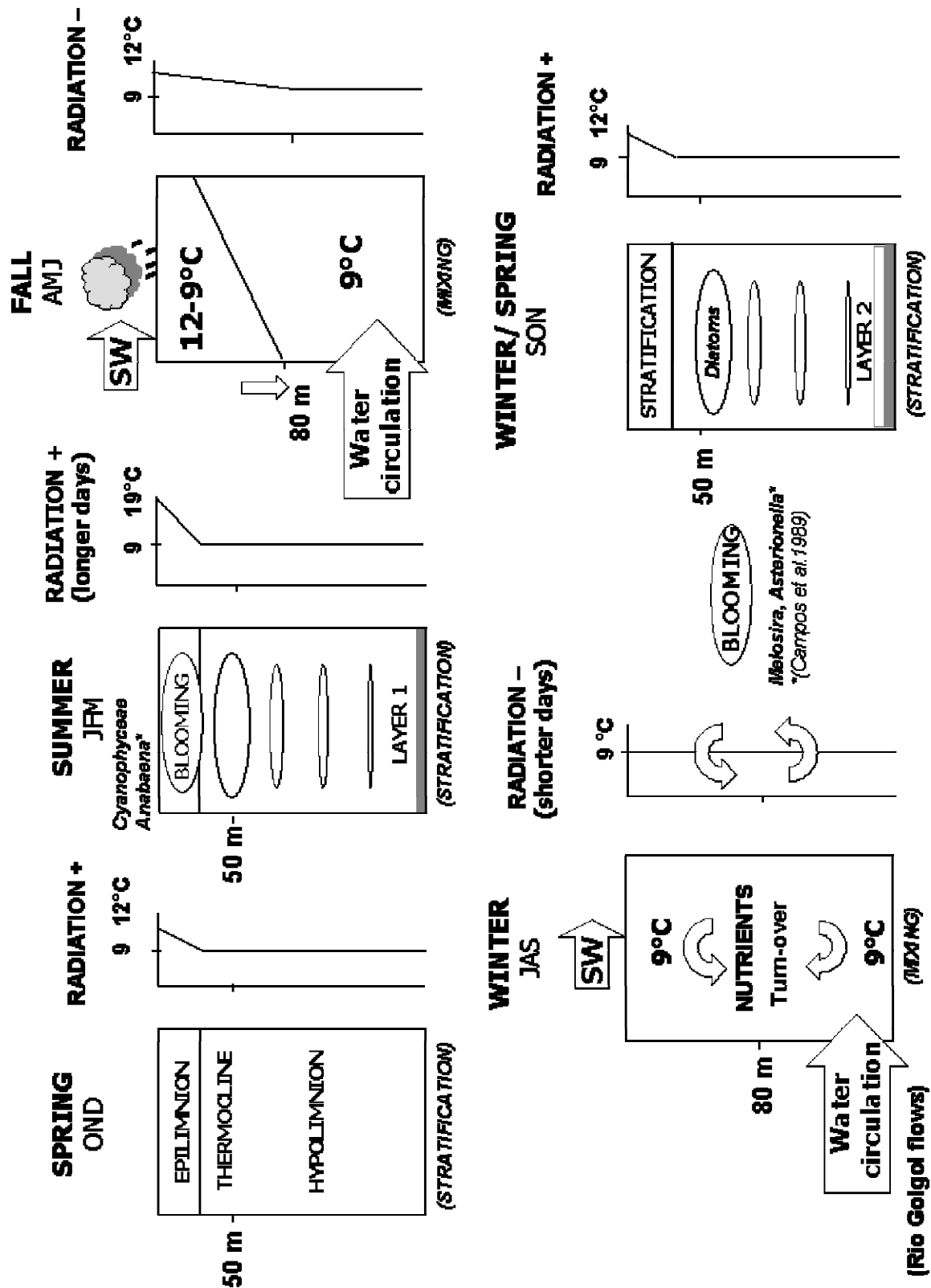


Figure 22: Schematic representation of the annual limnological cycle in Lago Puyehue, which gives rise to the formation of varved sediments (after Campos et al. 1989).

In PU-I-P3a, 6 % of the varve-thickness variability is explained by the annual precipitation (Fig. 23). There is no significant link between the varve thickness and the austral precipitation in summer/spring ( $r^2 < 0.08$ ), except a weak positive relation with the precipitation of January ( $r^2 = 0.10$ ;  $r = 0.32$ ;  $p = 0.00$ ). In contrast, the varve thickness and the precipitation in winter are positively correlated. The correlation is even more significant if we consider the maximum precipitation months:  $r^2 = 0.39$ ;  $r = 0.63$ ;  $p = 0.00$  in June, and  $r^2 = 0.23$ ;  $r = 0.48$ ;  $p = 0.00$  in August). About 39 % of the varve-thickness variability is explained by the maximum precipitation in winter (i.e., June, Fig. 23, Tab. 3).

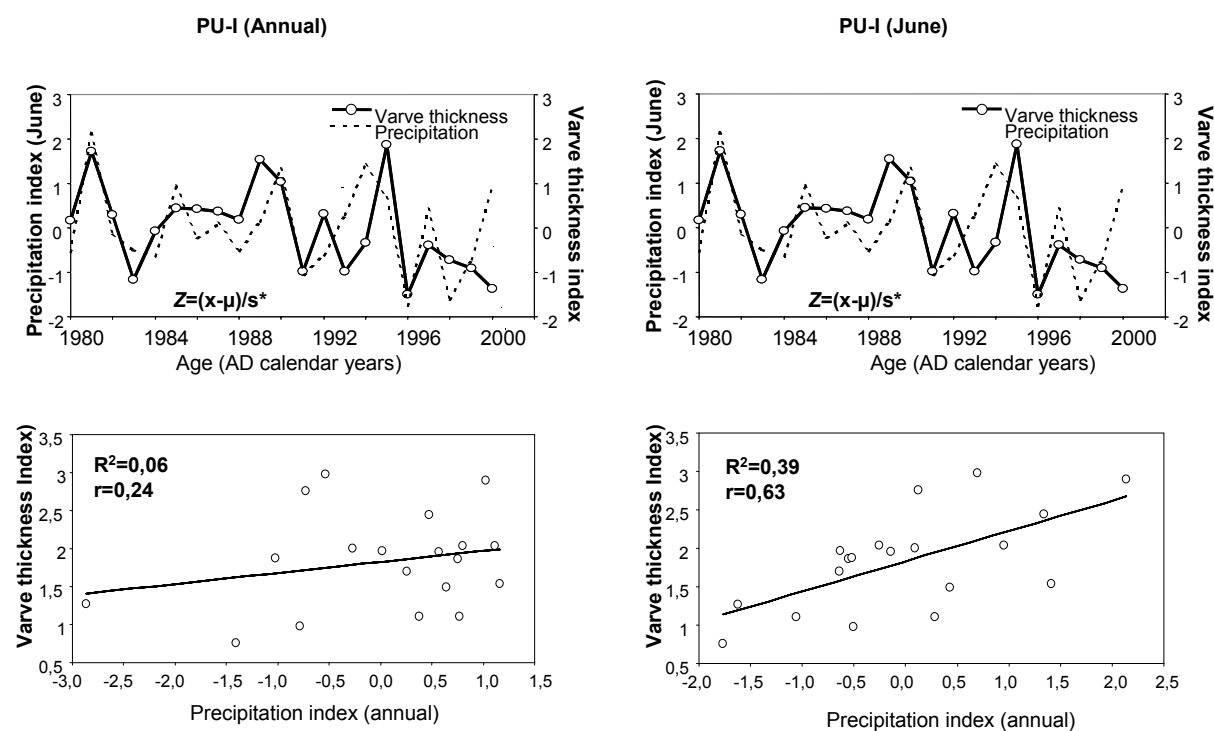


Figure 23: Core PU-I-P3a: relationships between standardized varve-thickness measurements and the local annual precipitation index (left diagrams). Positive correlation between the varve-thickness index and the precipitation index in June (right diagrams).

In PU-II-P5a, the annual precipitation explains 21 % of the varve-thickness variability ( $r = 0.46$ ) (Fig. 24). The comparison between the standardized varve thickness with the monthly instrumental climate data reveals no significant link between the varve thickness and precipitation in summer/spring. Only 1 to 3 % of the varve-thickness variability is explained by the austral summer/spring precipitation months (e.g.,  $r^2 = 0.03$ ;  $r = -0.16$ ;  $p = 0.00$  in December). As an exception, a better but still poor correlation is observed in February ( $r^2 = 0.22$ ;  $r = 0.47$ ;  $p = 0.00$ ). The overall variability is explained by the austral autumn/winter transition: about 63 % of the varve thickness is explained by the precipitation in May ( $r = 0.79$ ;  $p = 0.07$ ) (Fig. 24, Tab. 3). There is also a weak correlation with temperature at the same time ( $r = 0.51$ ). A weak negative correlation with westerly winds can be observed in June ( $r = -0.50$ ).

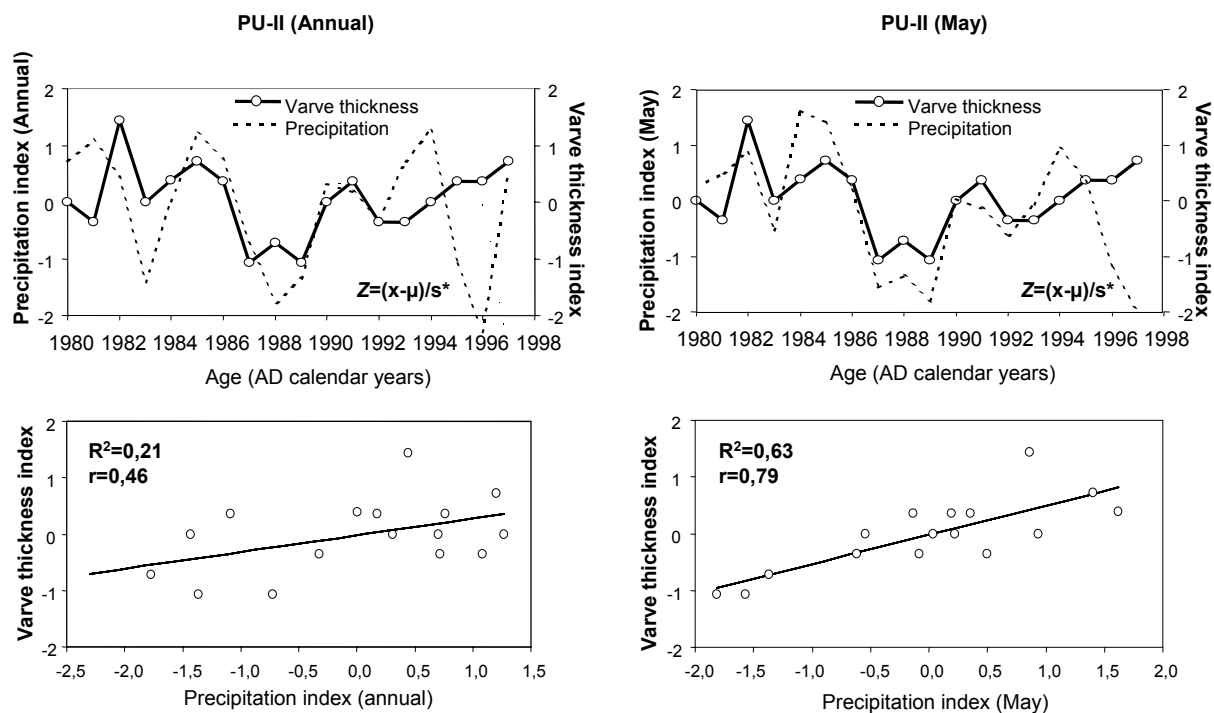


Figure 24: Core PU-II-P5a: relationships between standardized varve-thickness measurements and the local annual precipitation index (left diagrams). Positive correlation between the varve-thickness index and the precipitation index in May (right diagrams).

### Correlation between varve thickness and global climate factors

The varve-thickness index was also compared with different monthly atmospheric and ocean indices to test possible linkages between the Lago Puyehue varve record and more global climate forcing factors. The most significant indices for the South Pacific Ocean were selected from <http://www.cpc.ncep.noaa.gov/data/indices/> from and <http://jisao.washington.edu/pdo/PDO.latest> (Tab. 3):

- Tahiti-Darwin Southern Oscillation Index ( $SOI_{\text{Tahiti-Darwin}}$ );
- Equatorial-Eastern Pacific Southern Oscillation Index ( $SOI_{\text{Equatorial-Eastern Pacific}}$ );
- Indonesia Southern Oscillation Index ( $SOI_{\text{Indonesia}}$ );
- Pacific Decadal Oscillation (PDO);
- Quasi-Biennial Oscillation (QBO);
- Antarctic Oscillation (AAO).

The different SOI indices are relevant for El Niño-related periods (e.g., Trenberth and Shea 1987). In addition, the varve record was compared with climate oscillations relevant for the North Pacific Ocean: i.e., the Pacific Northwest Index (PNI) and the North Oscillation Index (NOI). The NOI is roughly the northern Pacific equivalent of the SOI. The NOI is based on the difference in sea-level pressure (SLP) anomalies between the northeastern Pacific and Darwin (Schwing et al. 2002). Except for PNI, the monthly index values were used to better assess the possible teleconnections (Tab. 3). Modern ENSO events cover a season that runs from the boreal summer to autumn (e.g., Cane 2005).

Climate parameters	J	F	M	A	M	J	J	A	S	O	N	D	Annual
Precipitation (mm)	187	162	234	331	457	<b>524</b>	395	351	255	271	235	231	302,7
Temperature (°C)	<b>13</b>	<b>13</b>	11	8,5	7	5	4,5	5,5	6,5	8,5	10,5	12,5	8,5
Radiation (w/m2)	<b>832</b>	695	540	375	261	198	277	314	387	594	654	786	493
Wind speed (m/s)	2	2	2	2	2	<b>4</b>	2	<b>4</b>	2	1	2	2	2
Wind direction	S	S	S	N	N	N	N	N	N	W	W	W	N
<b>Underflow site (PU-I)</b>													
Precipitation index	0,38	-0,13	-0,10	0,28	0,27	<b>0,53</b>	0,49	-0,22	0,34	-0,11	-0,02	-0,14	-0,22
Temperature index	0,32	-0,05	-0,11	0,15	0,19	<b>0,63</b>	-0,09	0,48	0,00	-0,11	-0,05	-0,28	-0,19
Westerly winds index	-0,14	-0,38	0,15	-0,14	0,02	<b>0,59</b>	0,18	0,46	0,08	0,08	-0,05	0,04	-0,25
SOI Tahiti Darwin	0,39	0,31	0,41	0,44	0,38	0,49	0,50	0,23	0,24	0,27	0,04	0,14	<b>0,52</b>
SOI Equat East Pacif	0,03	0,36	0,13	-0,14	0,17	0,26	0,32	0,11	0,35	0,35	0,05	0,39	0,34
SOI Indonesia	-0,12	0,01	-0,08	-0,16	-0,49	-0,13	-0,14	-0,45	-0,08	-0,19	-0,18	0,29	-0,19
PDO index	-0,06	-0,01	-0,21	-0,15	-0,19	-0,09	-0,17	-0,27	-0,06	-0,17	-0,23	-0,19	-0,21
QBO index	-0,04	-0,06	0,03	0,06	0,11	0,20	0,32	0,35	0,32	0,27	0,23	0,14	0,16
AAO index	0,36	0,34	-0,23	-0,22	0,05	0,18	-0,37	-0,28	0,24	-0,21	0,37	0,26	0,08
NOI	-0,01	0,35	0,11	0,10	0,35	-0,17	0,14	0,01	0,16	0,17	0,13	0,34	-0,12
PNI													0,12
<b>Interflow site (PU-II)</b>													
Precipitation index	0,03	0,47	0,05	-0,06	<b>0,79</b>	-0,05	0,22	0,14	-0,05	0,15	-0,08	-0,16	0,41
Temperature index	0,02	<b>-0,66</b>	-0,03	0,10	<b>0,51</b>	-0,10	0,17	0,20	0,47	-0,23	-0,20	0,34	0,18
Westerly winds index	-0,10	0,12	-0,19	-0,24	0,17	<b>-0,50</b>	0,10	-0,03	-0,40	-0,08	-0,28	<b>-0,58</b>	-0,36
SOI Tahiti Darwin	0,24	0,27	0,25	0,13	-0,30	-0,20	-0,25	-0,24	-0,42	-0,41	<b>-0,63</b>	-0,46	-0,21
SOI Equat East Pacif	0,36	0,08	-0,18	0,30	-0,03	-0,25	-0,28	-0,35	-0,26	-0,33	-0,39	-0,39	-0,25
SOI Indonesia	0,00	-0,42	-0,11	-0,15	0,02	0,07	0,00	0,11	0,35	0,30	0,28	-0,09	0,01
PDO index	-0,03	-0,06	-0,09	-0,26	-0,40	-0,21	-0,15	-0,17	0,03	0,02	-0,19	0,00	-0,26
QBO index	-0,10	-0,03	-0,01	0,06	0,12	0,19	0,20	0,13	0,13	0,18	0,20	0,17	0,15
AAO index	0,11	-0,08	0,41	0,40	-0,11	-0,03	-0,01	0,05	0,43	0,01	-0,48	-0,37	0,03
NOI	-0,10	0,15	0,06	0,26	-0,07	-0,10	-0,14	0,10	-0,31	0,06	-0,46	<b>-0,51</b>	-0,12
PNI													0,49

Table 3: Correlations between standardized instrumental climate data and varve-thickness records from the PU-I-P3a and PU-II-P5a PU-II short cores. Top: Monthly mean precipitation, temperature, and solar radiation derived from the 1980-2000 dataset (Station: Aguas Calientes). Centre and bottom: Correlation between varve index and different monthly atmospheric and ocean indices. Grey shading indicates the strongest correlations.

There appears to be no significant correlation between the varve thickness in PU-I-P3a with climate parameters, except a weak link with the annual SOI<sub>Tahiti-Darwin</sub> (Tab. 3). Any correlation coefficient higher or equal than 0.5 is considered relevant, because, even if the coefficient remains statistically low, it still contrasts with adjacent values and is significant for sedimentological interpretation. Among the different oscillation indices, the most significant correlation for PU-II-P5a is observed with the ENSO-related SOI<sub>Tahiti-Darwin</sub> during Austral spring ( $r = -0.63$  in November, Tab. 3). This interpretation is supported by additional negative correlation with the westerly wind index in December ( $r = -0.58$ ) and a weak negative correlation with the NOI in December ( $r = -0.51$ ).

### Varve thickness and ENSO

According to Montecinos and Aceituno (2003), the area of 38-41°S should be characterized by a significant relationship between ENSO variability and local rainfall. Austral summers (January, February, March) following an El Niño episode are mentioned to be characterized by reduced rainfall. However, the local monthly rainfall record for Lago Puyehue (Fig. 21) displays a precipitation deficit during the entire El Niño year (i.e. not only during austral summer, as postulated by Montecinos and Aceituno, 2003). The strongest precipitation anomaly occurs, in fact, during the

autumn/winter transition (May and June). Austral autumn/winter is also the period of dominant diatom primary productivity, the key factor determining varve thickness. El Niño years should be expressed in the varve-thickness record by thinner-than-normal varves.

Analysis of variations in varve thickness in relation to average annual precipitation highlights that, for the last 20 yrs, varve thickness was significantly reduced during El Niño years, in connection with marked precipitation deficits (Figs. 25, 26; Tab. 3). This is particularly obvious for the 1982-1983 El Niño event, which is one of the strongest of the 20<sup>th</sup> century (Dawson and O'Hara 2000). The 1982-1983 event is marked in the sedimentary record as a transition from a thick varve (positive varve thickness index) to a thin varve (negative varve thickness index) (Figs. 25, 26).

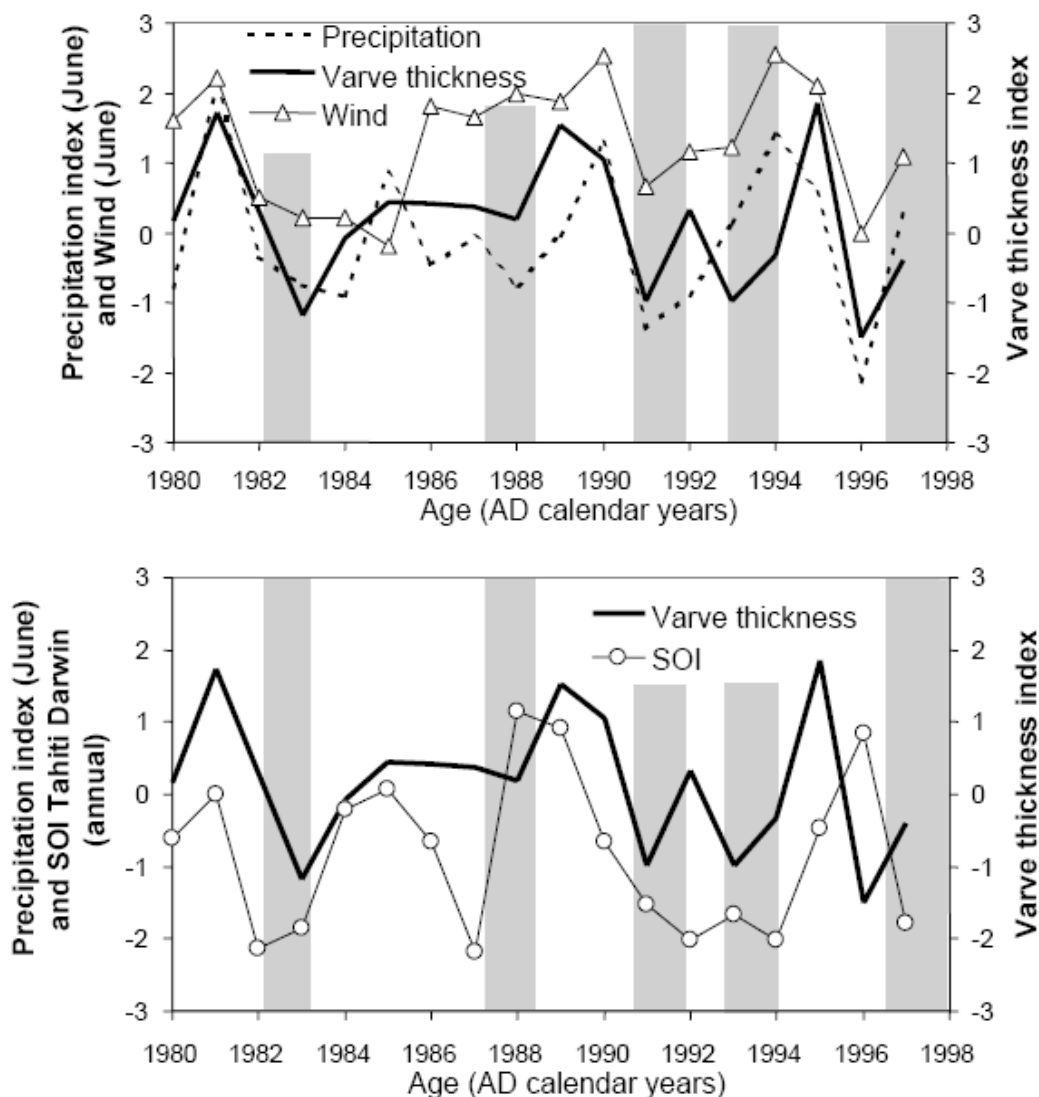


Figure 25: Top: Comparison of the varve-thickness index of PU-I-P3a with precipitation and wind indexes for the 1980-2000 period. Bottom: Comparison of the varve-thickness index of PU-I-P3a with SOI<sub>Tahiti-Darwin</sub>. Grey shading represents El Niño episodes.

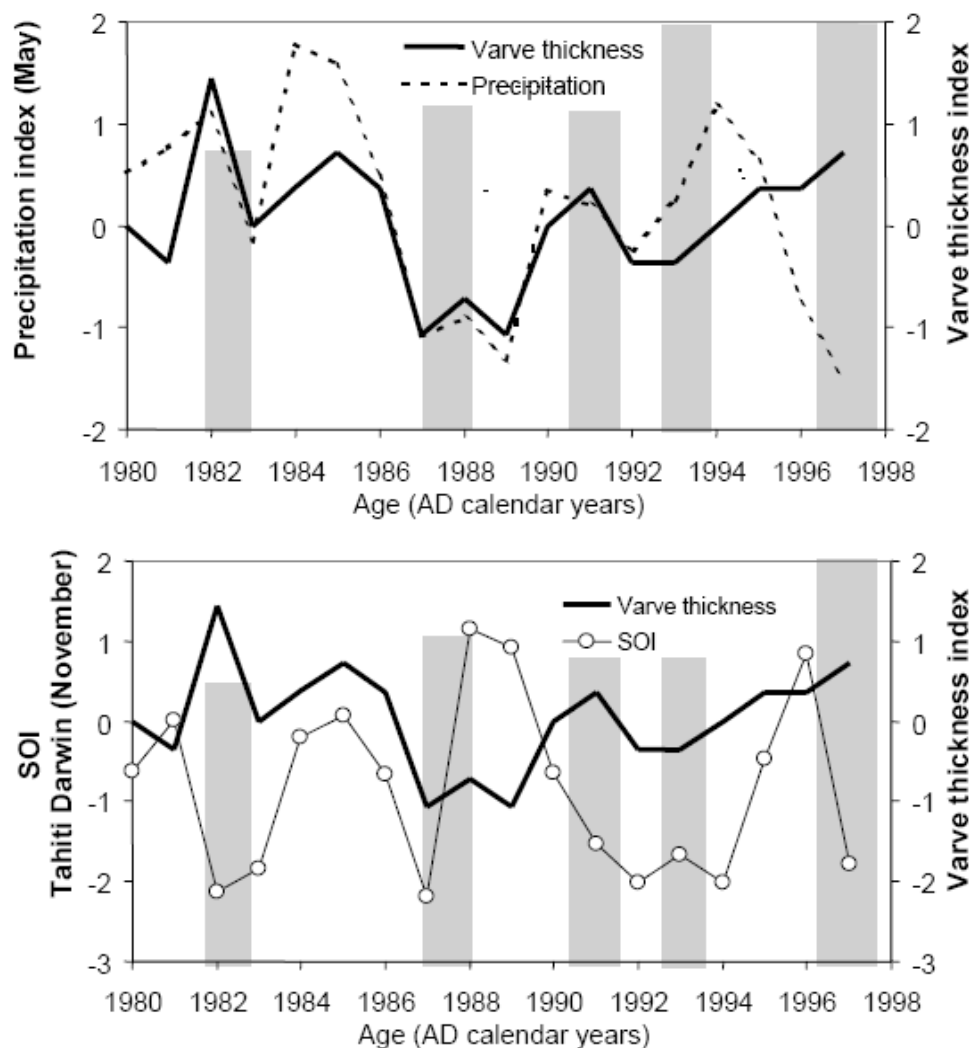


Figure 26: Top: Comparison of the varve-thickness index of PU-II-P5a with precipitation and wind indexes for the 1980-2000 period. Bottom: Comparison of the varve-thickness index of PU-II-P5a with  $SOI_{\text{Tahiti-Darwin}}$ . Grey shading represents El Niño episodes.

### III.3. Discussion

#### III.3.1. A 600 yr record of changes in precipitation in Lago Puyehue

##### Varve-thickness record

The total varve-thickness record of PU-I-P3a (Fig. 27) shows five distinct phases marked by a significant change in the mean varve-thickness values (mean =  $770 \mu\text{m} \pm 730$ ): 1730-1770, 1770-1820, 1820-1920, 1920-1950 and 1950-2000. The total varve-thickness record has four maximum thickness peaks in  $\sim 1722$ ,  $\sim 1845$ ,  $\sim 1923$  and  $\sim 1945$ .

The total varve-thickness record of PU-II-P5a (Fig. 27) shows eight varve-thickness intervals (mean =  $550 \mu\text{m} \pm 280$ ): 1400-1510, 1510-1630, 1630-1730, 1730-1780, 1780-1820, 1820-1920, 1920-1950 and 1950-2000. The intervals in the top part of

the record are similar as those observed in PU-I-P3a. The varve-thickness record shows three maximum thickness peaks in ~1845, ~1895 and ~1944.

#### Regional precipitation changes since 1400

Based on the positive correlation between the varve-thickness index of PU-II-P5a and the precipitation index calculated over the period 1980–2000 period (Fig. 24), the main variations in precipitation over the last 600 yrs can be evaluated (Fig. 27). Estimates of precipitation are derived from correlation with the historical instrumental autumn/winter precipitation datasets from Puyehue (1980-2000) and Valdivia (1900-1980). The long-term (i.e., for the period before 1900) estimates from the varve thickness are constrained by a significant correspondence between the highest varve-thickness index observed in the mid-20<sup>th</sup> century with the precipitation peak in autumn/winter observed during the same time period in the 1900-2000 Valdivia precipitation database (Fig. 27). The varve-thickness record was interpreted in terms of paleo-precipitation based on the differences in the standard deviation. A difference of  $+3\sigma$  to  $+4\sigma$  reflects a maximum precipitation above 700 mm/month in the autumn/winter transition; a difference of  $+2\sigma$  to  $+3\sigma$  corresponds to ~ 600-700 mm/month; a difference of  $+1\sigma$  corresponds to  $+2\sigma$  to ~ 500-600 mm/month; a difference of 0 to  $+1\sigma$  corresponds to ~ 400-500 mm/month; and a difference of 0 to  $-1\sigma$  corresponds to less than  $< 400$  mm/month.

The eight varve-thickness periods identified in the record of the last 600 yrs can be interpreted as follows (Fig. 27):

- (1) From ~ 1400 (bottom of the core) to ~ 1510, the varves are significantly thinner in comparison with those from the upper part of the record ( $-0.7$  and  $-1\sigma$ ). This could be consistent with a period of low nutrient supply (i.e., low primary diatom production) and thus with a dryer period characterized by precipitation minima during autumn/winter months ( $< 400$  mm/month). This could have been further reinforced by a lower lake level during a regional Late Medieval Warm Period. The existence of a Late Medieval Warm Period in the Southern Hemisphere has recently been proposed by Goose et al. (2004) from studies in the Southern Ocean.
- (2) Between ~ 1510 to ~ 1630, the varve-thickness index significantly increases ( $+0.5 \sigma$ ). This increase is interpreted as due to a period of increased autumn/winter precipitation (i.e.,  $>$  above 400 mm/month). This period is characterized by varve-thickness values slightly above the present-day values, suggesting that this period was slightly more humid than the present-day regional climate conditions.
- (3) From ~1630 to ~1730, the varve thickness significantly increases ( $+1.5\sigma$ ). This evolution could be consistent with a heavier autumn/winter precipitation (~ 500 mm/month) and also with a higher lake level in comparison with the present-day lake level.

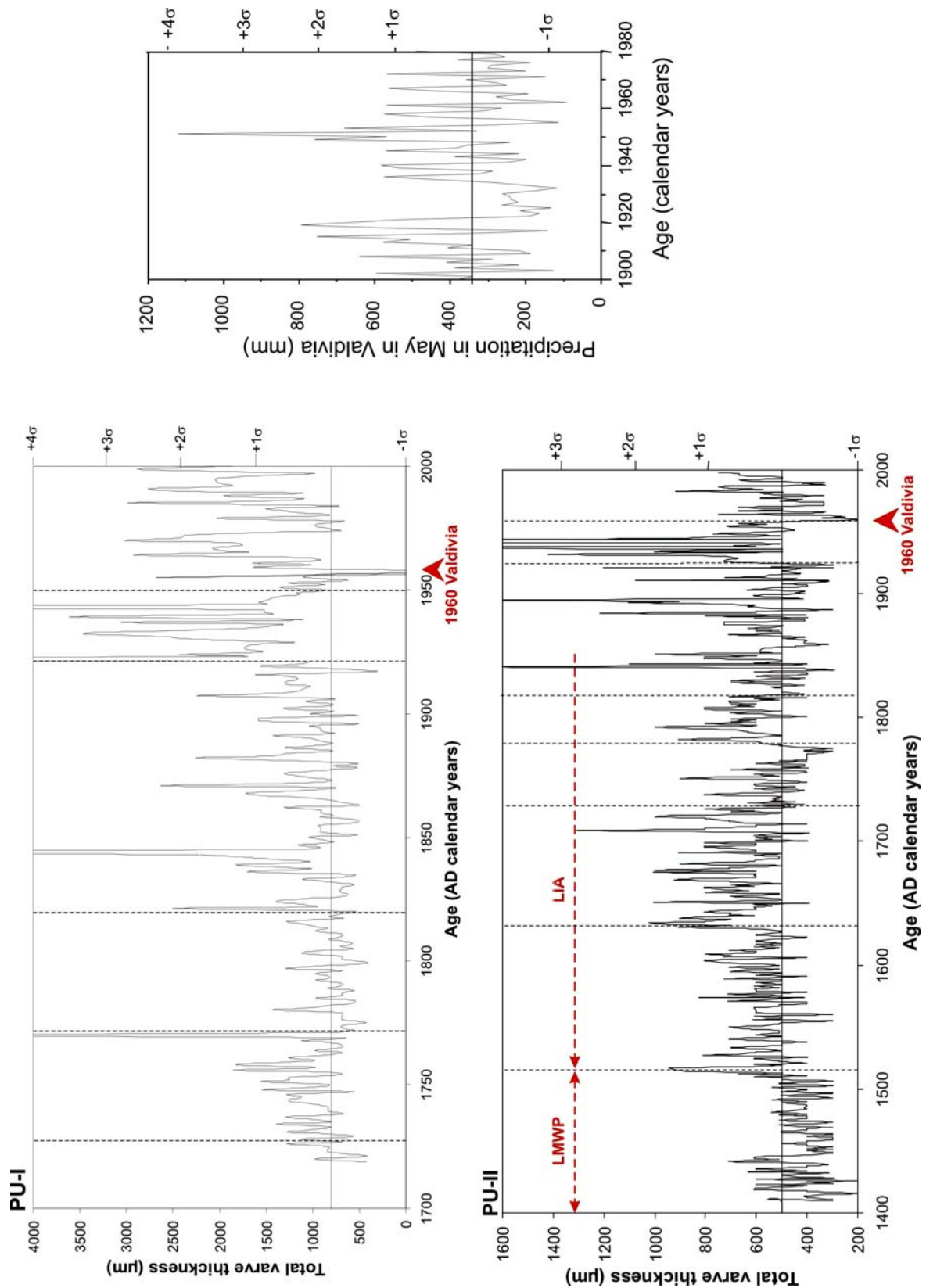


Figure 27: Left above: Total varve-thickness record for core PU-I-P3a (from 1706 to 2000). Left below: Total varve-thickness record for core PU-II-P5a (from 1408 to 2000). Right: Precipitation in May (austral autumn/winter transition) in Valdivia during the 1900-2000 period.

- (4) From ~ 1730 to ~ 1780, a significant decrease in the varve index can be observed (from  $+1\sigma$  to  $-0.5\sigma$ ). This could point to a short period of lower regional precipitation, i.e., dryer autumn/winter with less turbulence and less nutrient turn-over during the winter season.
- (5) From ~ 1780 to ~ 1820, the varve-thickness index increases ( $+1\sigma$ ) suggesting similar humid conditions than during the 1630 -1730 interval.
- (6) From ~ 1820 to ~ 1920, the varve index is lower than during the previous interval, but with a higher-amplitude variability. It may indicate a stronger variability in inter-annual precipitation.
- (7) During the interval between ~ 1920 and ~ 1950, the varve index strongly increases up to  $+3\sigma$ , pointing to an increase in precipitation up to  $> 700$  mm/month. This is consistent with a more humid phase, as observed in the precipitation dataset from Valdivia. For instance, precipitation during the autumn/winter months of the years 1919, 1922, 1926, 1949, 1951, 1953 was almost twice as high as the seasonal average calculated over the 1900-1980 period (i.e., 380 mm for May and June). This could be consistent with a higher lake level.
- (8) Between ~ 1950 and 2000, precipitation in autumn/winter decreased ( $-0.25 \sigma$ ) to present-day conditions close to the 1980-2000 seasonal average (~ 450 mm/month in May in Puyehue).

### ***III.3.2. Spectral analysis of ENSO variability over the last 600 yrs***

#### Dominant climate periodicities in the Lago Puyehue record

An evolutive MTM analysis was performed on the varve-thickness record of PU-I-P3a using a 100-yr long window shifted with a 10-yr step (Fig. 28a). The record covers the time interval between ~1706 and 2000, and contains 294 annual varve-thickness values. There are no clear, strong periodicities throughout the whole time interval. Nevertheless, a weak periodicity of ~ 3.0 yrs appears in a large part of the record, but especially in the recentmost part, as well as a periodicity of ~ 5.2 yrs. A weak periodicity of ~ 23 yrs is also present during most of the 19<sup>th</sup> and 20<sup>th</sup> centuries, although it has an ever lower significance level. This result is mainly related to the rapid and strong variations in the sedimentary record, which appear e.g. at ~ 1770, ~ 1844, ~ 1922 and ~ 1943. These events also clearly stand out in the wavelet transform (Fig. 28b). The wavelet transform also suggests the presence of some other periodicities: i.e., 22-24 yrs and 60-78 yrs.

Combining the different methods applied on the complete record, the following periodicities appear to be present with some degree of significance (although they may appear only in part of the record): 24, 12.6, 3.0, 2.7 and 2.1 yrs. The MTM-reconstructed signal based on the major periods identified by this method explains 18 % of the original signal.

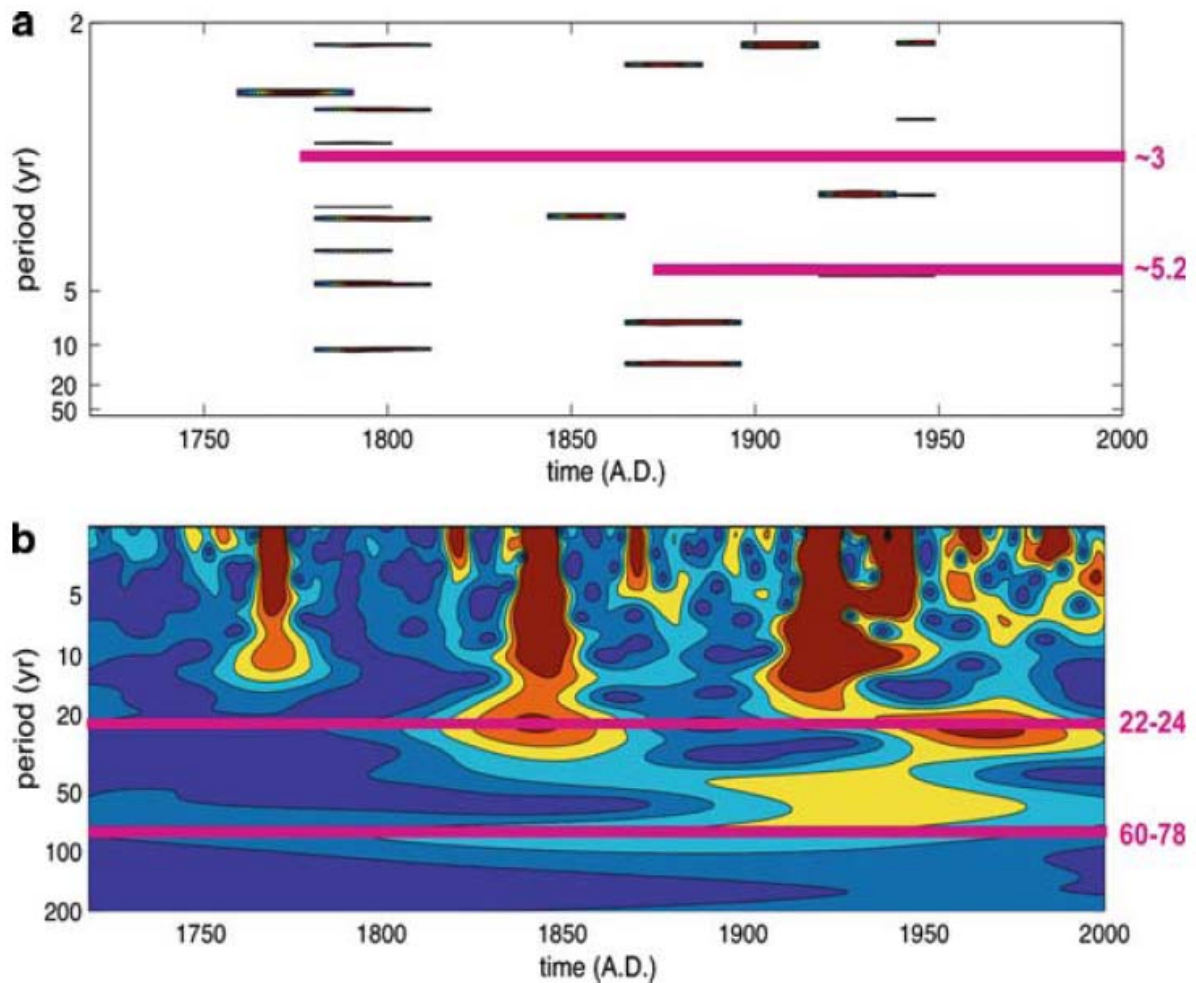


Figure 28: a) Evolutive MTM spectrum of the varve-thickness series of PU-I-P3a. Only the period at 90% significance level or higher are displayed. The bandwidth parameter is  $p = 5$ , and  $K = 7$  tapers are used. Dark lines indicate the time interval (X-axis) over which a periodicity (Y-axis) is identified. (b) PU-I wavelet analysis of the varve-thickness series of PU-I-P3a.

The varve-thickness record of PU-II-P5a covers the time interval between  $\sim 1408$  and 1998, and contains 590 annual varve-thickness values. The MEM estimate for the varve thickness record is computed using a number of lags (order of regression) of 20, 30 and 40. Fig. 29 clearly shows that the number of potentially spurious peaks increases with  $M$ . The more robust ones are at around 15, 9, 4.4, 3.2 and 2.4 yrs. These periods were confirmed by the Blackman-Tuckey and MTM methods (Fig. 29). Moreover MTM also identify a longer period around 43 yrs, possibly divided in two periods. The periods around 4.4, 3.0 and 2.4 yrs, as well as a period around 2.25 yrs are significant at the 95 % level, or more. The trend component identified in MTM captures 18 % of the total variance of the signal. The SSA method allows the reconstruction of the trend and oscillatory part of the signal. This reconstructed signal, which captures 39 % of the total variance of the signal, is characterized by periods of  $\sim 256$ ,  $\sim 78$ ,  $\sim 41$  and  $\sim 14$  yrs.

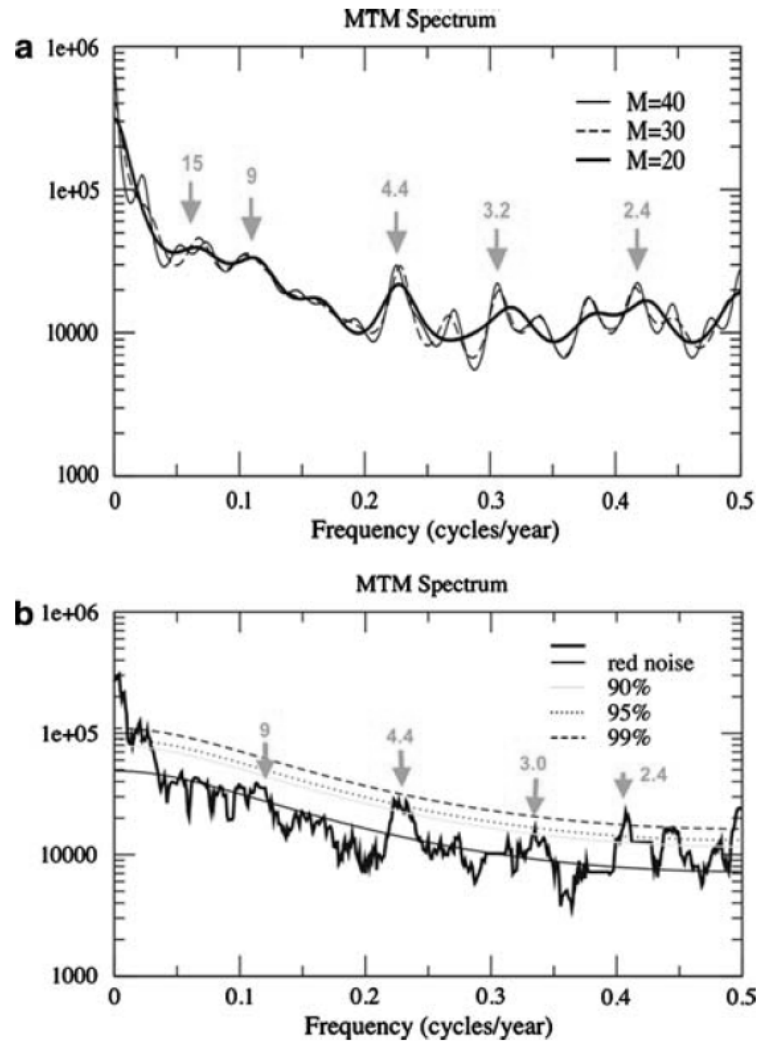


Figure 29: (a) Spectral estimate of the varve-thickness series of PU-II-P5a by the maximum entropy method. The autoregression orders are  $M = 40$ , 30 and 20 (light, dashed and thick curves, respectively). (b) MEM spectrum of the varve-thickness series of PU-II-P5a. The estimated red-noise background and associated 90, 95 and 99 % significance level are shown by the smooth curves. The bandwidth parameter is  $p = 5$ , and  $K = 7$  tapers are used.

Also an evolutive MTM analysis was performed using a 100-yr long window shifted with a 20-yr step (Fig. 30a). There is a striking break in the periodicities at around 1820. Most of the periods present before 1820 fade away to the benefit of new periodicities after this transition. From 1500 to 1700 there is a periodicity decreasing from 8.8 to 6.5 yrs. The periodicity at 4.4 yrs shows up at 1550 and decreases to 4.0 yrs at 1820. There are several periods shorter than 3 yrs: a.o., 2.6 yrs from 1500 to 1700, and 2.2 yrs from 1700 to 1860. This is one of the few highly significant periodicities to appear before and after 1820. Other periods are also identified after 1820: i.e.,  $\sim 21$  and  $\sim 3$  yrs. The wavelet analysis (Fig. 30b) identifies longer periods: a period of  $\sim 40$  yrs during the 15<sup>th</sup> century, a period of 31 yrs in the 17<sup>th</sup> century, increasing towards 35 yrs during the 18<sup>th</sup> century, and a 50-yr periodicity during the early 20<sup>th</sup> century. The method also identifies a 13-yr period during the 18<sup>th</sup> century and a 21-yr period during the 19<sup>th</sup> century.

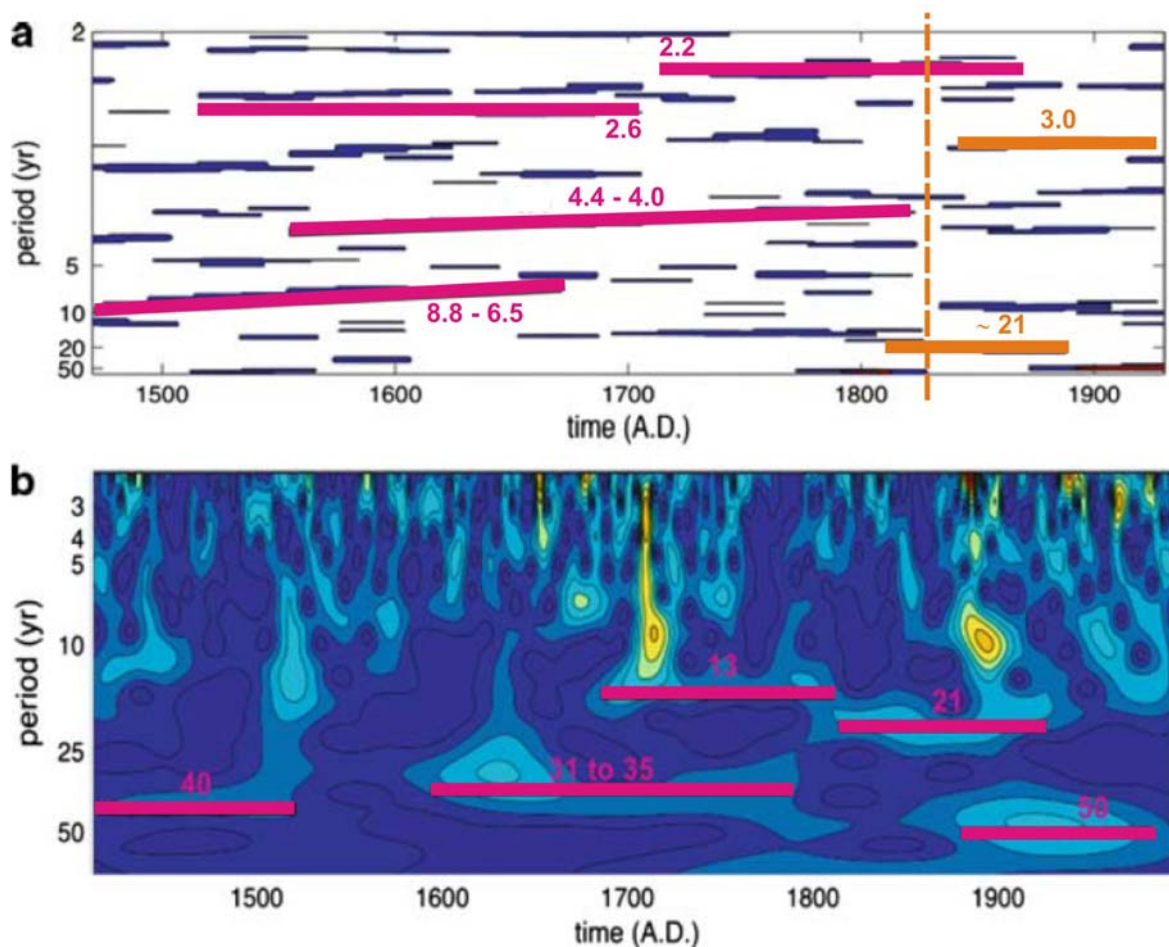


Figure 30: (a) Evolutive MTM spectrum of the varve-thickness series of PU-II-P5a. Only the periods at 90 % significance level or higher are displayed. The bandwidth parameter is  $p = 5$ , and  $K = 7$  tapers are used. Dark lines indicate the time interval (X-axis) over which a periodicity (Y-axis) is identified. (b) Wavelet analysis of the varve-thickness series of PU-II-P5a.

### A 600 yr record of ENSO-related periodicities and links with other climate modes

The spectral analyses performed on the Lago Puyehue high-resolution records reveal periodicities that are consistent with periodicities reported from a 2100 yr marine varved record from the North Pacific: i.e., Saanich Inlet, British Columbia (49°N) (Dean and Kemp 2004). The Saanich Inlet varve record displays periods at 2.5, 3.6 and 14.8 yrs, which were linked to QBO, ENSO and PDO, respectively (Dean and Kemp 2004). In the Lago Puyehue record, the observed frequency bands at 2.25 and 2.4 yrs can be related to QBO. The peaks of 3, 3.2, 4 yrs are in very good agreement with the most common periodicity of the El Niño phenomenon, which occurs every ~ 3-4 years in the Equatorial Pacific Ocean. Indeed the ENSO band is usually taken between 2-7 years (Cane 2005). In addition, the QBO signal is known to be a fundamental element in regulating ENSO variability (Rasmusson et al. 1990). The 15-yr periods identified in Lago Puyehue could be also relevant of the PDO. Finally the ~ 8-9 yrs band could be interpreted also as an alternate of weaker/stronger El Niño and stronger/weaker La Niña events in connection with solar

activity (Dean and Kemp 2004). In both Saanich Inlet and Lago Puyehue the multi-decadal periods at, respectively, 42.2 and 41 yrs might suggest harmonics of the PDO (Dean and Kemp 2004). Links between the South and North Pacific Oceanic circulation can be estimated from the Sea-Level Pressure (SLP) index. For instance, the North Oscillation Index (NOI) is the North Pacific counterpart of the Southern Oscillation Index (SOI, Schwing et al. 2002) and both SOI and NOI are dominated by inter-annual variations related to El Niño and La Niña events (Schwing et al. 2002).

### ***III.3.3. Precipitation and ENSO variability during millennium-scale abrupt climate changes***

#### ENSO variability during millennium-scale abrupt climate changes: the Little Ice Age

Of all millennium-scale abrupt climate changes that have been observed in Holocene climate records from the Northern Hemisphere, only the Little Ice Age (LIA) has been reported from several sites in South America and appears to have had a regional impact. The LIA in South America ranges from the 13<sup>th</sup> to the 19<sup>th</sup> century, but with variable regional duration and either a dry or wet climate response (Markgraf et al. 2000). For example, the Quelccaya ice-core record (14°S) shows that onset of the LIA in Peru was marked by an increase of net ice accumulation in the period between ~ 1480 and 1880 (Thomson et al. 1986).

The evolutive MTM analysis of the Lago Puyehue varve-thickness record shows a 4.4- to 4-yr periodicity (with 95 % level significance) between ~ 1550 to 1820 (i.e. during the LIA interval) (Fig. 30a). These 4.4 to 4 yr frequency bands are spectrally coherent with the El Niño phenomenon. It can therefore be inferred that the LIA in Lago Puyehue was characterized by an enhanced El Niño response: i.e., by significant precipitation deficits during the usual wetter season (austral autumn-winter transition).

#### A varve-thickness record of a Late-Glacial millennium-scale abrupt climate change: the Huelmo/Mascardi Cold Reversal

Apart from the PU-I-P3a and PU-II-P5a short cores, also a segment of the PU-II long core was examined in high resolution. This segment (from ~750 cm to ~1,113 cm core depth, in total ca. 3.5 m core length) is composed of laminated sediments characterized by glacial varve-like couplets (Fig. 31). A couplet is defined by two distinct layers, which represent sediment accumulated during one full season (~0.2 to 0.8 mm/yr): i.e., a high-reflectance (light-colored), phytoplankton-rich layer (Figs. 31, 32), and a low-reflectance (dark-colored) layer rich in terrigenous material (Figs. 31, 32). The investigated segment represents a regular varve increment undisturbed by turbidites, gas, or bioturbation.

A tephra layer at 774 cm clearly marks the top of the varve sequence (T1 in Fig. 33), and the age of the top of the studied varve sequence (i.e., at 767 cm) is 10,855 cal. yr BP, as calculated from the AMS <sup>14</sup>C age model (Fig. 7). In the studied varve sequence, 6,309 varve years were counted manually (i.e., between 10,855 and

17,163 cal. yr BP, Fig. 33), against 6,279 as counted semi-automatically using the grey-scale method.

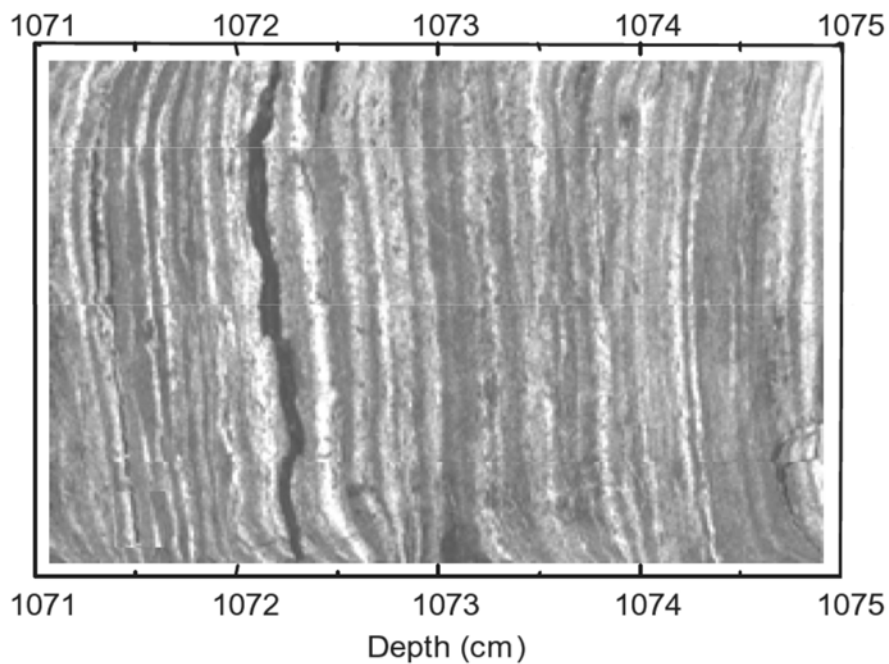


Figure 31: Micromorphological picture of core section between 1,071 and 1,075 cm core depth after varve pre-treatment.

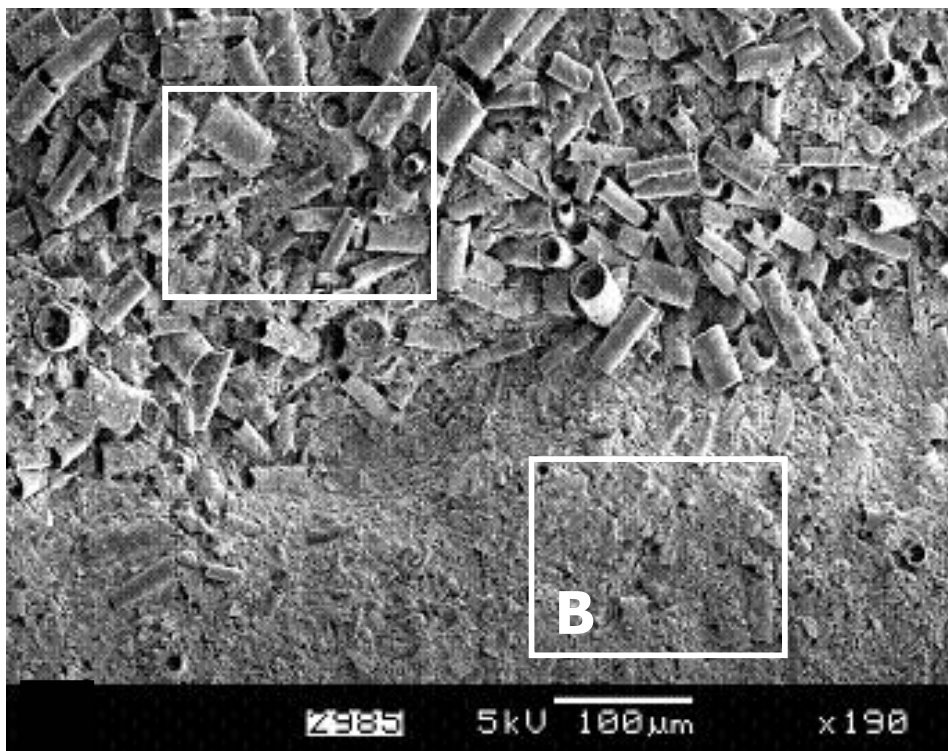


Figure 32: Micromorphological picture of core section between 1,071 and 1,075 cm core depth after varve pre-treatment. (A) Diatom layer. (B) Layer rich in organic matter.

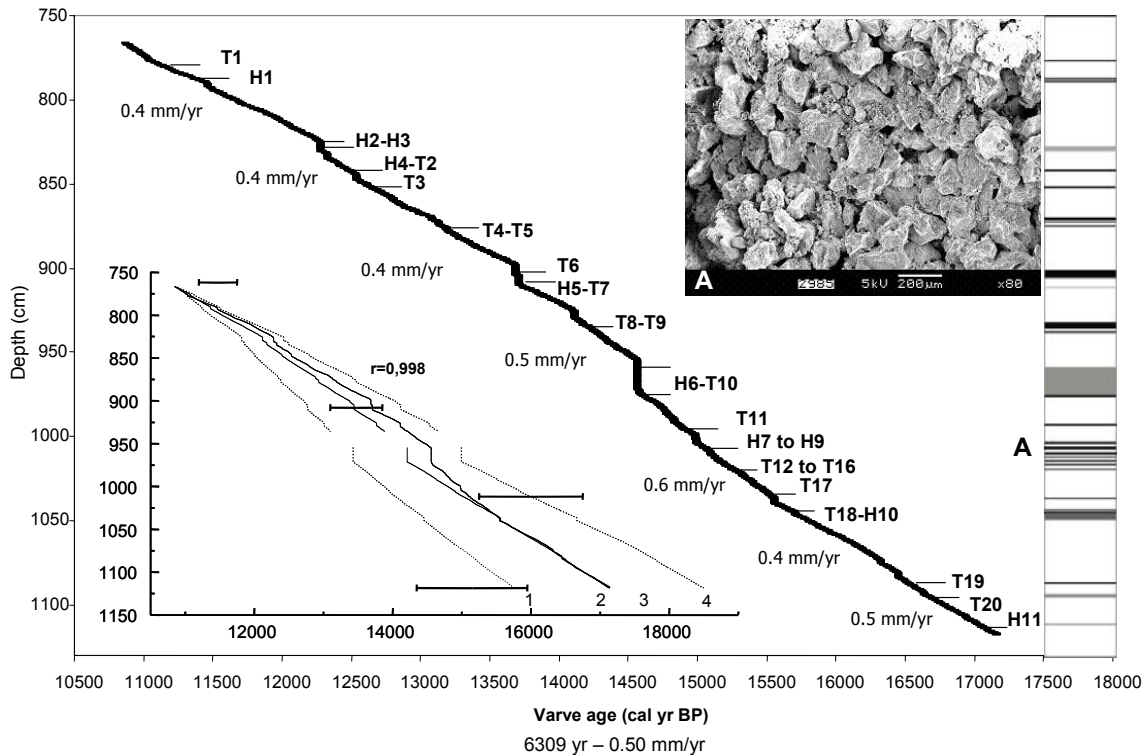


Figure 33: Varve chronology for the time-window 17,150-10,855 cal. yr BP derived from manual varve counting and corrected for intercalated deposits (which are indicated in the schematic stratigraphic column of the studied core on the right diagram): T = tephra layers, H = homogenite/seismically induced layers. Inset curve: manual and semi-automatic varve ages represented according to the four radiocarbon dated levels of the studied core sequence. 1 = 125  $\mu$ m filter, 2 = varve ages obtain by semi-automatic counts from the two filters, 3 = varve age obtain by the standard varve counting method, 4 = 100  $\mu$ m filter. The age error bars are presented in Fig. 34.

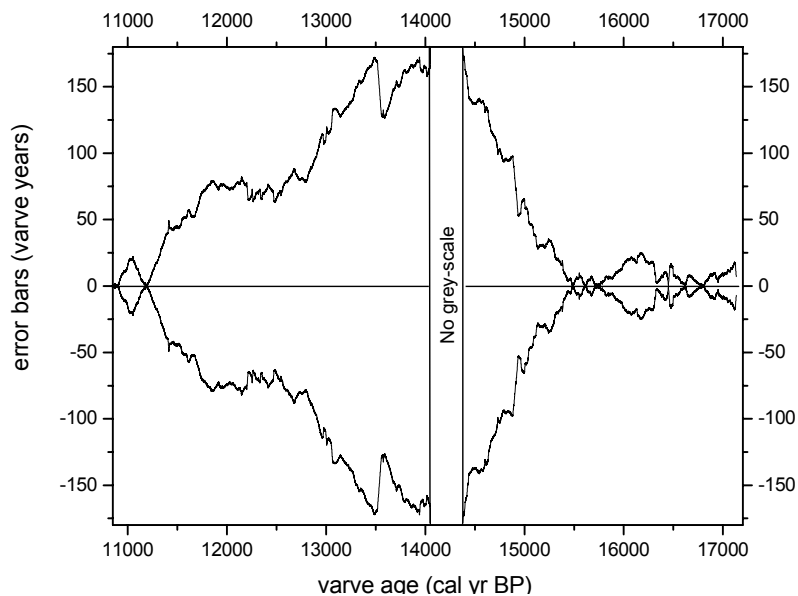


Figure 34: Assessment of the error bar on the varve-age estimation, calculated from the manual and semi-automatic varve-counting methods.

In the studied interval, the sedimentation rates vary between ~ 0.2 and 0.8 mm/yr (mean ~ 0.5 mm/yr), with higher sedimentation rates observed between ~ 15,100 and 14,500 cal. yr BP (Fig. 33). A number of homogeneous intercalated units (> 2 cm thick) occur at 15,550 cal. yr BP (H10), 14,560 cal. yr BP (H6), 13,710 cal. yr BP (H5), ~ 12,300 cal. yr BP (H2). In addition, two main volcanic layers occur at 14,100 cal. yr BP (T8) and 13,680 cal. yr BP (T6) and a period marked by a more frequent regional volcanic activity is manifested between ~ 15,500 and 14,980 cal. yr BP (T12 to T16) (Fig. 33).

The climatic interpretation of this record is based on the standardized annual grey-scale index and on variations in the annual thickness of the varves:

- The grey-scale values provide an indication of the accumulation of terrigenous versus biogenic components. When the diatom productivity is reduced (e.g., during cold phases), the resulting annual varve will be relatively enriched in terrigenous material and yield a negative grey-scale index. For most of the varve record the negative/positive grey-scale index mirrors the evolution of the dark/light varve thickness: i.e., when the dark (light) varve layer is thicker, the grey-scale index becomes negative (positive).
- The thickness of the biogenic varves in the more recent sediments of Lago Puyehue is mainly driven by strong winter precipitation, as increased winter precipitation causes an increase in the terrigenous supply into the lake as well as an increase in the nutrients, leading to thicker varves. In contrast, dry winters cause a reduction the terrigenous supply and in the water mixing, leading to less biogenic productivity and thinner varves.

Accepting a negative(positive) grey-scale index as evidence for cold(warm) climate, and thick(thin) varves as evidence of humid(dry) climate, the studied interval allows a high-resolution reconstruction to be made of climate variability between 17,200 to 11,000 cal. yr BP. Five main periods can be identified (Fig. 35):

- 17,200 to 16,150 cal. yr BP: this period is characterized by darker and thicker (negative annual grey-scale index, > 270  $\mu\text{m}$ ) varve couplets, which indicates a cold and humid climate phase.
- 16,150 to 15,500 cal. yr BP: during this period the varves remain dark but become slightly thinner (< 270  $\mu\text{m}$ ), which is consistent with a cold but dryer climate phase.
- 15,500 to 13,300 cal. yr BP: the varve record during this period reflects an instable climate with short, cold and warm pulses, as indicated by the oscillation of the grey-scale index. The period between 15,000 and 14,500 cal. yr BP is colder.
- 13,300 to 12,200 cal. yr BP: this period is generally characterized by darker and thicker varves. Detailed evaluation of the varve grey-scale index and varve thickness indicates the presence of two colder and wetter phases (~ 13,300-12,900 cal. yr BP, and ~ 12,500-12,200 cal. yr BP), separated by a dryer and warmer period (~ 12,800-12,600 cal. yr BP).

- 12,200 to 11,000 cal. yr BP: during this period, the varves are light and thin, which is consistent with a warm and dry climate (positive annual grey-scale index, < 270  $\mu\text{m}$ ). The warming significantly increases after  $\sim 11,500$  cal. yr BP.

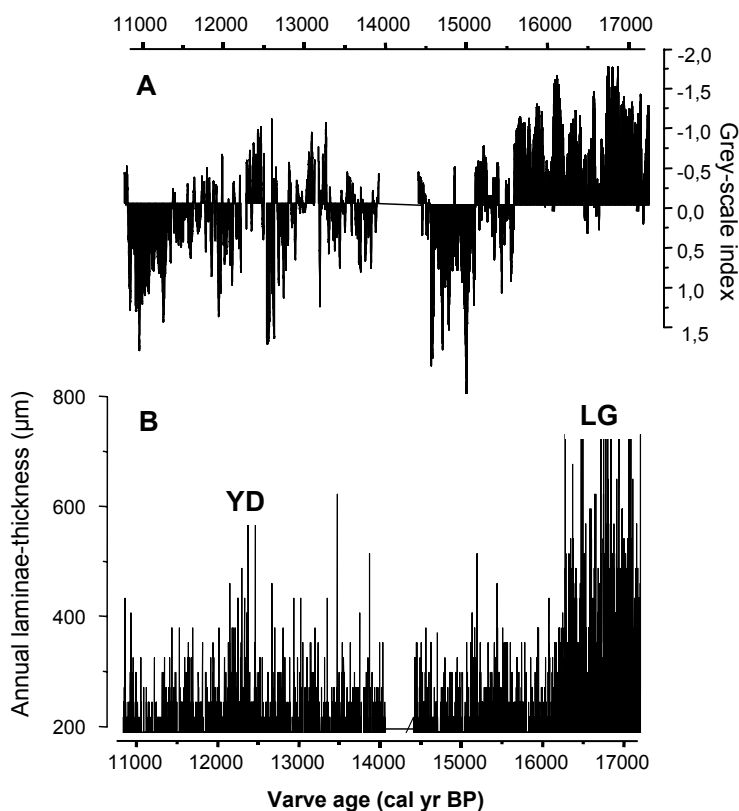


Figure 35: Smoothed annual grey-scale index and annual laminae thickness records between 17,200 and 10,850 cal. yr BP. YD = Younger Dryas, LG = Late Glacial.

This new varve record thus shows the occurrence of a distinct cold and humid period between  $\sim 13,300$  and  $\sim 12,200$  cal. yr BP, characterized by low grey-scale values (negative index) and higher varve thicknesses. This period coincides with the cold and humid interval identified in the PU-II long core based on sedimentological and geochemical analysis (i.e., at 13,100-12,300 cal. yr BP, chapter II.3.3) and which was interpreted as the local/regional expression of a Younger-Dryas-like Late-Glacial cold reversal. The high-resolution varve data demonstrate that this cold reversal actually consisted of two separate cold/humid phases ( $\sim 13,300$ -12,900 cal. yr BP and  $\sim 12,500$ -12,200 cal. yr BP), interrupted by a warmer event at  $\sim 12,800$ -12,600 cal. yr BP.

The first cold/humid phase appears to be synchronous with the final part of the Antarctic Cold Reversal as recorded in the Byrd ice core (Blunier et al. 1998), while the second cold/humid phase falls within the first part of the Younger Dryas event as recorded in several records in the Northern Hemisphere (e.g., Stuiver et al. 1995, Hughen et al. 1998) (Fig. 36). The timing of the cold phase between  $\sim 13,300$  and 12,900 cal. yr BP is in good agreement with that of the Huelmo/Mascardi Cold Reversal (Hajdas et al. 2003). The short climatic interruption of this cold reversal,

with warm and dry climate between ~ 12,800 and 12,600 cal. yr BP, attests that local disturbances may have affected the Late-Glacial climate evolution in south-central Chile, as also proposed by Moreno et al. (2001).

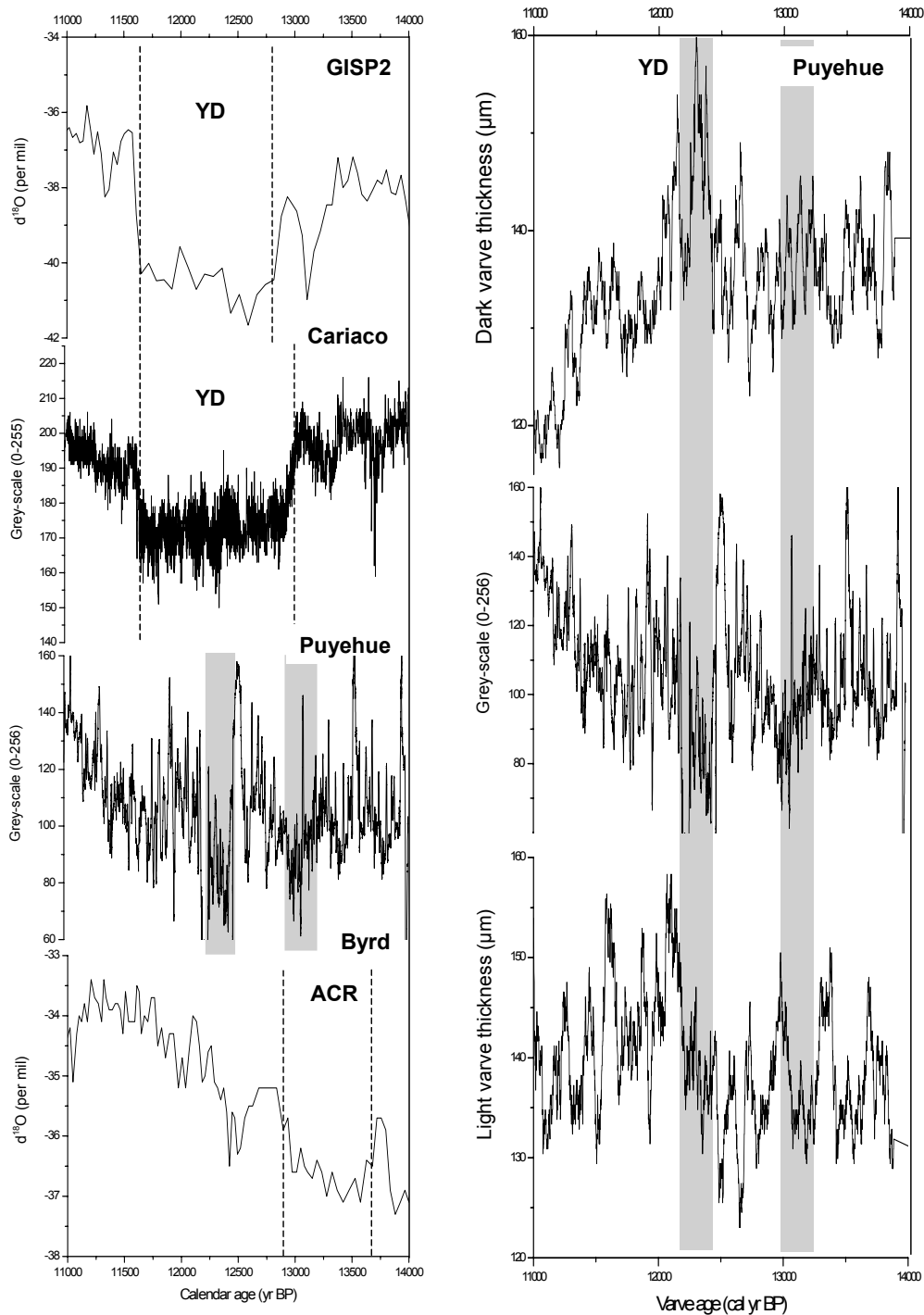


Figure 36: Comparison between the Lago Puyehue annual varve record with other annual-resolution records (i.e., ice cores and marine) along a North-South transect during the Late Glacial period.

#### IV. CONCLUSIONS

- The deep, glacial lakes of the Chilean Lake District do have the potential to contain a unique, long and high-resolution continuous sedimentary record of regional changes in climate. As such, this sequence of lakes, extending from North to South over a distance of 500 km, offers the possibility to yield a unique series of records, which will allow tracing climate evolution in South America across a wide latitudinal belt.
- An extensive regional study of several lakes in the Lake District (i.e., in terms of size, depth and limnological characteristics) and of their catchments (i.e., in terms of size, extent, geology, vegetation, etc.), resulted in the selection of one "master lake" for the further execution of the project: Lago Puyehue (40°40'S).
- The selection of the most suitable location for the collection of a long sediment core in Lago Puyehue was based on a thorough site investigation, involving high-resolution seismic profiling, short sediment coring and a multi-proxy study of the catchment, and on a good understanding of the lake dynamics and limnology, its geology and morphology, and the key meteorological factors.
- The long sediment core from Lago Puyehue extends back to 17,915 cal. yr BP and parts of it are annually laminated or varved. It thus contains both a long-term and a high-resolution record of regional climate change.

#### **Question 1: What are the effects of ENSO along the Pacific coast of southern South America ?**

- Regional climate around Lago Puyehue is dominated by the southern Westerlies and associated strong precipitation. Precipitation peaks during the transition from austral autumn to winter and during winter months. El Niño episodes are expressed as periods of reduced precipitation compared to normal years. Detailed analysis of available instrumental data shows the El-Niño-triggered precipitation anomalies to have the strongest expression during autumn/winter transition (as opposed to during the summer periods, as suggested in previous studies).
- The Westerly-driven precipitations also exert a strong control on the sedimentary processes in Lago Puyehue. Precipitation controls the amount of terrigenous material brought into the lake, and determines turn-over of the lake, nutrient cycling and primary productivity of phytoplankton. Diatom primary productivity is the dominant factor determining the thickness of the annual laminations. Varve-thickness records, in combination with varve color intensity (as revealed by grey-scale measurements) can thus be used as a proxy for precipitation and as a tracer of El Niño activity over time.

- Spectral analysis of varve-thickness and grey-scale records over the last 600 yrs reveal several multi-annual periodicities (i.e., 3, 3.2, 4 yrs). The dominant period over the last 100 yrs is that of 3 yrs. This periodicity is consistent with the most common frequency of the El Niño phenomenon, which occurs every ~ 3-4 yrs in the Equatorial Pacific Ocean.

**Question 2: Are multi-decadal cycles also present in the South Pacific and do they correlate with Northern Hemisphere ones ?**

- Spectral analysis of varve-thickness and grey-scale records over the last 600 yrs also reveals other multi-annual (i.e., 2.4 yrs) but also decadal (15 yrs, 41 yrs) periodicities. These are consistent with other southern Pacific indexes (QBO, PDO), and also with North Pacific oscillations (PNI or NOI).

**Question 3: Is the post-LGM period in southern South America also characterized by millennium-scale abrupt climate changes and do they relate to the tropical and/or the North Atlantic ones ? What is the long-term evolution of the ENSO system through the Holocene ?**

- The age of the base of the long core in Lago Puyehue is 17,915 cal. yr BP. Seismic-facies analysis in combination with extrapolation of sedimentation rates puts the age for the onset of open-water conditions in Lago Puyehue at ca. 28,000 cal. yr BP. This is in stark contrast with glacial-history reconstructions based on terrestrial records, which date the complete deglaciation of the basin as ca. 14,600 cal. yr. BP. This discrepancy cannot be easily explained. New lacustrine records are required to test the validity of our record and to resolve the apparent contradiction between the lacustrine and terrestrial records.
- A multi-proxy analysis of this much-longer-than-expected record, involving sedimentology, geochemistry, pollen and diatom analysis, reveals a number of climate fluctuations and shifts that are superimposed on a gradual and continuous climate improvement since the LGM (i.e., over the last 17,915 cal. yr BP). Among these climate fluctuations are: i) a first warming pulse sometime between 19,500 and 17,150 cal. yr BP, ii) a well-marked cold and humid interval at 13,100-12,300 cal. yr BP, roughly coeval with the Huelmo/Mascardi Cold Reversal, iii) a second pulse towards warmer and dryer conditions between 12,300 and 11,800 cal. yr BP, marking the onset of the Holocene, iv) warm and dry climate conditions between 11,800 and 7,800 cal. yr BP, reflecting an early Holocene climatic optimum, v) relatively stable climate conditions since 7,800 cal. yr BP, except for vi) an interval of cold and/or humid conditions at 3,400-2,900 cal. yr BP, and vii) a distinct wet period during the interval 1490-1700.
- The cold and humid interval at 13,100-12,300 cal. yr BP resembles other Late-Glacial cold reversals that have been documented both in the Northern and the Southern Hemisphere, but it is out of phase with them: i.e., it precedes the Northern-Hemisphere Younger Dryas by about 500 yrs, and post-dates the Antarctic Cold Reversal (i.e., 14,500 to 12,800 cal. yr BP) by about 1,400 yrs. It is roughly coeval with the Huelmo/Mascardi Cold Reversal (i.e., 13,475 to 12,000

cal. yr BP). Future records from further south in South America may reveal the exact link between this South American Huelmo/Mascardi Cold Reversal and the Antarctic Cold Reversal and may thus hold the key to a better understanding of the regional and interhemispheric teleconnections during millennium-scale abrupt climate changes.

- High-resolution analysis of varve-thickness and varve grey-scale records shows that this cold and humid reversal in fact consists of two separate cold phases (i.e., 13,300-12,900 cal. yr BP and ~ 12,500-12,200 cal. yr BP), interrupted by a warm and dry period.
- The period with warm and dry climate conditions, detected between 11,800 and 7,800 cal. yr BP, confirms the presence of an early Holocene climatic optimum in southern South America.
- The interval of cold and/or humid conditions at 3,400-2,900 cal. yr BP has not been detected in other records from Chile, although evidences exist for a period of climate change during this period from elsewhere in South America and in many places of the World. Climate disturbances around this period are generally attributed to changes in solar activity.
- The wet period during 1490-1700 is interpreted as the regional expression of the Little Ice Age in the area of the Lake District. In terms of timing, it is largely coeval with other cold and/or wet periods detected in other parts of Chile or South America, which have been attributed to the Little Ice Age. Spectral analysis of varve-thickness and grey-scale records shows that the most robust signal periodicity of all appears in the record exactly during this period: 4.4 to 4 yrs, which is coherent with El Niño phases in the Equatorial Pacific Ocean. The overall wet climate of the Little Ice Age, appears thus to result from successive pronounced El Niño events.



## ACKNOWLEDGEMENTS

This study was carried out with support from the Belgian Federal Science Policy Office (BELSPO) through project EV/12/10 "*A continuous Holocene record of ENSO variability in southern Chile*". Additional financial support was provided through the Chilean Millennium Science Initiative (Nuclei FORECOS, N° P04-065-F), the bilateral scientific and technical cooperation programme of Flanders with Chile, the Fonds National de la Recherche Scientifique (FNRS), the Patrimoine de l'Université de Liège and the Commissariat général aux Relations internationales de la Communauté française de Belgique (CGRI), as well as through Ph.D and post-doc grants (FNRS-FRIA, FWO – Flanders).

Many people have been instrumental for the success of this project, by providing collaboration during field-work, technical assistance or analytical resources, and by being available for stimulating discussions and for the sharing of data and ideas: a.o., Robert Brümmer (Universidad Austral de Chile, Valdivia, Chile), Maria Mardones, Waldo San Martin and Alejandro Peña (EULA, Universidad de Concepción, Chile), Christian Beck, Marc Tardy, Fabien Arnaud and Vincent Lignier (Université de Savoie, Chambéry, France), Olivier Magand (Université de Grenoble, Saint Martin d'Hères, France), Hedi Oberhänsli (GeoForschungsZentrum Potsdam, Germany), Mike Sturm (EAWAG, Dübendorf, Switzerland), Anna Pazdur and Natalia Piotrowska (Silesian University of Technology, Gliwice, Poland), Anson MacKay (University College London, UK), Henry Hooghiemstra (Universiteit van Amsterdam, the Netherlands), Chantal Tribolo (LSCE, Paris, France), Koen De Rycker, Koen Sabbe, Griet Terryn, Pieter Vanormelingen (Universiteit Gent), Jean-Jacques Garroi (Universiteit Antwerpen), Frédéric Boulvin, Bernard Charlier, Jean-Paul Culus, Thomas Gerards, Philippe Gerienne, Marcella Giraldo, Fernand Noebert, André Rulmont, Philippe Steemans, Michel Vanguetaine and Cécile Wastiaux (Université de Liège) and Christian Dupuis (Faculté Polytechnique de Mons).



## REFERENCES

- Ariztegui, D., Bianchi, M.M., Masferro, J., Lafargue, E. & Niessen, F., 1997. Interhemispheric synchrony of Late-glacial climatic instability as recorded in proglacial Lake Mascardi, Argentina. *Journal of Quaternary Science*, **12**, 333-338.
- Arnaud, F., Magand, O., Chapron, E., Bertrand, S., Boës, X., Charlet, F., Mélières, M.-A., 2006. Radionuclide dating ( $^{210}\text{Pb}$ ,  $^{137}\text{Cs}$ ,  $^{241}\text{Am}$ ) of recent lake sediments in a highly active geodynamic setting (Lakes Puyehue and Icalma—Chilean Lake District). *Science of the Total Environment*, **366**, 837-850.
- Battarbee, R.W. & Kneen, M., 1982. The use of electronically counted microspheres in absolute diatom analysis. *Limnology and Oceanography*, **27**, 184-188.
- Bentley, M., 1996. The role of lakes in moraine formation, Chilean Lake District. *Earth Surface Processes and Landforms*, **21**, 493-507.
- Bentley, M.J., 1997. Relative and radiocarbon chronology of two former glaciers in the Chilean Lake District. *Journal of Quaternary Science*, **12**, 25-33.
- Bertrand, S., Boës, X., Castiaux, J., Charlet, F., Urrutia, R., Espinoza, C., Charlier, B., Lepoint, G. & Fagel, N., 2005. Temporal evolution of sediment supply in Lago Puyehue (Southern Chile) during the last 600 years: climatic significance. *Quaternary Research*, **64**, 163-175.
- Bertrand, S. & Fagel, N., (in press). Nature, origin, transport and deposition of andosol parent material in south-central Chile (36-42°S). *CATENA*.
- Blackman, R.B. & Tukey, J.W., 1958. *The Measurement of Power Spectra From the Point of View of Communication Engineering*, Dover, Mineola, N.Y.
- Blinn, D.W., Hevly, R.H. & Davis, O.K., 1994. Continuous Holocene record of diatom stratigraphy, paleohydrology, and anthropogenic activity in a spring-mound in southwestern United-States. *Quaternary Research*, **42**, 197-205.
- Blunier, T. & Brook, E.J., 2001. Timing of millennial-scale climate change in Antarctica and Greenland during the last glacial period. *Science*, **291**, 109-112.
- Blunier, T., Chappellaz, J., Schwander, J., Dallenbach, A., Stauffer, B., Stocker, T., Raynaud, D., Jouzel, J., Clausen, H.B., Hammer, C.U. & Johnsen, S.J. 1998. Asynchrony of Antarctic and Greenland climate change during the last glacial period. *Nature*, **394**, 739-743.
- Boës, X. & Fagel, N., 2005. Impregnation method for tracking annual laminations in sediment cores: an overview. *Sedimentary Geology*, **179(3-4)**, 185-194.
- Bologne, G. & Duchesne, J.-C., 1991. Analyse des roches silicatées par spectrométrie de fluorescence X : précision et exactitude. *Professional Paper of the Belgian Geological Survey*. Brussels, 11 pp.
- Bradley, R.S., Briffa, K.R., Cole, J., Hugues, M.K. & Osborn, T.J., 2003. The climate of the Last Millenium. In: Pedersen, T.S. (Ed.), *Paleoclimate, Global Change and the Future*. Springer, Berlin, pp. 105-141.
- Brauer, A., 2004. Annually laminated lake sediments and their palaeoclimatic relevance. In: Fischer, H., Kumke, T., Lohmann, G., Flöser, G., Miller, H., von Storch, H. & Negendank, J.F.W. (eds.) *The Climate in Historical Times. Towards a Synthesis of Holocene Proxy Data and Climate Models*. Springer, pp. 109-128.
- Brauer, A. & Negendank, J.F.W., 2002. The value of annually laminated sediments in palaeoenvironment reconstructions. *Quaternary International*, **88**, 1-3.

- Brindley, G.W. & Brown, G., 1980. *Crystal structures of clay minerals and their x-ray identification*. Mineralogical Society Monograph, London, Vol. 5, 495 pp.
- Broomhead, D.S. & King, G.P., 1986. Extracting qualitative dynamics from experimental data. *Journal of Physics D.*, **20**, 217-236.
- Bronk Ramsey, C., 2001. Development of the Radiocarbon program OxCal. *Radiocarbon*, **43(2A)**, 355-363.
- Burg, J.P., 1978. Maximum entropy spectral analysis. In: Childers, E.G. (Ed.) *Modern Spectrum Analysis*. IEEE Press, Piscataway, N.J., pp. 42-48.
- Campos, H., Steffen, W., Aguero, G., Parra, O. & Zuniga, L., 1987. Limnology of Lake Riñihue. *Limnológica*, **18**, 339-345.
- Campos, H., Steffen, W., Aguero, G., Parra, O. & Zuniga, L., 1988. Limnological study of Lake Llanquihue (Chile). Morphometry, physics, chemistry, plankton and primary productivity. *Archiv für Hydrobiologie*, **81**, 37-67.
- Campos, H., Steffen, W., Aguero, G., Parra, O. & Zuniga, L., 1989. Estudios limnológicos en el Lago Puyehue (Chile): morfometría, factores físicos y químicos, plancton y productividad primaria. *Medio Ambiente*, **10**, 36-53.
- Campos, H., Steffen, W., Aguero, G., Parra, O. & Zuniga, L., 1990. Limnology study of lake Todos los Santos (Chile). Morphometry, Physics, Chemistry, Plankton and Primary Productivity. *Archiv für Hydrobiologie*, **117**, 453-484.
- Campos, H., Steffen, W., Aguero, G., Parra, O. & Zuniga, L., 1992a. Limnological studies of lake Rupanco (Chile). Morphometry, Physics, chemistry, plankton and primary productivity. *Archiv für Hydrobiologie, Suppl.*, **90**, 85-113.
- Campos, H., Steffen, W., Aguero, G., Parra, O. & Zuniga, L., 1992b. Limnology of Lake Ranco (Chile). *Limnológica*, **22**, 337-353.
- Cane, M.A., 2005. The evolution of El Niño, past and future. *Earth and Planetary Science Letters*, **230**, 227-240.
- Childers, D.G., 1978. *Modern Spectrum Analysis*. IEEE Press, 331 pp.
- Cholnoky, B.J., 1968. Die Ökologie der Diatomeen in Binnengewässern. J. Cramer, Lehre, 699 pp.
- Ciais, P., Petit, J., Jouzel, J., Lorius, C., Barkov, N.I., Lipenkov, V. & Nicolaiev, V., 1992. Evidence for an early Holocene climatic optimum in the Antarctic deep ice-core record. *Climate Dynamics*, **6**, 169-177.
- Clapperton, C.M., 1993. *Quaternary Geology and Geomorphology of South America*. Elsevier Science B.V., Amsterdam.
- Cook, H.E., Johnson, P.D., Matti, J.C. & Zemmels, I., 1975. Methods of sample preparation and x-ray diffraction data analysis, x-ray mineralogy laboratory. In: Kaneps, A.G. (ed.) *Initial reports of the DSDP*, **28**, Washington DC, 997-1007.
- Cox, E.J., 1996. *Identification of freshwater diatoms from live material*. Chapman and Hall, London, 158 pp.
- Czernik, T. & Goslar, T., 2001. Preparation of graphite targets in the Gwiliice radiocarbon laboratory for AMS <sup>14</sup>C dating. *Radiocarbon*, **43(2)**, 283-291.
- Daubechies, I., 1992. *Ten lectures on wavelets*. Society for Industrial and Applied Mathematics Press, vol 16 of CBMS-NSF Regional Conference Series in Applied Mathematics, Philadelphia USA, pp 357
- Dawson, A.G. & O'Hare, G., 2000. Ocean-atmosphere circulation and global climate. *Geography*, **85**, 193-208.

- Dean, J.M. & Kemp, A.E.S., 2004. A 2100 year BP record of the Pacific Decadal Oscillation, El Niño Southern Oscillation and Quasi-Biennial Oscillation in marine production and fluvial input from Saanich Inlet, British Columbia. *Palaeogeography, Palaeoclimatology, Palaeoecology*, **213**, 207-229.
- Denton, G.H., Heusser, C.J., Lowell, T.V., Moreno, P.I., Andersen, B.G., Heusser, L.E., Schlüter, C. & Marchant, D.R., 1999. Geomorphology, stratigraphy, and radiocarbon chronology of Llanquihue drift in the area of the southern Lake District, Seno Reloncaví, and Isla Grande de Chiloé, Chile. *Geografiska Annaler*, **81A(2)**, 167-212.
- Dettinger, M.D., Ghil, M., Strong, C.M., Weibel, W. & Yiou, P., 1995. Software expedites singular-spectrum analysis of noisy time series. *Eos Transactions*, **76(2)**, 12, 14, 21.
- Diaz, M.M., Pedrozo, F.L. & Temporetti, P.F., 1998. Phytoplankton of two Araucanian lakes of differing trophic status (Argentina). *Hydrobiologia*, **369-370**, 45-57.
- Erdtman, G., 1960. The acetolysis method. *Svensk Botanisk Tidskrift*, **54**, 561-565.
- Folk, R.L. & Ward, W.C., 1957. Brazos river bar: a study in the significance of grain size parameters. *Journal of Sedimentary Petrology*, **27(1)**, 3-26.
- Fraedrich, K., 1986. Estimating the dimension of weather and climate attractors. *Journal of Atmospheric Science*, **43**, 419-432.
- Frenquelli, J., 1942. Diatomeas del Neuquen (Patagonia). *Revista del Museo de la Plata Sección Botánica*, **5**, 73-219.
- Gerlach, D.C., Frey, F.A., Moreno-Roa, H. & Lopez-Escobar, L., 1988. Recent volcanism in the Puyehue-Cordon Caulle Region, Southern Andes, Chile (40.5°S): Petrogenesis of evolved lavas. *Journal of Petrology*, **29**, 333-382.
- Ghil, M., Allen, M.R., Dettinger, M.D., Ide, K., Kondrashov, D., Mann, M.E., Robertson, A.W., Saunders, A., Tian, Y., Varadi, F. & Yiou, P., 2002. Advanced spectral methods for climatic time series. *Reviews of Geophysics*, **40(1)**, 1003.
- Goodman, A.Y., Rodbell, D.T., Seltzer, G.O. & Mark, B.G., 2001. Subdivision of glacial deposits in Southeastern Peru based on pedogenic development and radiometric ages. *Quaternary Research*, **56**, 31-50.
- Goosse, H., Masson-Delmotte, V., Renssen, H., Delmotte, M., Fichet, T., Morgan, V., van Ommen, T., Khim, B.K. & Stenni, B., 2004. A late medieval warm period in the Southern Ocean as a delayed response to external forcing? *Geophysical Research Letters*, **31**, 1-5.
- Grimm, E.C., 1987. CONISS, a FORTRAN-77 program for stratigraphically constrained cluster analysis by the method of incremental sum of squares. *Computers and Geoscience*, **13**, 13-15.
- Grimm, E.C., 1991. Tilia version 2.0b4. Springfield: Illinois State Museum, Illinois.
- Grimm, E.G., 2001. TGView version 1.1.1.1. Springfield: Illinois State Museum, Illinois.
- Groote, P.M., Stuiver, M., White, J.W.C., Johnsen, S. & Jouzel, J., 1993. Comparison of oxygen isotope records from the GISP2 and GRIP Greenland ice cores. *Nature*, **366**, 552-554.
- Grosjean, M., Geyh, M.A., Messerli, B., Schreier, H. & Veit, H., 1998. A late-Holocene (<2600 BP) glacial advance in the south-central Andes (29°S), northern Chile. *The Holocene*, **8(4)**, 473-479.

- Hajdas-Skowronek, I., 1993. Extension of the radiocarbon calibration curve by AMS dating of laminated sediments of lake Soppensee and lake Holzmaar, Ph.D Thesis, 148 pp.
- Hajdas, I., Bonani, G., Moreno, P. & Ariztegui, D., 2003. Precise radiocarbon dating of Late-Glacial cooling in mid-latitude South America. *Quaternary Research*, **59**, 70-78.
- Håkansson, H., 2002. A compilation and evaluation of species in the general *Stephanodiscus*, *Cyclostephanos* and *Cyclotella* with a new genus in the family *Stephanodiscaceae*. *Diatom Research*, **17**, 1-139.
- Heusser, C.J., 1971. Pollen and spores of Chile. Modern types of the Pteridophyta, Gymnospermae, and Angiospermae. The University of Arizona Press, Tucson, Arizona, 167 pp.
- Heiri, O., Lotter, A.F. & Lemcke, G., 2001. Loss on ignition as a method for estimating organic and carbonate content in sediments: reproductibility and comparability of results. *Journal of Paleolimnology*, **25**, 101-110.
- Heusser, C.J., 2003. Ice age Southern Andes: A chronicle of Palaeoecological events. *Developments in Quaternary Science 3*, Elsevier, Amsterdam, 230 pp.
- Hubbard, A.L., 1997. Modelling climate, topography and palaeoglacier fluctuations in the Chilean Andes. *Earth Surface Processes and Landforms*, **22**, 79-92.
- Hughen, K.A., Overpeck, J.T., Lehman, S.C., Kashgarian, M., Southon, J., Peterson, L.C., Alley, R. & Sigman, D.M., 1998. Deglacial changes in ocean circulation from an extended radiocarbon calibration. *Nature*, **391**, 65-68.
- Jenny, B., Valero-Garcés, B.L., Villa-Martinez, R., Urrutia, R., Geyh, M. & Veit, H., 2002. Early to Mid-Holocene Aridity in Central Chile and the Southern Westerlies: The Laguna Aculeo Record (34°S). *Quaternary Research*, **58**, 160-170.
- Kalnay, E., Kanamitsu, M., Kistler, R., Collins, W., Deaven, D., Gandin, L., Iredell, M., Saha, S., White, G., Woollen, J., Zhu, Y., Leetmaa, A. & Reynolds R., 1996. The NCEP/NCAR Reanalysis 40-year Project. *Bulletin of the American Meteorological Society*, **77**, 437-471.
- Kendall, M. & Stuart, A., 1977. *The Advanced Theory of Statistics*. Vol. 2, 4<sup>th</sup> Ed. Macmillan, Old Tappan, N.J.
- Kilham, P., Kilham, S.S. & Hecky, R.E., 1986. Hypothesized resource relationships among African planktonic diatoms. *Limnology and Oceanography*, **31**, 1169-1181.
- Koch, J. & Kilian, R., 2005. 'Little Ice Age' glacier fluctuations, Gran Campo Nevado, southernmost Chile. *The Holocene*, **15(1)**, 20-28.
- Lamy, F., Hebbeln, D., Röhl, U. & Wefer, G., 2001. Holocene rainfall variability in Southern Chile: a marine record of latitudinal shifts of the Southern Westerlies. *Earth and Planetary Science Letters*, **185**, 369-382.
- Lamy, F., Kaiser, J., Ninnemann, U., Hebbeln, D., Arz, H.W., Stoner, J., 2004. Antarctic timing of surface water changes off Chile and Patagonian ice sheet response. *Science*, **304**, 1959-1962
- Lamy, F., Rühlemann, D., Hebbeln, D. & Wefer, G., 2002. High- and low-latitude climate control on the position of the southern Peru-Chile Current during the Holocene. *Paleoceanography*, **17(2)**, doi:10.1029/2001PA000727.
- Langhor, R., 1971. The volcanic ash soils of the central valley of Chile. *Pédologie*, **21(3)**, 259-293.

- Langhor, R., 1974. The volcanic ash soils of the central valley of central Chile. II. The parent materials of the Trumao and Nadi soils of the Lake District in relation with the geomorphology and quaternary geology. *Pédologie*, **24(3)**, 238-255.
- Lara, L.E., Naranjo, J.A. & Moreno, H., 2004. Rhyodacitic fissure eruption in Southern Andes (Cordon Caulle; 40.5°S) after the 1960 ( $M_w$ : 9.5) Chilean earthquake: a structural interpretation. *Journal of Volcanological and Geothermal Research*, **138**, 127-138.
- Lara, A. & Villalba, R., 1993. A 3620-year temperature record from Fitzroya cupressoides tree rings in Southern South America. *Science*, **260**, 1104-1106.
- Lau, K.M & Weng, H.Y., 1995. Climate signal detection using wavelet transform: how to make a time series sing. *Bulletin of the American Meteorological Society*, **76**, 2391-2402.
- Laugenie, C., 1982. La région des lacs, Chili méridional. Recherches sur l'évolution géomorphologique d'un piémont glaciaire quaternaire andin Unpublished PhD Thesis, Université de Bordeaux III, France, 822 pp.
- Leinen, M., 1977. A normative calculation technique for determining opal in deep-sea sediments. *Geochimica Cosmochimica Acta*, **41**, 671-676.
- Lotter, A.F. & Lemcke, G., 1999. Methods for preparing and counting biochemical varves. *Boreas*, **28**, 243-252.
- Lowell, T.V., Heusser, C.J., Andersen, B.G., Moreno, P.I., Hauser, A., Heusser, L.E., Schlüter, C., Marchant, D.R. & Denton, G.H., 1995. Interhemispheric correlation of Late Pleistocene glacial events. *Science*, **269**, 1541-1549.
- Luckman, B.H. & Villalba, R., 2001. Assessing the synchronicity of glacier fluctuations in the western cordillera of the Americas during the last millennium. In: Markgraf, V. (Ed.), *Interhemispheric Climate Linkages*. San Diego, pp. 119-140.
- Mallat, S., 1998. A wavelet tour of signal processing. Academic Press, San Diego, CA, USA, pp. 577.
- Markgraf, V., Baumgartner, T.R, Bradbury, J.P., Diaz, H.F., Dunbar, R.B., Luckman, B.H., Seltzer, G.O., Swetnam, T.W. & Villalba, R., 2000. Paleoclimate reconstruction along the Pole Equator Pole transect of the Americas (PEP 1). *Quaternary Science Reviews*, **19**, 125-140.
- Masson, V., Vimeux, F., Jouzel, J., Morgan, V., Delmotte, M., Ciais, P., Hammer, C., Johnsen, S., Lipenkov, V.Y., Mosley-Thompson, E., Petit, J.-R., Steig, E.J., Stievenard, M. & Vaikmae, R., 2000. Holocene climate variability in Antarctica based on 11 ice-core isotopic records. *Quaternary Research*, **54**, 348-358.
- Mauquoy, D., Blauw, M., van Geel, B., Borrromei, A., Quattrocchio, M., Chambers, F.M. & Possnert, G., 2004. Late Holocene climatic changes in Tierra del Fuego based on multiproxy analyses of peat deposits. *Quaternary Research*, **61**, 148-158.
- McCulloch, R.D., Bentley, M.J., Purves, R.S., Hulton, N.R.J., Sugden, D.E. & Clapperton, C.M., 2000. Climatic inferences from glacial and paleoecological evidence at the last glacial termination, southern South America. *Journal of Quaternary Science*, **15**, 409-417.
- Mercer, J.H., 1972. Chilean glacial chronology 20,000 to 11,000 carbon-14 years ago: some global comparisons. *Science*, **176**, 1118-1120.

- Mercer, J.H., 1976. Glacial history of southernmost South America. *Quaternary Research*, **6**, 125-166.
- Miller, A., 1976. The climate of Chile. In: Schwerdtfeger, W. (ed.). *World survey of Climatology*. Elsevier, Amsterdam, pp. 107-134.
- Moore, D.M. & Reynolds, R.C.J., 1989. X-ray diffraction and the identification and analysis of clay minerals. Oxford University Press, 332 pp.
- Montecinos, A. & Aceituno, P., 2003. Seasonality of the ENSO-Related Rainfall Variability in Central Chile and Associated Circulation Anomalies. *Bulletin of the American Meteorological Society*, **16**, 281-296.
- Moreno, P.I., 1997. Vegetation and climate near Lago Llanquihue in the Chilean Lake District between 20200 and 9500 <sup>14</sup>C yr BP. *Journal of Quaternary Science*, **12**, 485-500.
- Moreno, P., 2000. Climate, Fire, and Vegetation between About 13,000 and 9200 <sup>14</sup>C yr BP in the Chilean Lake District. *Quaternary Research*, **54**, 81-89.
- Moreno, P.I., 2004. Millennial-scale climate variability in Northwest Patagonia over the last 15 000 yr. *Journal of Quaternary Science*, **19**, 35-47.
- Moreno, P.I., Jacobson, G.L., Lowell, T.V. & Denton, G.H., 2001. Interhemispheric climate links revealed by a late-glacial cooling episode in southern Chile. *Nature*, **409**, 804-808.
- Moreno, P.I. & León, A.L., 2003. Abrupt vegetation changes during the last glacial to Holocene transition in mid-latitude South America. *Journal of Quaternary Science*, **18**, 787-800.
- Moreno, P.I., Lowell, T.V., Jacobson, G.L.J. & Denton, G.H., 1999. Abrupt vegetation and climate changes during the last glacial maximum and last termination in the Chilean Lake District: a case study from Canal de la Puntilla (41°S). *Geografiska Annaler*, **81A(2)**, 285-311.
- Morlet, J., 1983. Sampling theory and wave propagation. NATO ASI series, F1, Springer, pp. 233-261.
- Mortlock, R.A. & Froelich, P.N., 1989. A simple method for the rapid determination of biogenic opal in pelagic marine sediments. *Deep-Sea Research*, **36(9)**, 1415-1426.
- Nederbragt, A.J. & Thurow, J.W., 2001. A 6000 yr varve record of Holocene climate in Saanich Inlet, British Columbia, from digital sediment colour analysis of ODP Leg 169S cores. *Marine Geology*, **174**, 95-110.
- Parada, M.G., 1973. Pluviometria de Chile. Isoyetas de Valdivia-Puerto Montt. CORFO Departamento de Recursos hydraulicos. 73 pp.
- Park, J., 1992. Envelope estimation for quasi-periodic geophysical signals in noise: A multitaper approach. In: Walden, A.T. & Guttorp, P. (eds.) *Statistics in the Environmental and Earth Sciences*. Edward Arnold, London, pp. 189-219
- Patrick, R. & Reimer, C.W., 1966. The diatoms of the United States, exclusive of Alaska and Hawaii. Volume 1. Academy of Natural Sciences of Philadelphia, Philadelphia, 688 pp.
- Percival, D.B. & Walden, A.T., 1993. Spectral Analysis for Physical Applications. Cambridge Univ. Press, New York, 583 pp.
- Porter, S.C., 1981. Pleistocene glaciation in the southern Lake District of Chile. *Quaternary Research*, **16**, 263-292.

- Rasmusson, E.M., Wang, X. & Ropelewski, C.F., 1990. The biennial component of ENSO variability. *Journal of Marine Systems*, **1**, 71-96.
- Round, F.E. & Bukhtiyarova, L., 1996. Four new genera based on *Achnanthes* (*Achnanthidium*) together with a re-definition of *Achnanthidium*. *Diatom Research*, **11**, 345-361.
- Round, F.E., Crawford, R.M. & Mann, D.G., 1990. The diatoms: biology and morphology of the genera. Cambridge University Press, Cambridge, 747 pp.
- Rumrich, U., Lange-Bertalot, H. & Rumrich, M., 2000. Diatoms of the Andes, from Venezuela to Patagonia/Tierra del Fuego, and two additional contributions. ARG Gartner Verlag KG, Koningstein, 673 pp.
- Schick, M., 1980. Flora del parque nacional Puyehue. *Universitaria*, Santiago, 557 pp.
- Schwing, F.B., Murphree, T. & Green, P.M., 2002. The Northern Oscillation Index (NOI): a new climate index for the northeast Pacific. *Progress in Oceanography*, **53**, 115-139.
- SERNAGEOMIN, 2003. Mapa Geológico de Chile: versión digital. Servicio Nacional de Geología y Minería, Publicación Geológica Digital 4 (CD-ROM, version 1.0, 2003). Santiago
- Soon, W. & Baliunas, S., 2003. Proxy climatic and environmental changes of the past 1000 years. *Climate Research*, **23**, 89-110.
- Soto, D., 2002. Patrones oligotróficos en lagos del sur de Chile: relevancia de los nutrientes y de la profundidad de mezcla. *Revista Chilena de Historia Natural*, **75**, 377-393.
- Stockmarr, J., 1971. Tablets with spores used in absolute pollen analysis. *Pollen et Spores*, **13**, 615-621.
- Stuiver, M., Grootes, P.M. & Braziunas, T.F., 1995. The GISP2 <sup>18</sup>O climate record of the past 16,500 years and the role of the sun, ocean and volcanoes. *Quaternary Research*, **44**, 341-354.
- Stuiver, M., Reimer, P.J., Bard, E., Beck, J.W., Burr, G.S., Hughen, K.A., Kromer, B., McCormac, G., van der Plicht, J. & Spurk, M., 1998. Intcal98 radiocarbon age calibration, 24,000-0 cal BP. *Radiocarbon*, **40(3)**, 1041-1083.
- ter Braak, C.J.F. & Smilauer, P., 1997-2002. CANOCO for Windows 4.5., Biometris - Plant Research International, Wageningen, The Netherlands.
- ter Braak, C.J.F. & Prentice, I.C., 1988. A theory of gradient analysis. *Advances in Ecological Research*, **18**, 271-317.
- Thomasson, K., 1963. Araucanian Lakes, plankton studies in North Patagonia with notes on terrestrial vegetation. Almqvist & Wiksells Boktryckeri A.B., Uppsala, 139 pp.
- Thompson, L.G., Mosley-Thompson, E., Bolzan, J.F. & Koci, B.R., 1985. A 1500-year record of tropical precipitation in ice cores from the Quelccaya ice cap, Peru. *Science*, **229**, 971-973.
- Thompson, L.G., Mosley-Thompson, E., Dansgaard, W. & Grootes, P.M., 1986. The Little Ice Age as recorded in the stratigraphy of the tropical Quelccaya ice cap. *Science*, **234**, 361-364.
- Thomson, D.J., 1982. Spectrum estimation and harmonic analysis. *Proceedings of the IEEE*, **70**, 1055-1096.

- Torrence, C. & Compo, G.P., 1997. A practical guide to wavelet analysis. *Bulletin of the American Meteorological Society*, **79**, 61-78.
- Trenberth, K.E. & Shea, D.J., 1987. On the evolution of the Southern Oscillation. *Monthly Weather Review*, **115**, 3078-3096.
- Urrutia, R., Sabbe, K., Crucès, F., Pozo, K., Becerra, J., Araneda, A., Vyverman, W. & Parra, O., 2000. Paleolimnological studies of Laguna Chica of San Pedro (VIII Region): Diatoms, hydrocarbons and fatty acid records. *Revista Chilena de Historia Natural*, **73**, 717-728.
- Valero-Garcés, B.L., Delgado-Huertas, A., Navas, A., Edwards, L., Schwalb, A. & Ratto, N., 2003. Patterns of regional hydrological variability in central-southern Altiplano (18°S–26°S) lakes during the last 500 years. *Palaeogeography, Palaeoclimatology, Palaeoecology*, **194**, 319-338.
- van Geel, B., Heusser, C.J., Renssen, H. & Schuurmans, C.J.E., 2000. Climate change in Chile at around 2700 BP and global evidence for solar forcing: a hypothesis. *The Holocene*, **10**(5), 659-664.
- van Geel, B. & Renssen, H., 1998. Abrupt climate change around 2,650 BP in North-West Europe: evidence for climatic teleconnections and a tentative explanation. In: Issar, A. & Brown, N. (eds). *Water, environment and society in times of climatic change*. Kluwer, Dordrecht, pp. 21-41.
- Van Rensbergen, P., De Batist, M., Beck, C. & Manalt, F., 1998. High resolution seismic stratigraphy of late Quaternary fill of Lake Annecy (Northwestern Alps): evolution from glacial to interglacial sedimentary processes. *Sedimentary Geology*, **117**, 71-96.
- Vautard, R. & Ghil, M., 1989. Singular spectrum analysis in nonlinear dynamics, with applications to paleoclimatic time series. *Journal of Physics D.*, **35**, 395-424.
- Villagrán, C., 1980. Vegetationsgeschichtliche und pflanzensoziologische Untersuchungen im Vicente Pérez Rosales Nationalpark (Chile). *Dissertationes Botanicæ*, **54**, 1-165.
- Villalba, R., 1990. Climatic fluctuations in Northern Patagonia during the last 1000 years as inferred from tree-ring records. *Quaternary Research*, **34**, 346-360.
- Villalba, R., 1994. Tree-ring and glacial evidence for the medieval warm epoch and the little ice age in Southern South America. *Climatic Change*, **26**, 183-197.
- Villalba, R., D'Arrigo, R.D., Cook, E.R., Jacoby, G.C. & Wiles, G., 2001. Decadal-scale climatic variability along the extratropical western coast of the Americas: evidence from tree-ring records. In: Markgraf, V. (Ed.), *Interhemispheric Climate Linkages*. Academic Press, San Diego, pp. 155-172.
- Williams, P.W., King, D.N.T., Zhao, J.-X. & Collerson, K.D., 2004. Speleothem master chronologies: combined Holocene <sup>18</sup>O and <sup>13</sup>C records from the North Island of New Zealand and their paleoenvironmental interpretation. *The Holocene*, **14**, 194-208.
- Willner, A.P., Glodny, J., Gerya, T.V., Godoy, E. & Massonne, H.-J., 2004. A counterclockwise PTt path of high-pressure/low-temperature rocks from the Coastal Cordillera accretionary complex of south-central Chile: constraints for the earliest stage of subduction mass flow. *Lithos*, **75**, 283-310.
- Zippi, P., 1996. NADP Fossil Pollen Data file to spreadsheet conversion utility. *INQUA Newsletter*, **14**, 23.

Zolitschka, B., 1996. High resolution lacustrine sediments and their potential for palaeoclimatic reconstruction. In: Jones, P.D., Bradley, R.S. & Jouzel, J. (eds) *Climatic variations and forcing mechanisms of the last 2000 years*. NATO ASI series. **141**, pp. 453-478.



## PROJECT OUTPUT

### Project publications

- Araneda, A., Cruces, F., Torres, L., Bertrand, S., Fagel, N., Treutler, H.C., Chirinos, L., Barra, R. & Urrutia, R., 2007. Changes of sub-fossil chironomid assemblages associated with volcanic sediment deposition in an Andean lake (38°S), Chile. *Revista Chilena de Historia Natural*, **80(2)**, 141-156.
- Arnaud, F., Magand, O., Chapron, E., Bertrand, S., Boës, X., Charlet, F., Mélières, M.-A., 2006. Radionuclide dating ( $^{210}\text{Pb}$ ,  $^{137}\text{Cs}$ ,  $^{241}\text{Am}$ ) of recent lake sediments in a highly active geodynamic setting (Lakes Puyehue and Icalma—Chilean Lake District). *Science of the Total Environment*, **366**, 837-850.
- Bertrand, S., Castiaux, J. & Juvigné, E., (submitted). Tephrostratigraphy of the Late Glacial and Holocene sediments of Puyehue Lake (Southern Volcanic Zone, Chile, 40°S). *Quaternary Research*.
- Bertrand, S., Castiaux, J., Boes, X., Charlet, F., Urrutia, R., Espinoza, C., Lepoint, G., Charlier, B. & Fagel, N., 2005. Temporal evolution of sediment supply in Lago Puyehue (Southern Chile) during the last 600 years: climatic significance. *Quaternary Research*, **64(2)**, 163-175.
- Bertrand, S., Charlet, F., Chapron, E., Fagel, N. & De Batist, M., (in press). Reconstruction of the Holocene seismotectonic activity of the Southern Andes from seismites recorded in Lago Icalma, Chile, 39°S. *Palaeogeography, Palaeoclimatology, Palaeoecology*. doi: 10.1016/j.palaeo.2007.10.013
- Bertrand, S., Charlet, F., Charlier, B., Renson, V. & Fagel, N., (in press). Climate variability of southern Chile since the Last Glacial Maximum: a continuous sedimentological record from Lago Puyehue (40°S). *Journal of Paleolimnology*. doi: 10.1007/s10933-007-9117-y
- Bertrand, S. & Fagel, N., (in press). Nature, origin, transport and deposition of andosol parent material in south-central Chile (36-42°S). *CATENA*. doi:10.1016/j.catena.2007.08.003
- Boës, X. & Fagel, N., 2005. Impregnation method for tracking annual laminations in sediment cores: an overview. *Sedimentary Geology*, **179(3-4)**, 185-194.
- Boës, X. & Fagel, N., (in press a). Relationships between southern Chilean varved lake sediments, precipitation and ENSO for the last 600 years. *Journal of Paleolimnology*. doi: 10.1007/s10933-007-9119-9
- Boës, X. & Fagel, N., (in press b). Timing of Late Glacial and Younger Dryas cool reversal in southern Chile varved sediments. *Journal of Paleolimnology*. doi: 10.1007/s10933-007-9118-x
- Chapron, E., Ariztegui, D., Mulsow, S., Villarosa, G., Pino, M., Outes, V., Juvigné, E. & Crivelli, E., 2006. Impact of the 1960 major subduction earthquake in Northern Patagonia (Chile, Argentina). *Quaternary International*, **158**, 58-71.
- Chapron, E., Juvigné, E., Mulsow, S., Ariztegui, D., Magand, O., Bertrand, S., Pino, M. & Chapron, O., 2007. Recent clastic sedimentation processes in Lake Puyehue (Chilean Lake District, 40.5°S). *Sedimentary Geology*, **201(3-4)**, 365-385.

- Chapron, E., Bertrand, S., Charlet, F., Boes, X., De Batist, M., Fagel, N., Magand, O., Arnaud, F., Melieres, M.A., Pino, M. & Urrutia, R., 2004. Sedimentary processes in Lake Puyehue over the last 500 years: Implications for paleoenvironmental reconstructions in the Chilean Lake District (41°S). *Bolletino di Geofisica*, **45(2) supp.**, 238-242.
- Charlet, F., De Batist, M., Chapron, E., Bertrand, S., Pino, M. & Urrutia, R., (in press). Seismic stratigraphy of Lago Puyehue (Chilean Lake District): new views on its deglacial and Holocene evolution. *Journal of Paleolimnology*. doi: 10.1007/s10933-007-9112-3
- Charlet, F., Marchand, C., Bertrand, S., Chapron, E., Pino, M., Urrutia, R. & De Batist, M., 2004. Geophysical reconstruction of the sedimentary infill of Lago Icalma (39°S, Chilean Lake District) since the last deglaciation. *Bolletino di Geofisica*, **45(2) supp.**, 179-184.
- Chirinos, L., Urrutia, R., Fagel, N., Bertrand, S., Gamboa, N., Araneda, A. & Zaror, C., 2005. Chemical profiles in lake sediments in Laguna Chica de San Pedro (Bio-bio region, Chile). *Journal of the Chilean Chemical Society*, **50(4)**, 697-710.
- Cruces, F., Urrutia, R., Parra, O., Araneda, A., Treulter, H., Bertrand, S., Fagel, N., Torres, L., Barra, R. & Chirinos, L., 2006. Changes in diatom assemblages in an Andean lake in response to a recent volcanic event. *Archiv für Hydrobiologie*, **165**, 23-35.
- De Batist, M., Fagel, N., Loutre, M.F. & Chapron, E., (in press). A 17,900 year multiproxy lacustrine record of Lago Puyehue (Chilean Lake District): Introduction. *Journal of Paleolimnology*. doi: 10.1007/s10933-007-9113-2
- De Batist, M., Fagel, N., Loutre, M.F. & Chapron, E. (Eds.), (in press). Lacustrine record of Late Pleistocene and Holocene climate evolution, volcanism and seismic activity in Lake Puyehue (Chilean Lake District). *Journal of Paleolimnology*.
- De Vleeschouwer, F., Juvigné, E., Renson, V. & Naranjo, J.A., 2005. Mineral chemistry of Llaïma Pumice, Southern Chile: Evidence of magma mixing. *Geologica Belgica*, **8(1-2)**, 135-143.
- Fagel, N., Boës, X. & Loutre, M.F., (in press). Climate oscillations evidenced by spectral analysis of Southern Chilean lacustrine sediments: the assessment of ENSO over the last 600 years. *Journal of Paleolimnology*. doi: 10.1007/s10933-007-9116-z
- Juvigné, E., Bertrand, S., Heuschen, B. & Tallier, E., (submitted). Tephrostratigraphy of lake sediments located in geodynamically active areas: Lessons from Lake Icalma (Chile, Southern Volcanic Zone, 38°S). *Quaternaire*.
- Heirman, K., De Batist, M., Charlet, F., Moernaut, J., Chapron, E., Brümmer, R., Pino, M. & Urrutia, R., (submitted). Detailed seismic stratigraphy of Lago Puyehue: implications for mode and timing of glacier retreat in the Chilean Lake District. *Quaternary Science Reviews*.
- Magand, O. & Arnaud, F., 2007. Response on the comment from Ribeiro Guevara and Arribere on the article 'Radionuclide dating (Pb-210, Cs-137, Am-241) of recent lake sediments in a highly geodynamic setting (Lakes Puyehue and

- Icalma-Chilean Lake District)'. *Science of the Total Environment*, **385(1-3)**, 312-314.
- Melnick, D., Charlet, F., Echtler, H. & De Batist, M., 2006. Incipient axial collapse of the Main Cordillera and strain partitioning gradient between the Central and Patagonian Andes, Lago Laja, Chile. *Tectonics*, **25(5)**, TC5004. doi:10.1029/2005TC001918
- Moernaut, J., De Batist, M., Charlet, F., Heirman, K., Chapron, E., Pino, M., Bruemmer, R. & Urrutia, R., 2007. Giant earthquakes in South-Central Chile revealed by Holocene mass-wasting events in Lake Puyehue. *Sedimentary Geology*, **195(3-4)**, 239-256.
- Sterken, M., Verleyen, E., Sabbe, K., Terryn, G., Charlet, F., Bertrand, S., Boës, X., Fagel, N., De Batist, M. & Vyverman, W., 2007. Late Quaternary climatic changes in southern Chile, as recorded in a diatom sequence of Lago Puyehue (40°40'S). *Journal of Paleolimnology*. doi: 10.1007/s10933-007-9114-1
- Urrutia, R., Araneda, A., Cruces, F., Torres, L., Chirinos, L., Treutler, H.-C., Fagel, N., Bertrand, S., Alvial, I., Barra, R. & Chapron, E., 2007. Changes in diatom, pollen, and chironomid assemblages in response to a recent volcanic event in Lake Galletué (Chilean Andes). *Limnologica - Ecology and Management of Inland Waters*, **37(1)**, 49-62.
- Vargas, L., Roche, E., Gerrienne, Ph. & Hooghiemstra, H., (in press). Pollen-based record of Lateglacial-Holocene climatic variability in southern Lake District, Chile. *Journal of Paleolimnology*. doi: 10.1007/s10933-007-9115-0

### **Multimedia products**

- Mémoires chiliennes*. Wetenschapspopulariserende film-documentaire, 2003. Door: Anouk, La Rotonde, Teraa. Duur: 25'40"